

DESIGN OF NON-PNEUMATIC TYRES

A THESIS

submitted by

ANAND SURESH KUMAR

for the award of the degree

of

MASTER OF SCIENCE

(by Research)



**DEPARTMENT OF ENGINEERING DESIGN
INDIAN INSTITUTE OF TECHNOLOGY MADRAS
CHENNAI-600 036**

APRIL 2016

THESIS CERTIFICATE

This is to certify that the thesis entitled "**DESIGN OF NON-PNEUMATIC TYRES**" submitted by **ANAND SURESH KUMAR** to the Indian Institute of Technology Madras, Chennai for the award of the degree of **Master of Science**, is a bonafide record of research work carried out by him under my supervision. The contents of this thesis, in full or in parts, have not been submitted and will not be submitted to any other Institute or University for the award of any degree or diploma.

Prof. R. Krishna Kumar
Research Guide
Professor
Department of Engineering Design
IIT Madras, 600036

Place : Chennai

Date : 8th April 2016

ACKNOWLEDGEMENTS

Does writing the ‘acknowledgements’ section of a thesis have therapeutic effects, or am I the only one feeling like a 7 year old on Christmas Eve? I’ve always been fond of reading this section as it is one those few things which adds a human touch to a book which can get rather overwhelming with its content (the other one being, incorrect labelling of the coordinate axes :P). It is not very often that we come across an opportunity in life to thank the people around us. I would like to begin this with my research advisor.

If there is one quality that students who have worked under Prof. R Krishna Kumar often repeat about him, it would be his infectious enthusiasm for learning new things, and to paraphrase one of his grad students*, “You need to be bold to tackle new and hard problems”. These were the two predominant reasons why this thesis saw the light of day. I would like to thank Dr. RKK for considering me and giving me an opportunity to work on a problem statement which is one of its kind and in a domain where research is highly competitive and proprietary. It is not every day that a professor hands over an open-ended problem to one of his students to work on. The fact that I was given complete freedom on how to tackle the problem made the process even more pleasurable. The time that I have spent in the ‘hallowed portals of IIT Madras’** has been nothing short of enlightening and I owe it all to my advisor.

Another person whose contributions have been significant in the completion of this work is, Dr. K. V. Narasimha Rao, DGM, JK Tyres & Industries Ltd. His participation was vital in drawing up a road-map for the research work. I am extremely grateful for his active contribution and meticulous critique (which I cannot stress enough!) of the work done during this period. I am honoured to have worked alongside a person of his stature. I would like to thank JK Tyres & Industries Ltd. along with IIT Madras for establishing a research center with top of the line computational facilities which engineers can only dream of working in! I highly doubt if I would ever get a chance to work in such a facility outside this institute. I would also like to thank my General Test Committee members Dr. Nilesh J Vasa, Dr. Shankar Krishnapillai and Dr. G. Saravanakumar for their contributions during the progress review meetings.

The following is a list of people who “made” my life in this institute. Each person on this list has at some point during the course of my research, made invaluable tangible and

priceless intangible contributions; ranging anywhere from academic to administrative; from psychological to philosophical. With an environment filled with such amazingly brilliant and diverse people, tackling challenging problems was always fostered. Although my mettle is yet to be proved in the ‘real world’, I believe I have gained insights which I can bank on when facing tough situations in the future. No matter how hard I try, the fact that I cannot think of a way to repay them for their contributions is what makes this page special. I will always be indebted to these people.

Vinid – Unofficial mentor

Jaiganesh Sir

Prasanth Sir

Sabarinath

Jeevan

Hem*

Girish

Suresh

Mythreyi

Pradeeba

Jayakala

Neerav

Nikhil

Arun

Govindabalan

Saravanan Sir

Vijay Alagappan

Apoorva

Yagnanaryanan**

Kashif

Sakthivel Sir

Sindhoor

Srinivasan

Arun Nelson

Aban

Radhika – For boldly saying what no man had said before, “Send me the draft of your thesis, I’ll check it out”

Baalu Sir

Gayathri

Finally, I would like to thank my Mom who prayed for my “paper to get selected” and Dad, for coming up with innovative motivational quotes like “Is your MS project going to take longer than your braces?” Given the duration of my project, they were nothing but thoroughly patient and supportive. As for my brother, he snapped!

Anand Suresh Kumar

ABSTRACT

KEYWORDS: *Non-Pneumatic Tyre, Rhombi tessellation, Flexible spoke, Force and Moment characteristics, Reinforcing belts*

A pneumatic tyre has four primary functions; they are (i) to support vehicular load (ii) help maintain and change the course of travel (iii) transmit power from the engine to the road and finally (iv) absorb road shocks to provide a smoother ride. These functions are made possible due to the tyre's inflation pressure. Incorrect maintenance of inflation pressure is one of the major causes of premature mechanical failure in tyres. The adverse effects of improper maintenance of inflation pressure also results in lowering of the fuel efficiency, instability at high speeds, affects longitudinal/lateral performance as well as the ride comfort. Solutions like run-flat tyres and self-sealing tyres have been developed to curb this problem. But these alternatives seem more of a temporary fix to a rather permanent issue. The solution is to either develop a containment that does not tear, break, fail during operation or eliminate the concept of inflation pressure.

A Non-Pneumatic Tyre (NPT) is one which performs all the operations of a pneumatic tyre devoid of inflation pressure. In the present work, an NPT is designed to perform the functions of a pneumatic tyre. The NPT is designed with an aperiodic rhombi tessellated spoke acting as the load bearing member, where the 'unit cell' design is based on the vertical, circumferential and lateral stiffness offered by the structure. The theory of cellular structures is used in order to design the spoke. A parametric study is conducted to capture the effect of different geometric properties on the overall stiffness of the structure.

In order to validate the design, the NPT is compared with an equivalent pneumatic tyre. Apart from its static behaviour, an evaluation of the tyre's performance is done by observing its Force and Moment (F&M) characteristics. A 3D Finite Element (FE) model has been used to capture the mechanics of load distribution in the spoke, contact patch and variation of contact pressure distribution when the tyre is subjected to different operating conditions. SIMULIA/Abaqus, a commercial finite element software has been used to conduct static loading, acceleration/braking and cornering analyses. The F&M characteristics have been extracted from these simulations and compared with those of a 165/70R14 passenger car tyre. The variation in the vertical and circumferential stiffness, based on the spoke geometry has

also been highlighted. The use of conventional pneumatic tyre's belts to alter the NPT's lateral stiffness, despite the tyre behaving like a 'bottom loader', adds uniqueness to the design. An alternative design has been proposed in the form of circumferential spoke. This model decouples circumferential stiffness from the lateral and vertical stiffness thereby eliminating one of the governing design criteria in conventional NPT design. A comparison is made between the three tyre models to evaluate their performance.

Some of the basic design criteria which go into tyre design have been highlighted in this thesis. It also proposes modifications in the existing assembly in the form of reinforcing belts and introduces the concept of circumferential spokes thus reiterating the freedom available in NPT design which is one of underlying theme of the work done.

TABLE OF CONTENTS

ACKNOWLEDGEMENTS	i
ABSTRACT	iv
LIST OF TABLES	x
LIST OF FIGURES	xi
ABBREVIATIONS	xv
NOTATION	xvi
1. INTRODUCTION	
1.1 Motivation.....	1
1.2 Research Background.....	3
1.3 Objective and Scope of the Research.....	6
1.4 Organisation of the Thesis.....	7
2. HONEYCOMBS, TESSELLATIONS AND SPOKE DESIGN	
2.1 Introduction.....	8
2.2 Mechanics of Loading.....	8
2.3 Solid Tyre.....	9
2.4 Cellular Structures.....	10
2.5 Tessellations.....	11

2.5.1	What are tessellations?.....	11
2.5.2	Economics of Tessellation – Unit Cell Dependence.....	12
2.5.3	Economics of Tessellation – Unit Cell Grouping.....	13
2.5.4	Mechanical Properties of Regular Honeycombs.....	14
2.6	Unit Cell Parameters and its Effects on the In-Plane Properties.....	16
2.6.1	Unit Cell.....	16
2.6.2	Mechanics of Cell Wall Deformation.....	17
2.7	Summary.....	19
3.	DESIGN, ASSEMBLY AND FINITE ELEMENT MODEL OF A NON-PNEUMATIC TYRE	
3.1	Introduction.....	21
3.2	Finite Element (FE) Model of a Pneumatic Tyre.....	21
3.3	FE Procedures for Characterizing Pneumatic Tyre’s Performance...	24
3.3.1	Inflation and Loading.....	24
3.3.2	Steady State Rolling.....	25
3.4	NPT Design.....	26
3.4.1	NPT – FE Model.....	26
3.4.2	Unit Sector.....	27
3.5	Flexible Spoke Design – Parametric Analysis.....	29
3.5.1	Radial Stiffness.....	29
3.5.2	Circumferential Stiffness.....	29

3.6	Results and Discussion.....	32
3.6.1	Radial Stiffness.....	32
3.6.2	Circumferential Stiffness.....	35
3.7	Static Loading and Steady State Rolling.....	38
3.7.1	Loading.....	38
3.7.2	Contact Patch.....	40
3.7.3	Longitudinal Force.....	40
3.7.4	Lateral Force.....	41
3.7.5	Self-Aligning Torque (SAT).....	41
3.8	Summary.....	43
4.	EFFECT OF DESIGN ATTRIBUTES ON THE FORCE AND MOMENT CHARACTERISTICS	
4.1	Introduction.....	44
4.2	Effect of In-Plane Geometry on Lateral Stiffness.....	44
4.3	Belt Model as Reinforcements.....	47
4.4	FE Model of Belt Reinforced NPT.....	48
4.5	Results and Discussions.....	50
4.5.1	Vertical Stiffness.....	50
4.5.2	Contact Patch.....	51
4.5.3	Longitudinal Force.....	53
4.5.4	Lateral Force.....	53

4.5.5	Self-Aligning Torque (SAT).....	55
4.6	Characterization of NPT's F&M Behaviour.....	55
4.6.1	Spoke Material Variation.....	56
4.6.2	Normal Load Variation.....	58
4.6.3	Tread Material Variation.....	60
4.7	Circumferential Spoke NPT.....	61
4.7.1	Vertical Stiffness.....	63
4.7.2	Contact Pressure Distribution.....	64
4.7.3	Longitudinal Force.....	64
4.7.4	Lateral Force.....	65
4.7.5	Self-Aligning Torque (SAT).....	66
4.8	Limitation.....	66
4.9	Summary.....	67
5.	CONCLUSION	
5.1	Contributions.....	68
5.2	Conclusions.....	69
5.3	Future Work.....	69
	REFERENCES	71
	LIST OF PUBLICATIONS	74

LIST OF TABLES

Table	Title	Page No
2.1	Perimeter variations for polygons of same area.....	12
3.1	Reinforcement material properties.....	22
3.2	Properties of different reinforcements.....	23
3.3	Hyperelastic material coefficients for different regions in the tyre..	23
3.4	NPT material compositions.....	28
3.5	Radial stiffness with relative density.....	33
4.1	Embedded element – material properties.....	49
4.2	Host element – material properties.....	49
4.3	Contact area of different NPT models.....	53
4.4	Vertical deflection with varying material stiffness.....	57

LIST OF FIGURES

Figure	Title	Page No
1.1	Schematic diagram of (a) Run flat tyres with crescent shaped reinforcing members (Source: Willard, 1996) (b) Support device for run flat tyres. (Source: Gardetto., 1997)	3
1.2	Cross-section of a self-sealing tyre. The sealant layer (2) is located between ply (3) and the inner liner (4) (Source: Wilson, Joshua L., 2013).....	3
1.3	Variants of Non-Pneumatic Tyres (a) Rhyne <i>et al.</i> , 2007 (b) Kodaira <i>et al.</i> , 2014 (c) Manesh <i>et al.</i> , 2012 (d) Russel, B. A., 2012.....	5
2.1	Illustration of Top and Bottom loading mechanism (Source: Cron <i>et al.</i> , 2008).....	9
2.2	Embodiment of a solid tyre (Source: Reinhard Hoppenheit <i>et al.</i> , 1996).....	10
2.3	Unit cell characterization and illustration of Euler’s law.....	13
2.4	Tessellations of different polygons. (a) Circle (b) Triangle (c) Square (d) Pentagon (e) Hexagon. (The hatched area indicates that additional material is required for filling the openings).....	14
2.5	Normalized in-plane modulus for various polygonal structures (Wang <i>et al.</i> , 2004).....	15
2.6	Components of a unit cell.....	17
2.7	Unit cell loading and mechanics of cell wall deformation.....	17
2.8	Stress-Strain curves of hexagonal honeycombs.....	19
3.1	2D axisymmetric FE model of a 165/70R14 tyre.....	22

3.2	SAE superseded tyre axis system. (Source Milliken and Milliken, 1995).....	24
3.3	Unit sector of the designed NPT.....	27
3.4	Complete revolved model of the tyres.....	28
3.5	Change in spoke configuration with varying Half Cell Angle (HCA).....	30
3.6	Variation in spoke configuration with varying Cell Wall Thickness (CWT).....	31
3.7	Variation in spoke configuration with varying Half Cell Length (HCL)	31
3.8	HCA and its effect on the vertical stiffness.....	34
3.9	CWT and its effect on the vertical stiffness.....	34
3.10	HCL and its effect on the vertical stiffness.....	35
3.11	HCA and its effect on the circumferential stiffness.....	36
3.12	CWT and its effect on the circumferential stiffness.....	36
3.13	HCL and its effect on the circumferential stiffness.....	37
	Figure (a) illustrates an NPT with adequate vertical stiffness.	
3.14	Figure (b) shows the same spoke configuration with inadequate circumferential stiffness and the resultant contortion of the structure when subjected to rolling.....	37
3.15	Vertical load – deflection curves for different tyre models.....	38
3.16	Illustration of the ‘bottom –loading’ phenomena in the Steel Ringed NPT.....	39
3.17	Contact pressure distribution and contact area variation for different tyre models.....	39

3.18	Longitudinal force variation for different tyre models.....	41
3.19	Lateral force variation for different tyre models.....	42
3.20	Self-Aligning Torque (SAT) variation for different tyre models....	42
4.1	Variation of lateral force generation with HCA.....	45
4.2	Variation of lateral force generation with CWT.....	46
4.3	Variation of lateral force generation with HCL.....	46
4.4	Variation of vertical load – deflection curves with varying outer ring material properties.....	47
4.5	Lateral section and unit sector of Belt Reinforced NPT.....	49
4.6	Vertical load – deflection curve for different tyre models.....	50
4.7	Vertical load – deflection curve for NPT varying reinforcement angles.....	51
4.8	Contact pressure distribution for different tyre models.....	52
4.9	Contact pressure distribution for tyres with different reinforcement angles.....	52
4.10	Variation of longitudinal force for different tyre models.....	54
4.11	Variation of lateral force for different NPT models.....	54
4.12	Variation of SAT for different NPT models.....	55
4.13	Variation of lateral force with varying spoke material stiffness.....	57
4.14	Variation of SAT magnitudes with varying spoke material properties.....	58
4.15	Variation of lateral force with varying normal loads.....	59
4.16	Variation of SAT magnitudes with varying normal loads.....	59

4.17	Variation of lateral force with varying tread hyperelastic properties.....	60
4.18	Variation of SAT magnitudes with varying tread hyperelastic properties.....	61
4.19	Unit sector and lateral section of a circumferential spoke NPT.....	62
4.20	Sectional view of (a) axial spoke NPT and (b) circumferential spoke NPT.....	62
4.21	Load – deflection curves for different tyre models.....	63
4.22	Contact pressure variation for different tyre models.....	64
4.23	Variation of longitudinal force for different tyre models.....	65
4.24	Variation of lateral force for different tyre models.....	65
4.25	Variation of SAT for different tyre models.....	66

ABBREVIATIONS

2D	Two Dimensional
3D	Three Dimensional
ALE	Arbitrary Lagrangian Eulerian
BC	Boundary Condition
C3D8H	Continuum 3 Dimensional 8 Noded Hybrid
CAD	Computer Aided Design
CWT	Cell Wall Thickness
F&M	Force and Moment
FEA	Finite Element Analysis
FR	Free Rolling
HCA	Half Cell Angle
HCL	Half Cell Length
IITM	Indian Institute of Technology Madras
NCRB	National Crime Records Bureau
NPT	Non-Pneumatic Tyre
PCR	Passenger Car Radial
SAE	Society of Automotive Engineers
SAT	Self-Aligning Torque
SIAM	Society of Indian Automobile Manufacturers
TPMS	Tyre Pressure Monitoring System

NOTATION

ρ^*	Density of the cellular structure
ρ_s	Density of the constituent material
F_c	Face of the unit cell
E_c	Edge of the unit cell
V_c	Vertex of the unit cell
θ_h	Horizontal half cell angle
θ_v	Vertical half cell angle
l	Cell wall length
T	Cell wall thickness
L	Half cell length
E	Young's Modulus
E_{45}	Young's Modulus with unit cell oriented at 45 degrees
E_s	Young's Modulus of the constituent material
F_{45}	Force acting at 45 degrees to the principal axis
I	Moment of Inertia
P_{cr}	Critical Buckling Load
κ	Slip Ratio
ω	Angular velocity
ω_o	Free rolling angular velocity
α	Slip Angle
V_x	Longitudinal Velocity
V_y	Lateral Velocity
C_{i0}	Yeoh material constants with index i

μ	Coefficient of friction
B	Left Cauchy-Green Tensor
J^{el}	Volumetric Ratio

CHAPTER 1

INTRODUCTION

1.1 MOTIVATION

Ever since John Boyd Dunlop performed the famous ‘cobble stone test’, the design of pneumatic tyres has undergone a radical change. But the phenomenon of load-carrying in a pneumatic tyre although has largely remained unchanged. The performance of a vehicle is either traction dependent or powertrain dependent (Gillespie, 1992), and with more and more powerful engines being installed in everyday passenger vehicles, there is a constant race between the powertrain and the tyre, not to be the ‘weakest link in the performance chain’. The Indian automobile industry is the 4th largest in the world in terms of volume and over 2.2 million vehicles were manufactured during the period of March-April 2015 (SIAM, 2015). This mercurial rise in the number of vehicles has also unwittingly increased the number of road related accidents. A total of 4.8 lakh vehicles were involved in road accidents in the year 2011 (NCRB, 2013). It is estimated that approximately 10% of the vehicles report tyre related problems in the pre-crash phase when the tyre was underinflated by 25%, and this number increased by three folds when the tyre is underinflated more than 25% (Choi, 2012). Apart from delivering peak performance during operation, the onus of safety is also borne by the humble tyre.

The pneumatic tyre is a highly complex composite which is designed to endure millions of loading cycles before it is deemed unfit for road use. Despite exhibiting such high durability, tyres are prone to mechanical failure. Failure of pneumatic tyres, like tyre blowout at high speeds can result in catastrophic consequences. Incorrect maintenance of inflation pressure can lead to premature failure of tyres. Reduced fuel efficiency, instability at high speeds, uneven tyre wear, poor ride and handling characteristics are some of the major consequences of incorrect maintenance of inflation pressure. It must be noted that the performance as well as the safety characteristics of a tyre has one underlying factor: inflation pressure.

Various solutions have been sought to curb this problem. Run-flat tyres were introduced to prevent the immobilization of a vehicle in the event of a complete loss in inflation pressure.

The tyre included a thickened sidewall along with multiple pairs of reinforcing members and a specially designed bead seat area to prevent the bead from unseating when operating without inflation pressure as shown in Figure 1.1(a) (Willard, 1996). Figure 1.1(b) shows another embodiment of run-flat tyres which included a rigid circular support attached to the rim, thereby preventing the sidewall from collapsing completely in the event of a loss in inflation pressure (Gardetto, 1997). Another major alternative was the introduction of self-sealing tyres. These tyres were manufactured with a layer of sealant lined between the various components of the tyre. The sealant usually consists of a combination of high and low molecular weight butyl rubbers, a liquid polybutylene tackifier and appropriate curing agents (Stang *et al.*, 1976). The sealants were highly sticky in nature and when a foreign object penetrated the air cavity, the sealant flowed around the object and the region of rupture, preventing further loss of inflation pressure. The typical construction of a self-sealing tyre is shown in Figure 1.2. Recently, Tyre Pressure Monitoring Systems (TPMS) are being installed in tyres which update the driver regarding the inflation pressure in the tyre (Fiorletta, 1994). Though TPMS is effective in identifying the state of the tyre, the responsibility lies with the user to ensure the proper maintenance of the tyre. The introduction of these systems only seems to further complicate an already complex entity. For example, run-flat tyres have a mileage limitation when operating without inflation pressure and thus prolonged use can damage the tyre beyond repair (Willard, Jr, 1995). The issue of tyre imbalance during motion due to the flow of the sealant around the tyre is a persistent issue (Kent *et al.*, 1978). Effective functioning of self-sealing tyres is governed by the operating and ambient temperatures (Stang *et al.*, 1976), which are susceptible to large variations depending on the geographical location. All the existing solutions seem temporary, to a problem that is rather permanent. The solution is to either design a containment which does not tear, break or fail during operation or eliminate the concept of inflation pressure.

A Non-Pneumatic Tyre (NPT) is one which performs all the functions of the pneumatic tyre without the requirement of inflation pressure.

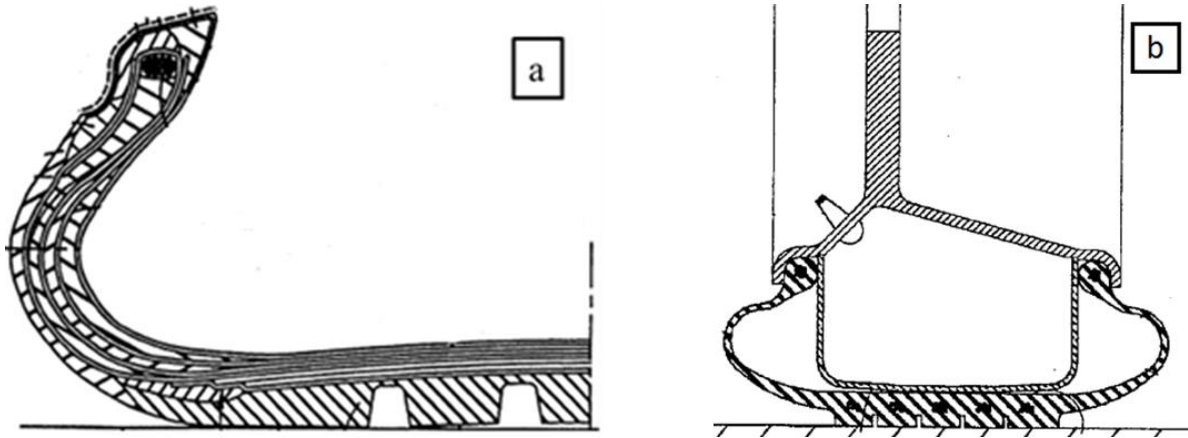


Figure 1.1: Schematic diagram of (a) Run flat tyres with crescent shaped reinforcing members (Source: Willard, 1996) (b) Support device for run flat tyres. (Source: Gardetto., 1997)

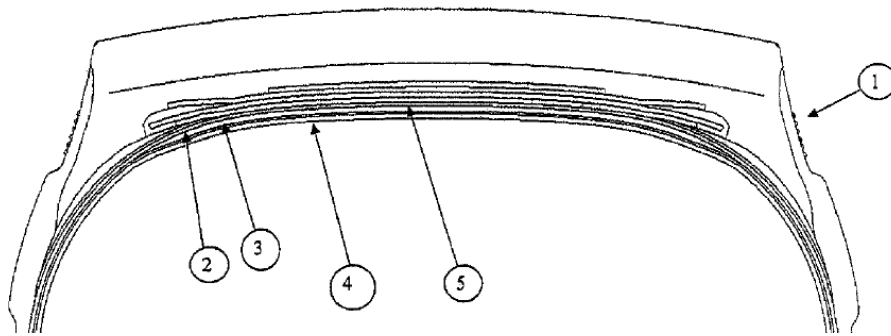


Figure 1.2: Cross-section of a self-sealing tyre. The sealant layer (2) is located between the Ply (3) and the inner liner (4) (Source: Wilson, Joshua L., 2013)

1.2 RESEARCH BACKGROUND

The concept of airless tyres has intrigued automobile manufacturers for years. Several patents have been filed in the field of NPTs, some as early as 1897. The earliest recorded patent for a non-pneumatic bicycle tyre by E. Humbercht (1897), highlighted the arrangement of ‘spring around the periphery of the rim with a circular rubber section forming the outer portion of the tyre’. Later patents introduced the concept of flexible spoke like arrangement which functioned as the load carrying member of the tyre. Pajtas S. R. (1990) designed a ‘Honeycomb NPT with a single web on one side’. The model consisted of angular ribs arranged in an alternative manner sandwiched between the inner and outer hoops with a circumferential web on the side which functioned as the sidewall. The profile helped the tyre exhibit excellent handling characteristics even at speeds in excess of 120 kmph. Rhyne *et al.* (2007) successfully designed an NPT (commercially called Tweel™) in which loads were carried in tension rather than compression by introducing the concept of ‘shear beam’. The

shear beam along with the spokes worked analogous to an arch under compression, where the structure's bending stiffness caused an increase in the shear beam's diameter, resulting in spokes being subjected to a tensile load. The Tweel™ claimed of superior load carrying efficiency, decoupled the vertical stiffness and contact pressure, and demonstrated lower energy losses while running over obstacles. Georges M. Fadel (2011) improved on the previous design of Tweel™ by introducing honeycomb based shear beams to replace the continuous elastomeric layer, which was conventionally used, and in turn help lower the hysteresis loss. Manesh *et al.* (2012) developed the 'tension based non-pneumatic tyre' which carried the loads in tension with the aid of a plurality of web elements. The design included a flexible cellular structure with polygons of different geometric properties used along with a 'shear beam' in order to carry the loads. With tyre noise being one of the major issues with NPTs, Arakawa *et al.* (2012) went about developing an NPT which claimed improved ride and noise performance. The design comprised of web elements that suppressed buckling of spoke in the contact region by dispersing the fluctuation of the spoke's strains into the tyre's body structure.

Gasmi *et al.* (2012) developed an analytical model for a 2D compliant NPT. The spokes were modelled as linear spring and the effect of spoke stiffness on the vertical deflection, contact patch and the rolling resistance was highlighted. A parametric study was conducted to rationalize the conceived design. The elastomer in the shear beam exhibited high hysteresis loss and to overcome this problem, Berglund *et al.*, (2012) suggested the use of aluminium tapered bristles (which exhibited the same mechanical properties as the shear beam) as a replacement effectively reducing the hysteretic loss and thus, the rolling resistance. The introduction of compliant cellular structures has prompted further investigation into its applicability for tyres. Ju *et al.* (2012) conducted an FE study comparing different cellular spoke designs for fatigue life resistance. Different spoke models were subjected to a rated load and the structure which developed the least stress was chosen. Kim *et al.* (2013) studied the development of contact pressure in a 3D hexagonal spoke NPT during loading. Gibert *et al.* (2013) developed models to predict the steady and transient energy losses due to rolling resistance in NPTs. With the number of patents increasing every year, it is evident that there lies a growing interest among tyre manufacturers in this relatively nascent field. Research on optimizing spoke geometry and shear band for lowering rolling resistance, studying vibration characteristics and lowering energy losses have been satisfactorily undertaken.

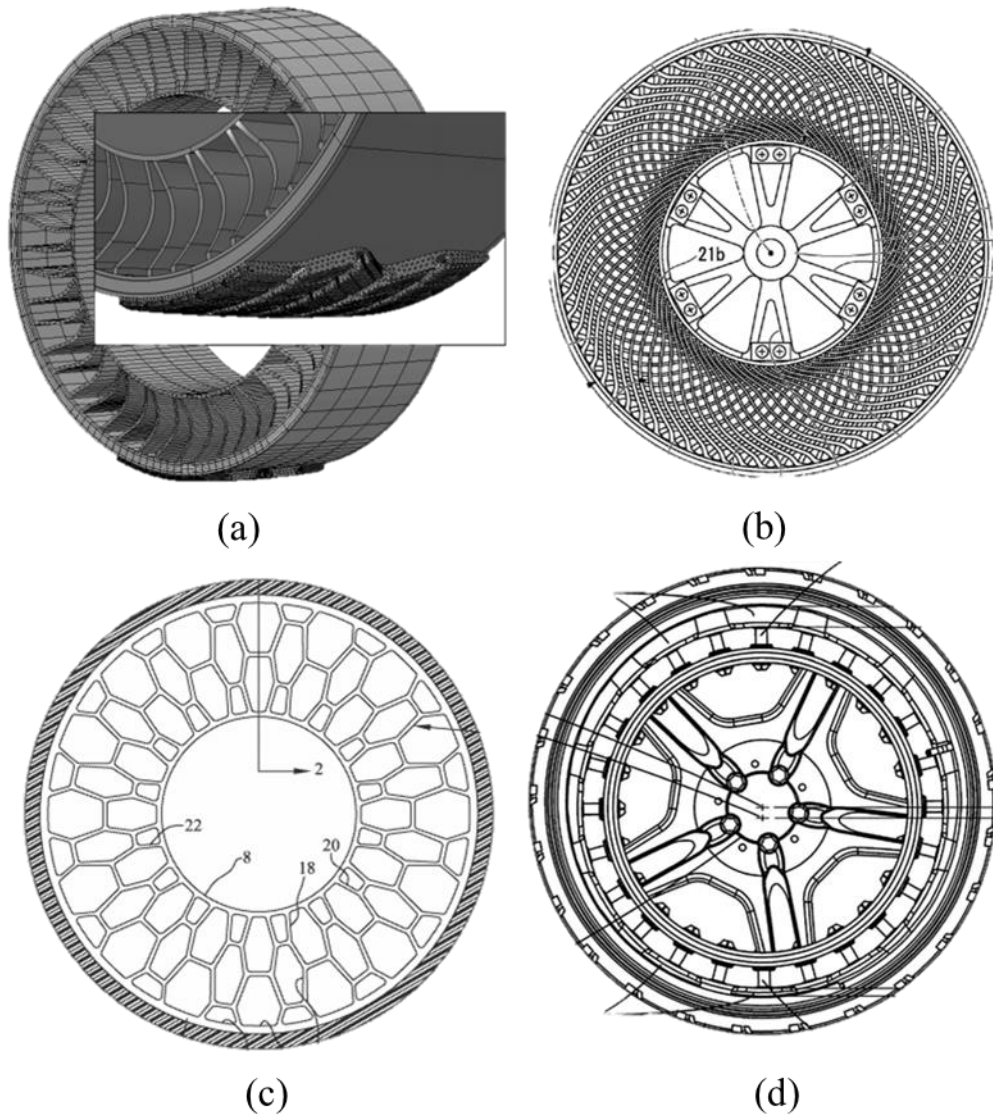


Figure 1.3: Variants of Non-Pneumatic tyres (a) Rhyne *et al.*, 2007 (b) Kodaira-shi *et al.*, 2014 (c) Manesh *et al.*, 2012 (d) Russell, B. A., 2012

However, due to the highly competitive nature of the field, none of the available literature delves into validation of their design in comparison with a pneumatic tyre or other NPTs. Validation of an NPT's design is incomplete without comparing their performance with an equivalent pneumatic tyre. Apart from the static properties, comparison of a tyre's dynamic characteristics is of prime importance. Force and Moment (F&M) characteristics of a tyre are imperative in understanding the vehicle's handling characteristics. F&M characteristics of tyres bring out the relation between (i) longitudinal force (ii) lateral force and (iii) Self Aligning Torque (SAT) variation with slip ratio and slip angle. The physics of tyre force generation is directly captured in these plots. The objective and the scope of the thesis have been planned, with this available data.

1.3 OBJECTIVE AND SCOPE OF THE RESEARCH WORK

The objective of the present work is to design an NPT for passenger car applications and to evaluate the designed tyre's performance with an equivalent pneumatic tyre using numerical techniques.

Most of the available research on NPTs stops at the design phase alone and realistic validation of the design is only possible by evaluating its performance with an equivalent pneumatic tyre. The aim of this work is to bridge this void by performing a one to one comparison of various static and steady-state properties of an NPT with its equivalent pneumatic counterpart. To achieve the aforementioned objective, the following work has been undertaken

- A 'rhombi tessellated flexible spoke' is designed to replace inflation pressure as the load carrying component of the tyre. The philosophy of cellular structures has been used in designing the spoke.
- A parametric study is conducted to observe the mechanics of carrying the load and, to record the effect of geometric properties on the spoke design using commercial Finite Element (FE) codes.
- A FE model of the NPT assembly is conceived and performance evaluation of the static and steady-state characteristics of the NPT with an equivalent 14" passenger car radial (PCR) tyre have been conducted.
- A design modification is proposed where conventional pneumatic tyre's belts are used as reinforcements to achieve varying performance characteristics in NPTs
- The concept of 'circumferential spokes' has been introduced in order to demonstrate the decoupling of various stiffness, in the designed NPT.

1.4 ORGANISATION OF THE THESIS

The work done regarding the design, modelling and validation of an NPT is explained in the following chapters

Chapter 1 gives an introduction to the nature of the problem statement, motivation, and objective of the research undertaken. A review of the available literature on modelling NPTs and evaluating NPT's various performance characteristics using analytical and numerical techniques has been conducted.

Chapter 2 introduces the concept of cellular structures and tessellations. The design requirements for an NPT are identified and the mechanical characterization of cellular structures is shown.

Chapter 3 captures the mechanical behaviour of an annular rhombi tessellated structure through a parametric study. Based on this study, a spoke design is conceived and a Finite Element (FE) model is developed. A static and steady-state FE simulation for the designed NPT and equivalent pneumatic tyre are conducted.

Chapter 4 suggests a design modification to the existing conventional NPT design. The effect of this modification is observed through the tyre's force and moment characteristics. The effect of different loading conditions on the NPT's performance has also been highlighted. A circumferential spoke NPT is designed and its performance compared with other tyre models.

Chapter 5 summarizes the work done, the contributions made, conclusions and the scope for future work.

CHAPTER 2

HONEYCOMBS, TESSELLATIONS AND SPOKE DESIGN

2.1 INTRODUCTION

The flexible spoke is the load bearing component of the Non-Pneumatic Tyre (NPT) and the philosophy behind its design has been addressed in this chapter. The chapter begins with an introduction about the basic load carrying methods. It is followed by an outline on the construction of solid tyres and the subsequent need for cellular structures. The concepts of cellular solids and cell tessellations have been introduced from the perspective of their mechanical behaviour and the economics of construction.

Inflation pressure is responsible for rendering stiffness to a tyre. The radial, tangential and lateral stiffness of the tyre are functions of the inflation pressure. In the absence of inflation pressure, a suitable structure needs to be conceived to perform the role of the pneumatic tyre. As mentioned in the previous chapter, several designs have been ideated depending on the tyre's requirement and operating conditions. In this work, the designed NPT is a bottom loader and hence priority has been given to a structure which does not buckle under vertical loading and contort when subjected to tangential load.

2.2 MECHANICS OF LOADING

Load carrying is one of the four primary functions of a pneumatic tyre (Wong, 1992). In this section, the mechanics of load carrying in a tyre is explained using the concept of 'top loaders' and 'bottom loaders' (Cron *et al.*, 2008) as this is one of the primary characteristics involved in the design of NPTs.

Conventionally, rigid wheels carry loads by directly compressing the material above the contact area. When rigid wheels roll, the material above the contact area undergoes both compression and shear whereas the material in the rest of the structure is in a stress free state. This is realized by observing the stress contours in a loaded rigid wheel. It can be intuitively understood that when all the material, except the ones above the contact area, is removed, the wheel is still capable of carrying the required load. Wheels that exhibit this kind of load carrying phenomenon are called 'bottom loaders'.

In the case of pneumatic tyres, inflation pressure is responsible for the load carrying process. When inflated, the entire structure of the tyre is under tension. The pressure in the contact area is equilibrated by an increase in the overall pressure inside the cavity. This is manifested as an increase in the tension of the structure. As the load increases, the inflation pressure causes an increase in tension in the entire structure. Depending on the stiffness of the sidewall, the region above the contact patch carries a part of the load whereas the rest of the tyre carries the majority of the load. Structures which exhibit this phenomenon of carrying loads in tension are known as ‘top loaders’. The concept of top and bottom loaders is illustrated in Figure 2.1. It can be observed that in bottom loaders, only the region above the contact patch carries the entire load. In a top loading mechanism, the loads are suspended from the structure and the inherent tension in the structure is involved in the load carrying process.

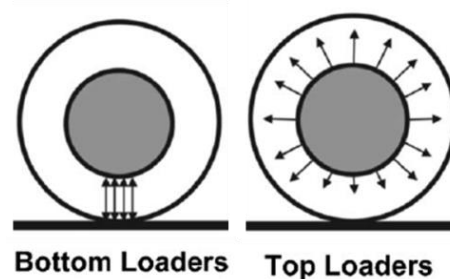


Figure 2.1: Illustration of Top and Bottom loading mechanism (Source: Cron *et al.* 2008)

2.3 SOLID TYRE

The simplest embodiment of an NPT is a solid tyre. They are designed for carrying heavy loads and negotiating harsh terrain while operating at low speeds. Thus these tyres are required to be heavy, wear resistant and offer very high stiffness in the radial direction. Figure 2.2 shows the composition of a typical solid tyre (Reinhard Hoppenheit *et al.*, 1996). The air cavity of a pneumatic tyre is replaced by a layer of elastomer surrounded by different types of reinforcements. There are four components that make up the primary assembly of the tyre. A high viscosity hard rubber forms the bottom layer, which is adjacent to the rim. It is surrounded by a reinforcement layer which is wound overlay with cords, cables and wires. The cords are made of stainless steel, natural or synthetic fibres. The tread forms the final and the biggest component of the tyre. The tyre’s excess mass is due its high tread content. A highly wear resistant tread material is chosen owing to its operation in extreme environments.

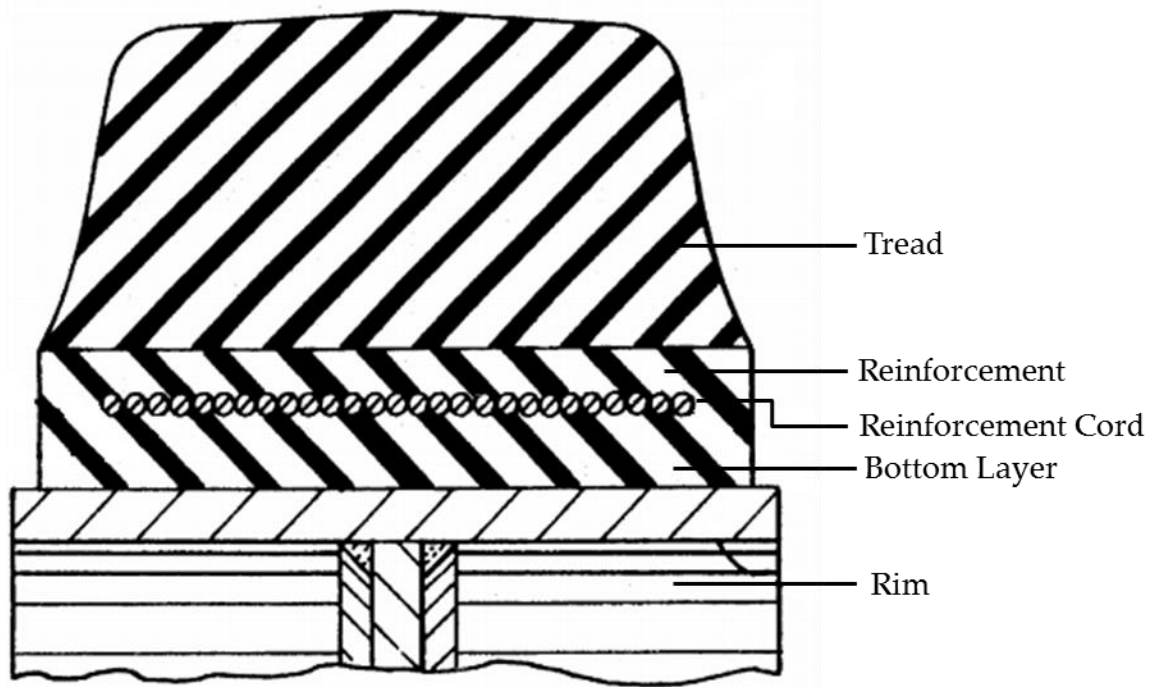


Figure 2.2: Embodiment of a solid tyre (Source: Reinhard Hoppenheit *et al.*, 1996)

From the purview of a passenger car's requirements, solid tyres do not satisfy the necessary performance criteria. The weight affects the fuel efficiency, longitudinal and lateral performance of the tyre. The excessive stiffness affects the ride quality. It does not satisfy the handling, performance or comfort characteristics which make up three of the four primary characteristics of a pneumatic tyre. Thus, a structure needs to be conceived which carries the required load, generates the required traction and handling forces and offers ride quality equivalent to those of a pneumatic tyre.

2.4 CELLULAR STRUCTURES

Cellular structures are preferred where there is a requirement for an entity to exhibit high strength yet offer low weight characteristics. Cellular structures are made up of interconnected networks of struts or columns arranged in either regular or in a random manner (Gibson *et al.*, 1997). A three dimensional (3D) cellular structure can be made of different polyhedral cells. A unit cell is the primary repeating entity of a cellular structure. The arrangements of these cells are important as they determine the behaviour of the structure. When the arrangement is regular, i.e. polyhedral cells are packed together to fill a volume, the solids are called as honeycombs and when it is random, they are known as foams. Depending on the kind of polygon used, different combinations of cellular solids can

be obtained. Hexagonal honeycombs are common examples of cellular solids in which a plane is packed with hexagons. The mechanical behaviour of cellular solids is predominantly a function of its constituent material and its geometric properties. The effect of the structure's geometric properties are given by its relative density (ρ^*/ρ_s). Relative density is defined as the ratio of the density of the cellular structure to the density of the constituent material from which the structure is made (Gibson *et al.*, 1997). In a broader sense, relative density indicates the volume of material used in making up the structure to the total amount of the material that can occupy the given volume. Greater the relative density of a structure, greater is the mass.

Manesh *et al.*, (2012) showed for the first time, the mechanism of carrying loads by a cellular structure. They designed a spoke with hexagonal honeycombs which was used in combination with shear beams to carry loads in tension. The structure comprised of web elements (individual entities that make up the cellular structures) of varying geometric properties which facilitated buckling above a critical load thereby ensuring that the loads are carried in tension rather than compression. The spoke structure was made of web elements of varying thickness in order to favour directional buckling. A cellular structure is required, which can exhibit low mass and adequate stiffness characteristics to replace the elastomeric portion of the solid tyre; yet perform the functions of inflation pressure in a pneumatic tyre.

2.5 TESSELLATIONS

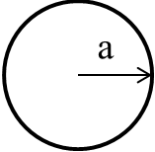
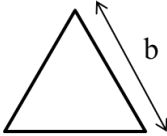
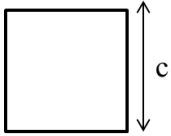
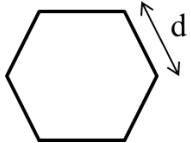
2.5.1 What are Tessellations?

Tessellation is the process of tiling different polygonal cells without any gaps or overlaps (Weisstein *et al.*, 2001). The repeating entity of a cellular structure is called as a 'unit cell'. A polygon forms the fundamental entity (the unit cell) of the structure. Depending on the nature of polygon used, tessellations are classified as regular or semi-regular tessellation. If a tessellation consists of polygons of same shape and size, then the tessellation is said to be a regular. When a group of polygons or similar polygons of varying sizes are combined to form a fundamental repeating unit, then they're called semi-regular tessellations. Tessellations are the basis for the design of cellular structures. The selection of a polygon for tessellating is dependent on (i) the quantity of material required for construction and (ii) its mechanical behaviour. In this section, a comparison is made between different tessellations to identify the one which not only is the most economical but offers the required in-plane behaviour.

2.5.2 Economics of Tessellations - Unit Cell Dependence

Tessellations are possible using different regular polygons. Tessellations are governed by topological laws. As mentioned previously, a group of interconnected columns combine to form a cell. The columns that make up an individual cell are termed as cell walls (Gibson *et al.*, 1997). The material required for the construction of a unit cell is dependent on the geometric properties of individual cell wall. When different polygons of same area are selected, the material requirement is dependent on the polygon with the least cell wall length. Since the cell wall length is equal to the perimeter of the polygon (for a unit cell), a shape is chosen with the least perimeter. It is observed from the Table 2.1 that, for different polygons of the same area, the increase in the number of sides of a polygon decreases the perimeter of the cell. Since a circle is assumed to be a polygon with infinite sides, it has the lowest perimeter, whereas the triangle with only 3 sides requires the maximum amount of material. Apart from the perimeter of the unit cell, the amount of material required to construct a tessellated structure is also dependent on how a polygon can be arranged with other similar or dissimilar polygons.

Table 2.1: Perimeter variations for polygons of same area

Polygon \ Property	Circle (a)	Triangle (b)	Square (c)	Hexagon (d)
Shape				
Area	$A = \pi a^2$	$A = \frac{\sqrt{3}}{4} b^2$	$A = c^2$	$A = 3 \frac{\sqrt{3}}{2} d^2$
Perimeter	$P = 2.32a$	$P = 3a$	$P = 2.632 a$	$P = 2.45a$

2.5.3 Economics of Tessellations - Unit Cell Grouping

Unit cells of same or different polygons combine together to form a cellular structure. For regular tessellations, individual polygons are arranged in such a manner that there are no gaps or overlaps in the structure. A gap or overlap indicates that additional material is required in tessellating the structure. All cellular structures can be characterised by its face (F_c), edge (E_c), vertex (V_c) and cell (C) information. These components of the cell are highlighted in Figure 2.3. For a regularly tessellated pattern to exist, the sum of the internal angles of all the edges joining at a vertex must be 360 degrees. If the sum exceeds 360 degrees, there will be an overlap and when the sum is lesser than 360, an opening is formed (Harris, 2000).

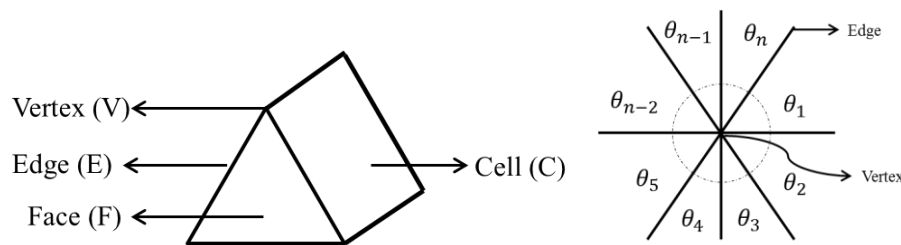


Figure 2.3: Unit cell characterisation and illustration of Euler's law

The concept of regular tessellations can also be shown through Euler's law (Gibson *et al.* 1997) which connects the face (F), cell (C), edges (E) and vertices (V) of an aggregate of cells by stating that

$$F - E + V = 1 \text{ (2D Cells)}$$

$$-C + F - E + V = 1 \text{ (3D Cells)}$$

In the above formula, the edges represent the number of 'shared' edges with similar polygons. The number of cell walls shared by a polygon determines the material required by the structure. It has been shown that, when tessellating polygons, only triangles, squares and hexagons can be arranged in a regular fashion without violating the Euler's law i.e. only the aforementioned polygons can be used to make a regularly tessellated pattern. When two cells

share a cell wall, only half of the original material is required to construct that particular cell wall. Triangles, squares and hexagons can share all of their cell walls, which results in a 50% drop in the material requirement. A polygon which shares half the total number of sides saves 25% on the material required for construction and so on. Polygons like pentagon require additional material to fill the openings as a result of unshared walls. The hatched region, as seen in Figure 2.4, for circular and pentagonal tessellated structure shows the inability of the structure to form regular tessellation thus leading to gaps in the structure. The hatched region in this model indicates that additional material is required to fill the plane. A circle is treated as a polygon with infinite sides and thus circular honeycombs do not share even a single cell wall and are considered to be the least economical shape for tessellation. On the other hand, hexagonal honeycombs have been found to possess the lowest material requirement of the 3 regular honeycombs (Gibson *et al.*, 1997). Apart from the economic consequence of tessellations, it is imperative to observe the mechanical properties of these honeycombs.

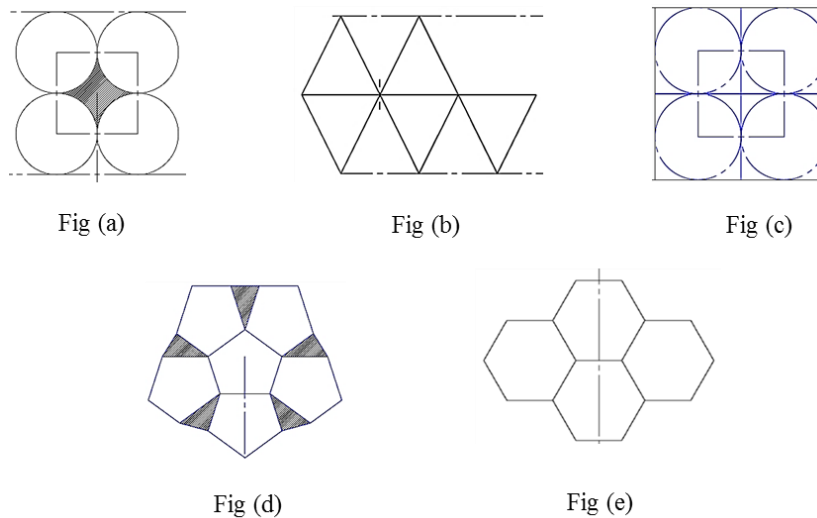


Figure 2.4: Tessellation of different polygons. (a) Circle (b) Triangle (c) Square (d) Pentagon (e) Hexagon (The hatched area indicates that additional material is required for filling the opening)

2.5.4 Mechanical Properties of Regular Honeycombs

Wang *et al.* (2004) investigated the in-plane behaviour of various periodic honeycombs and developed analytical models for these structures by treating the individual cell walls as beam elements. Simple beam theory was used to derive the mechanical properties of honeycombs.

Figure 2.5 shows the variation in the in-plane modulus of various honeycombs with increasing relative density. A triangular honeycomb behaves like a truss and hence it does not accommodate any deflection. The structure is rigid in nature. From the perspective of tyres, this behaviour translates to poor ride quality and hence it is unsuitable for tyres. A square honeycomb exhibits a similar behaviour when its orthogonal sides are oriented parallel to the two principal directions. When loaded along these directions, the cell walls are subjected to axial compression until elastic buckling of the cell walls take place. It has been observed that when the structure is loaded diagonally i.e. when the structure is rotated by 45 degrees and loaded along the two principal directions, the structure becomes compliant as bending becomes the primary mode of deformation. As in the case of axially loaded square honeycombs, hexagonal honeycombs too carry loads due to their cell wall's bending resistance. Wang *et al.* (2004) showed that square honeycombs have the highest in-plane moduli in the two principal directions and hexagonal honeycombs, the lowest. Additionally, the designed tyre behaves like a bottom loader and hence a structure with high circumferential stiffness is required. Circumferential stiffness is the resistance offered by the structure when subjected to a torsional load. In the following chapter, the effect of inadequate radial and circumferential stiffness in a tyre has been highlighted.

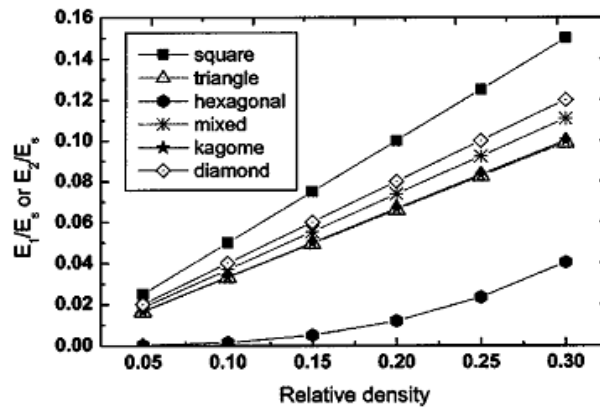


Figure 2.5: Normalised in-plane modulus for various polygonal structures (Wang *et al.*, 2004)

2.6 UNIT CELL PARAMETERS AND ITS EFFECT ON ITS IN-PLANE PROPERTIES

The overall behaviour of a tessellated structure can be discretized to the behaviour of individual web element in the structure. The geometric properties of these individual web elements govern the mechanics of deformation in the structure. Predominantly all of the available research has been undertaken with the assumption that the honeycombs are planar in nature. This has been used to derive the in-plane stiffness in the 2 principal directions. Since the tyre is required to offer sufficiently high stiffness in the circumferential direction, a square honeycomb was chosen over triangular and hexagonal geometries. The effect of geometric parameters on the in-plane moduli is highlighted in this section.

2.6.1 Unit Cell

The unit cell is the fundamental repeating entity of a regular tessellation. The unit cell and its geometric parameters are labelled in Figure 2.6. Relative density of a cellular structure is conventionally used as an indicator to quantify their mechanical behaviour. Relative densities of honeycombs are a function of the cell wall thickness and cell wall length. Figure 2.7 shows the loading mechanism of the individual cell wall. The cell walls are treated as cantilever beams and the mechanism of loading is shown in Figure 2.7. A reaction force is developed which is due to the bending stiffness offered by the cell wall. The compliance in the structure is due to the rotation of the hinge (point at which cell walls meet). The relative density $\left(\frac{\rho^*}{\rho_s}\right)$ of the structure is given by

$$\frac{\rho^*}{\rho_s} = 2 \frac{t}{l} \left(1 - \frac{1}{2} \frac{t}{l}\right)$$

where t is the cell wall thickness and l is the length of the cell wall. The Young's modulus in the loading direction is given by

$$E_{45}^* = E_s * 2 \left(\frac{t}{l}\right)^3$$

Where E_s is the Young's modulus of the constituent material.

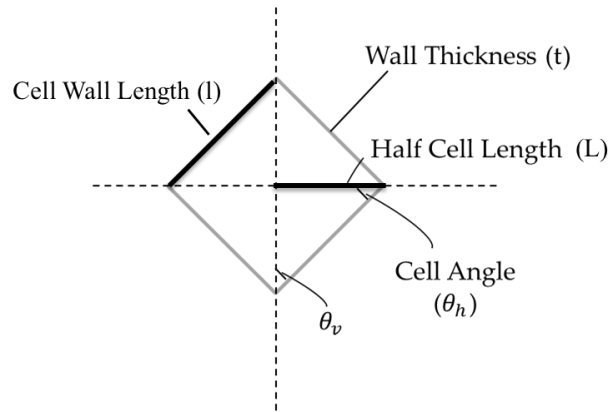


Figure 2.6: Components of a unit cell

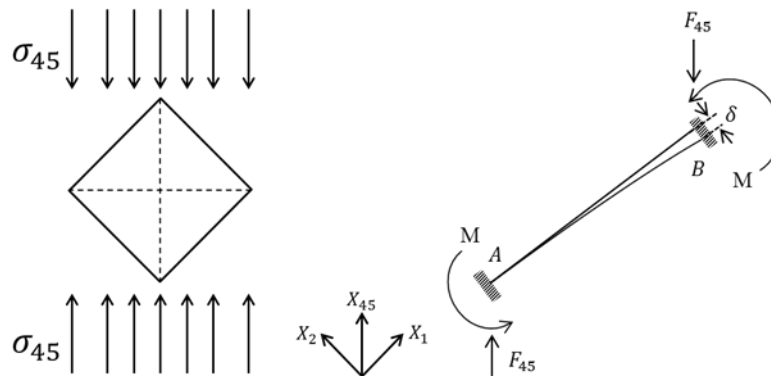


Figure 2.7: Unit cell loading and mechanics of cell wall deformation (Source: Wang et al., 2004)

2.6.2 Mechanics of Cell Wall deformation

The mechanics of cell wall deformation for a hexagonal honeycomb was analytically modelled by Gibson *et al.* (1981). They analysed the in-plane mechanical properties of a three-connected cellular structure (as each vertex accommodates three edges in a hexagonal tessellation). Figure 2.8 shows the stress-strain behaviour of honeycomb structures. It can be observed that there are 3 distinct behavioural regions in the plot. The initial linear-elastic region where the deformations are recoverable, the intermediate plateau region where buckling of cell wall takes place and finally the densification of the collapsed cell walls which causes a sharp rise in the stiffness. The length of the intermediate plateau region is a function of its relative density. Conventionally, tyres are subjected to high impact loads when

encountering an obstacle, and thus buckling of the spoke is inevitable. Thus structures with low relative densities result in large strains, which is undesirable in a tyre especially when operating at high speeds. Increasing the relative density of the cell reduces this plateau region thereby resulting in small strains in the structure even after the loads have crossed the critical buckling load. Wang *et al.* (2004) showed that, for square honeycombs with a $\frac{t}{l}$ ratio greater than 0.2, buckling is not a mode of failure as the cell walls can be treated as short columns. A tyre structure with inadequate relative density is susceptible to large geometry change when it encounters an obstacle and this can have adverse effects on the vehicle's handling characteristics when operating at high speeds. By designing a structure with its relative density greater than the aforementioned critical value, it can be ensured that the tyre does not buckle and has a small intermediate plateau region.

Wang *et al.* (2004) analysed the mechanical properties of square honeycombs with its cell walls inclined 45 degrees to the principal directions. The inclined cell walls are modelled as beams which are subjected to axial, shear and bending loads. Depending on the end connectivity of a cell wall, each cell wall can be modelled as a beam with appropriate boundary condition. In the case of rhombi tessellated structure, each cell wall is modelled as a cantilever with a fixed-free boundary condition. When subjected to σ_{45} as shown in the Figure 2.7, the force F_{45} and a bending moment M act on the beam. Due to the virtue of its loading, the force F_{45} is equilibrated. The moment M causes a deflection δ . The difference between the hexagonal and rhombi honeycombs lies in the calculation of their critical buckling load. Like any other columnar structure, the cell walls are also subjected to buckling. Euler's buckling theory can be applied to predict the critical buckling loads of the cell walls. The critical buckling load is given by

$$P_{cr} = \frac{n^2 \pi^2 EI}{l^2}$$

where 'E' is the Young's modulus of the material used, 'n' is the effective length factor and 'l' is the length of the column. 'I' is the moment of inertia of the column and it is given by $I = \frac{bt^3}{12}$, where 'b' is the breadth of the beam and 't', the thickness. The effective length factor 'n' is a function of the column's end boundary condition. Depending on the boundary condition, the value of 'n' lies between $0.5 \leq n \leq 2$. In the case of rhombi tessellated structures, a fixed-free boundary condition is imposed and hence the value of 'n' is assigned

to be 1. For hexagonal tessellated structures, rotation is permitted at the ends, indicating a pinned joint and hence a value of 0.5 is chosen.

All the previously mentioned design criteria have been chosen based only on the vertical stiffness that a structure offers. A rolling tyre is generally subjected to vertical loads due to its sprung mass and a tangential force created due to the friction that exists between the tyre and the road. A pneumatic tyre is a continuous toroidal structure in which inflation pressure is responsible for its stiffness. But in the case of a NPT, the structure suffers deformation in both vertical and longitudinal direction. Hence care is to be taken so as to ensure that the NPT does not deform in both radial and circumferential direction.

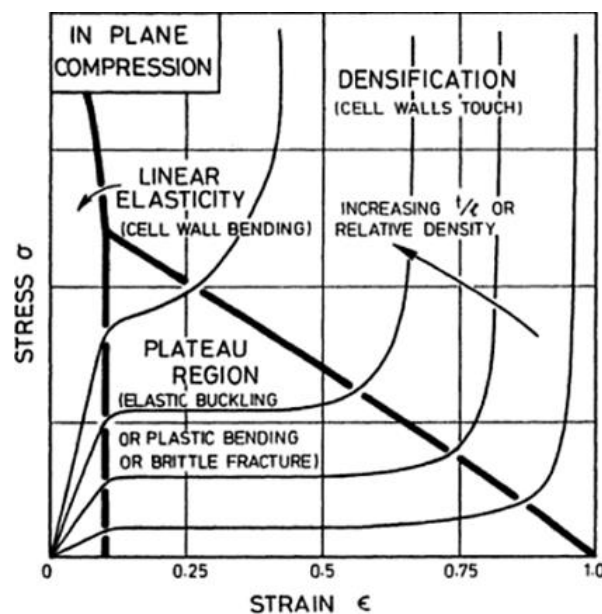


Figure 2.8: Stress-Strain curve of hexagonal honeycombs (Gibson *et al.*, 1982)

2.7 SUMMARY

The concept of cellular structures has been introduced in this chapter. It is shown that, for designing the flexible spoke, the structure should exhibit low vertical stiffness and high circumferential stiffness. Literature has established that a square honeycomb exhibits the maximum stiffness in both the direction, and thus it was chosen as the basis for the flexible spoke design. Apart from this, to ensure that the structure does not buckle, a relative density greater than 0.2 has been fixed as a design criteria. This ensures that the buckling would not

be a mode of failure in the structure and the intermediate plateau region is maintained as small as possible, thereby ensuring that the strains in the structure are low when the load crosses the critical buckling load.

With the available design rules, an annular rhombi tessellated structure is conceived. The design of the spoke is based on the stiffness offered by the structure in the two directions. The following chapter discusses in detail, the effect of geometric properties on the in-plane behaviour of these structures.

CHAPTER 3

DESIGN, ASSEMBLY AND FINITE ELEMENT MODEL OF A NON-PNEUMATIC TYRE

3.1 INTRODUCTION

Apart from characterizing the mechanical properties of cellular structures based on the preliminary understanding of the economics and in-plane behaviour, a study needs to be performed to understand the effect of geometric parameters on the overall behaviour of the structure. An annular model of the structure is created. A three dimensional (3D) FE model of the Non-Pneumatic Tyre (NPT) is developed with the required material properties assigned to it. A static analysis is conducted to simulate the load carrying behaviour, the vertical stiffness offered and the development of the contact patch. The evaluation of the model's design is further extended by comparing its Force and Moment (F&M) characteristics with respect to the pneumatic tyre's data.

3.2 FINITE ELEMENT MODEL OF A PNEUMATIC TYRE

An axisymmetric FE model of the of a 165/70R14 pneumatic tyre is shown in the Figure 3.1. Various materials that make up the 2D section of the tyre are tabulated in Table 3.1. The elastomeric behaviour of different rubber components are modelled using Yeoh hyperelastic model (SIMULIA/Abaqus, 2014). The material constants for the various elastomeric components of the tyre are shown in Table 3.1. The material constants for the elastomers are obtained from 100% uniaxial tension tests. 4-noded axisymmetric elements make up the elastomeric portion of the tyre whereas the reinforcements are modelled using surface elements. The model consists of two belts and its reinforcement material properties are provided in Table 3.2 and Table 3.3. The material properties for different elastomeric components of the tyre (Table 3.1 – 3.3) are from the work done by Vijay A. Alagappan (2014). The tyre is subjected to an inflation pressure of 220 kPa. The road and the rim are modelled as analytical rigid surfaces. All the numerical experiments performed on the tyre are for a rated load of 3000 N and a coefficient of friction value of 0.7 is assigned between the tyre and the road. A smooth tread profile is considered which is consistent with the

designed NPT's tread profile in order to minimize variability when comparing the performance of the two tyres.

The procedure to simulate the static behaviour is well documented (SIMULIA/Abaqus 2014). Narasimha Rao *et al.* (2006) established a steady-state method to extract the F&M data of a pneumatic tyre. A static loading operation is conducted to obtain the vertical stiffness of the tyre and the subsequent contact pressure distribution. Steady-state acceleration and cornering simulations are conducted for the aforementioned rated loading conditions in order to obtain the traction force, cornering force and self-aligning torque (SAT) magnitudes. A SAE superseded tyre axis system is considered while designing the pneumatic tyre. It is similar to the conventional SAE tyre axis system, barring the direction of the z-axis, which is pointed downwards unlike the conventional system. The force and moments acting in their respective axes is provided in Figure 3.2.

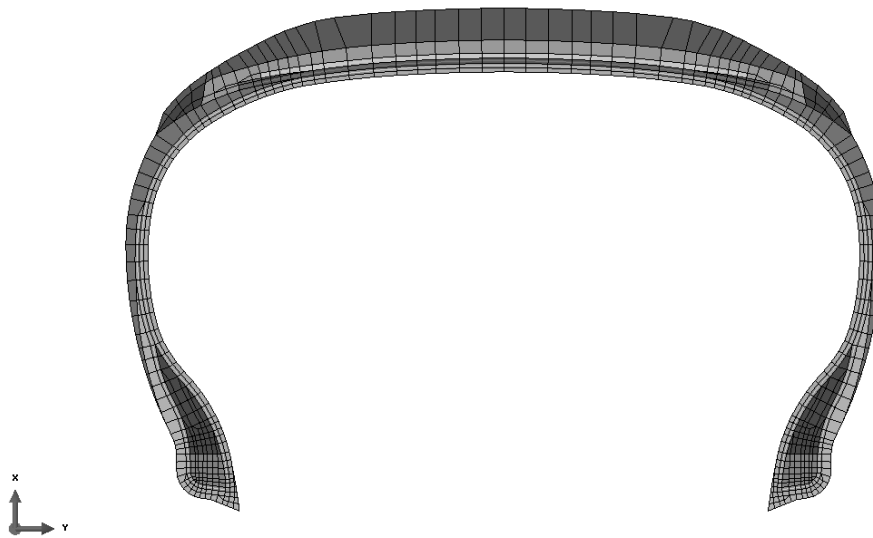


Figure 3.1: 2D axisymmetric FE model of a 165/70R14 tyre

Table 3.1: Reinforcement Material Properties

Tyre Component	Density (kg/m^3)	Young's Modulus (N/m^2)	Poisson's Ratio
Bead	7430	206.39E+09	0.30
Membrane Ply	1050	4.71E+09	0.49
Belt 1	7485	140.76E+09	0.30
Belt 2	7485	140.76E+09	0.30

Table 3.2: Properties of different reinforcements

Tyre Component	Reinforcement cross-sectional area (m^2)	Reinforcement Spacing (m)	Orientation of reinforcement (deg)
Membrane Ply	3.5256E-07	8.686E-04	0.724
Belt 1	2.1205E-07	1.647E-03	59.74
Belt 2	2.1205E-07	1.647E-03	-59.32

Table 3.3: Hyperelastic material coefficients for different regions in the tyre

Tyre Component	Density (kg/m^3)	C_{10} (N/m^2)	C_{20} (N/m^2)	C_{30} (N/m^2)
Belt 1	1177	8.96732E+05	-2.80203E+05	0.78807E+05
Belt 2	1177	8.96732E+05	-2.80203E+05	0.78807E+05
Belt Edge Gum	1100	12.19269E+05	-4.85253E+05	1.96638E+05
Filler	1182	8.76048E+05	-2.93303E+05	0.79358E+05
Inner Liner	1177	3.14469E+05	-1.10385E+05	0.26544E+05
Ply	1177	3.72454E+05	-0.96940E+05	0.24338E+05
Rim Strip	1100	11.33636E+05	-4.43953E+05	1.18934E+05
Sidewall	1100	4.87666E+05	-1.41342E+05	0.38610E+05
Tread cap	1100	6.16046E+05	-1.90709E+05	0.47504E+05
Wing Tip	1100	6.16046E+05	-1.90709E+05	0.47504E+05
Tread	1100	6.16046E+05	-1.90709E+05	0.47504E+05

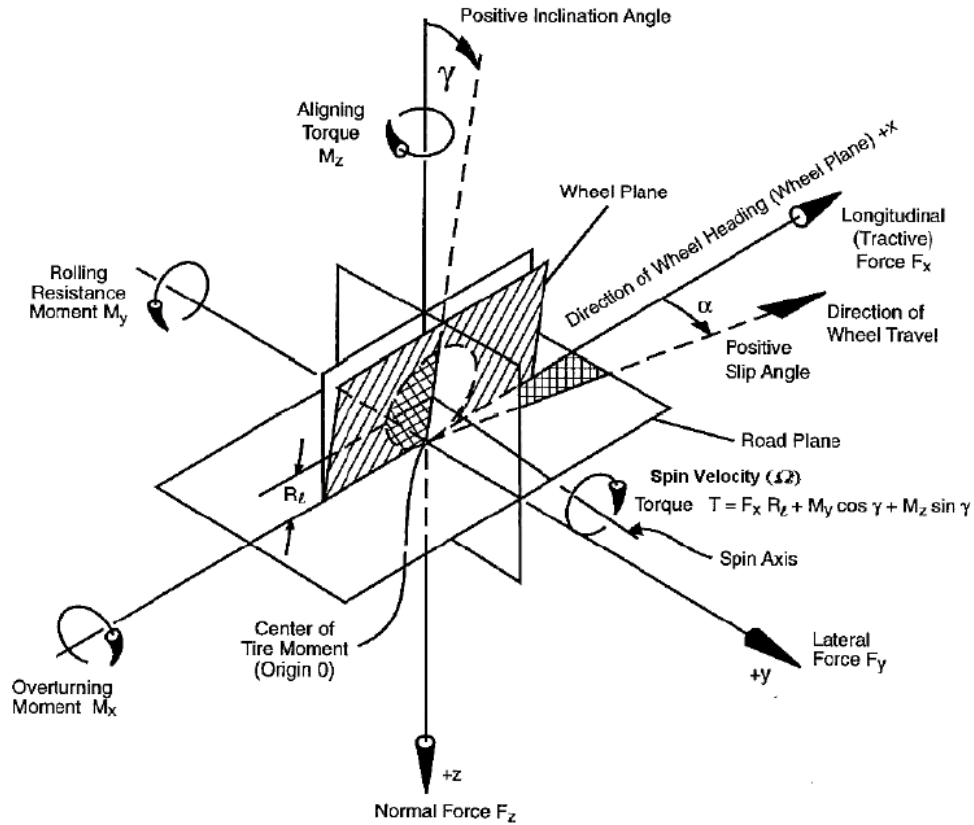


Figure 3.2: SAE superseded tyre axis system. (Source: Milliken and Milliken, 1995)

3.3 FE PROCEDURE FOR CHARACTERIZING PNEUMATIC TYRE'S PERFORMANCE

3.3.1 Inflation and Loading

Procedures to simulate the inflation and loading phenomenon in a pneumatic tyre are well established. The axisymmetric FE model, shown in Figure 3.1 is subjected to an inflation pressure. The results from the 2D inflation analysis are transferred to the 3D revolved model by making use of the software's symmetric result transfer facility and brought to equilibrium. The effect of inflation pressure on the tyre's structure can be visualized.

To perform the loading simulation, a displacement-based boundary condition is initially provided to the road and a frictionless contact is established between the road and the tyre. In the following step, depending on the required normal load, a load-based boundary condition is applied. The effect of inflation and loading combined with the foot print obtained can be visualized through these simulations.

3.3.2 Steady State Rolling

A steady state rolling simulation is conducted to extract the longitudinal and lateral forces produced by the tyre when subjected to rolling. Unlike implicit dynamic rolling simulations, this method has lower computational requirements (SIMULIA/Abaqus 2014). Apart from this, the results obtained from the implicit dynamic simulations are noisy and must be filtered in order to obtain meaningful results (Narasimha Rao *et al.*, 2004). Abaqus's steady state transport facility is used and this feature models the problem using an Arbitrary Lagrangian Eulerian (ALE) formulation where the deformations are modelled in a Lagrangian manner whereas rigid body motions are modelled in an Eulerian manner. In the first step, the required coefficient of friction is assigned between the road and the tyre. The value is increased in steps, from 0 to the required amount and the solution is brought to equilibrium. This is done to overcome convergence constraints when trying to achieve a steady state solution. A translational velocity is assigned to the tyre-rim assembly and based on the loaded radius of the tyre, a range of angular velocities are assigned to the tyre-rim assembly. For a constant load and translational velocity, there exists a condition where the tyre rolls without any torque acting at the axle of the tyre. This velocity is called as the Free Rolling (FR) velocity. The longitudinal force generated by the tyre at this velocity is zero, indicating that the tyre is neither accelerating nor braking. The tyre is said to be accelerating if its angular velocity is above the FR velocity and braking when vice versa. The longitudinal force generated is a non-linear function of the slip ratio. Slip ratio κ is defined below:

$$\kappa = \frac{\omega - \omega_0}{\omega_0}$$

where ω is the angular velocity of the tire and ω_0 is its FR velocity. For a steady state straight line rolling simulation, the slip angle (α) is considered to be 0. The angle between the tire's longitudinal plane and its heading direction is called slip angle. A tire corners with a non-zero slip angle. Slip angle (α) is given as

$$\alpha = \tan^{-1} \frac{V_y}{V_x}$$

where V_x is the longitudinal velocity and V_y is the lateral velocity of the tyre. The tyre is brought to a FR condition in first step and subsequently, lateral and longitudinal velocities are assigned depending on the required slip angle till which the simulation is to be carried out. The magnitude of lateral force and the SAT generated with varying slip angles are extracted

from this simulation. The longitudinal force, lateral force and SAT combined together to form the Force and Moment (F&M) characteristics of a tyre.

The method to record the static behaviour for the designed NPT is explained in the following section, whereas the F&M characteristics of the NPT can be extracted in a similar method as prescribed above.

3.4 NPT DESIGN

The challenge in the design of an NPT lies in conceiving the load-bearing component of the tyre. The consequence of replacing the inflation pressure is that, the designed structure should be capable of providing the required stiffness in all the 3 principal directions. The preliminary design of the spoke is based on the stiffness offered by the structure in the vertical and the circumferential direction i.e. torsional stiffness. During straight line rolling, a tyre is subjected to both vertical loads, due to the sprung mass and torsional loads, due to the traction force developed between the tyre and the road. Thus, a tyre structure is preferred which offers the required stiffness in the two directions. In this work, circumferential stiffness is considered to be the governing design parameter, followed by the vertical stiffness and finally the lateral stiffness.

3.4.1 NPT - FE Model

Exploiting the NPT geometry's circular symmetry is the key to modelling an annular honeycomb. A unit sector is the fundamental repeating entity in an annular tessellated structure. The 3D model of the unit sector and its lateral section is shown in Figure 3.3. The assembly of the various components of the NPT is based on the work done by Kim *et al.* (2013). The designed NPT consists of 5 components. The layer adjacent to the rim is the inner beam. Two stainless steel rings, namely inner and outer rings are embedded in the assembly. These rings are used to render structural rigidity to the model. Sandwiched between the inner and the outer ring, is the load carrying component of the tyre, a flexible spoke. The outermost layer, which comes in contact with the road, is the tread. The following assumptions are made while designing the current model. (i) The rim and the road are modelled as analytical rigid bodies. (ii) The adhesion properties between different surfaces have not been defined. The nodes of the innermost layer of the tyre are tied to the rim. To simulate the tyre's elastomeric behaviour, Yeoh model has been defined and its strain energy density is written as (SIMULIA/Abaqus, 2014)

$$\psi = \sum_{i=1}^3 C_{i0} (I_1 - 3)^i + \sum_{i=1}^3 \frac{1}{D_i} (J^{el} - 1)^{2i}$$

where I_1 is the first invariant of the deviatoric left Cauchy-Green tensor \mathbf{B} and J^{el} is the volumetric ratio. The values of the coefficients are provided in Table 3.4. Hybrid continuum elements (C3D8H) are assigned to mimic the behaviour of the elastomeric components whereas C3D8 elements are assigned for the steel rings.

3.4.2 Unit Sector

As stated previously, only a unit sector is to be designed whereas the rest of the model can be generated using the Abaqus's symmetric model generation capability. The sector dimensions are based on its unit cell parameters. Three parameters have been considered in the design of the flexible spoke. The parameters are (i) Half Cell Angle (HCA) (ii) Half Cell Length (HCL) and (iii) Cell Wall Thickness (CWT). A radially varying cell geometry is considered i.e. the size of the cell increase as we progress in a radially outward direction. A parametric study is performed based on the unit cell properties to highlight the variation in the radial stiffness and circumferential stiffness. A complete annular model is generated by repeating the sector multiple times. The number of the sectors required to complete the model is a function of the sector angle. The sector angle is dependent on the size of the unit cell. An illustration of the complete model of the tyre is shown in Figure 3.4.

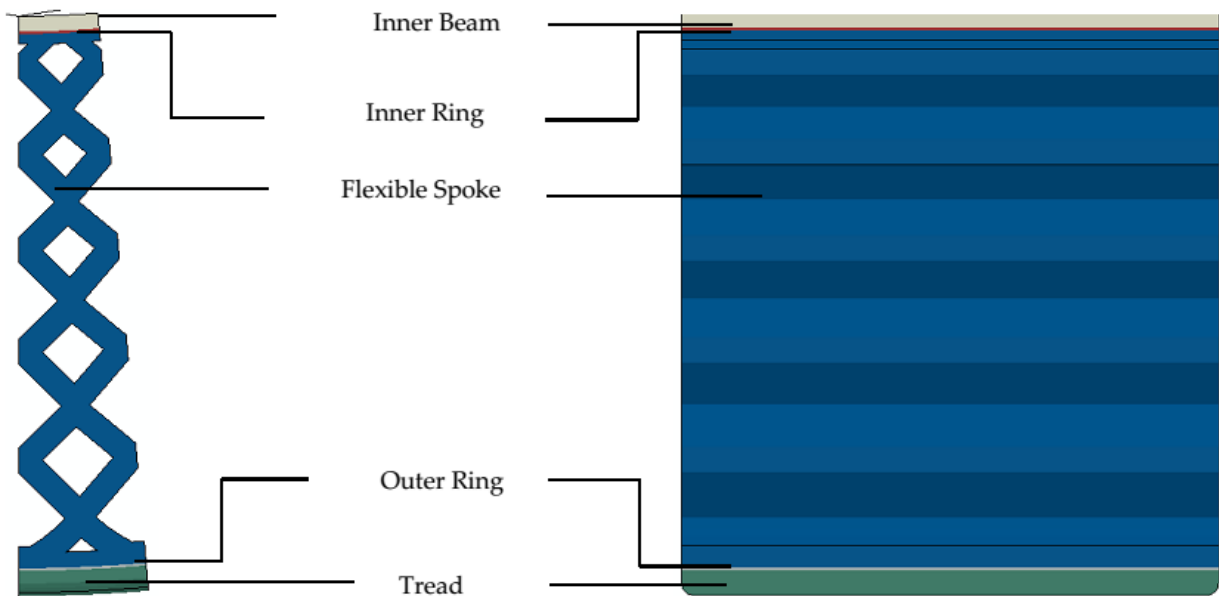
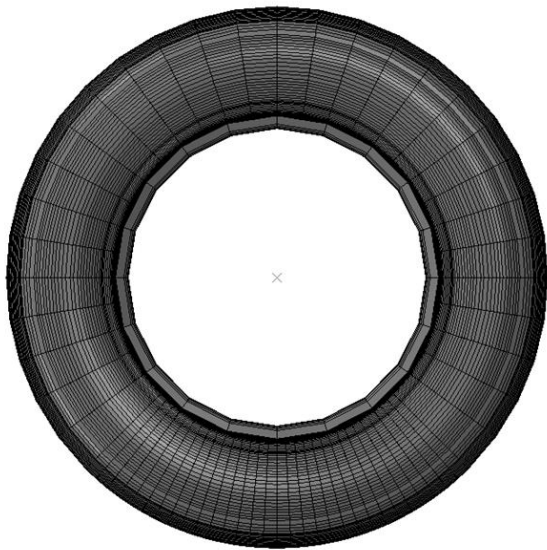


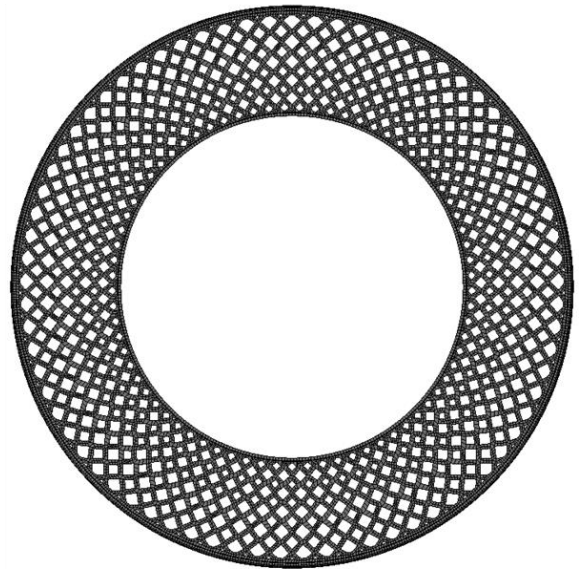
Figure 3.3: Unit sector of the designed NPT

Table 3.4: NPT material composition (Rao *et al.*, 2006)

Component	Density (kg/m^3)	Material		
		Hyperelastic - Reduced Polynomial Form - $n=3$		
		C_{10} (N/m^2)	C_{20} (N/m^2)	C_{30} (N/m^2)
Inner Beam	1204	1.04 E+06	-0.39 E+06	0.13 E+06
Spoke				
Tread	1170	0.77 E+06	-0.27 E+06	0.09 E+06
Linear Elastic				
	Density (kg/m^3)	Young's Modulus (N/m^2)		Poisson's Ratio
Inner Ring	8193	221 E+09		0.3
Outer Ring				



165/70R14 Pneumatic Tyre



Steel Ringed Non-Pneumatic Tyre

Figure 3.4: Complete revolved model of the tyres

3.5 FLEXIBLE SPOKE DESIGN - PARAMETRIC ANALYSIS

The in-plane mechanical properties of the spoke are a function of the relative density and hence the spoke configuration has to be selected based on the stiffness offered by the structure in the radial and circumferential direction. Improper design of spoke may cause the structure to buckle radially thereby rendering the structure unusable. Thus a configuration that is selected which does not buckle offers the lowest vertical stiffness. Inadequacy of stiffness in the circumferential direction may cause contortion of the spoke and hence a structure with high circumferential stiffness is preferred. A FE experiment is conducted to record the stiffness offered by the structure when it is subjected to both vertical and shear loading. The simulation is conducted for a range of unit cell parameters and variations in the structure's configuration with varying unit cell parameters. The HCAs are varied from 25 degrees to 65 degrees. The HCLs are varied from 5 mm to 10 mm whereas the CWT is varied from 3 mm to 7 mm. The variation in the spoke geometry due to the change in the unit cell parameters are shown in Figures 3.5, 3.6 and 3.7.

3.5.1. Radial Stiffness

The procedure for determining the radial stiffness of the structure is explained below

- From the designed 'unit sector', the entire model is generated by taking advantage of the model's circular symmetry. SIMULIA/Abaqus's *SYMMETRIC MODEL GENERATION keyword is used to generate the complete model shown, as shown in the Figure 3.4.
- A 'fixed' boundary condition is imposed on the rim which eliminates all the 6 degrees of freedom of the tyre.
- The rigid road is displaced by 15 mm towards the centre of the tyre and the reaction force offered by the tyre is recorded.

3.5.2 Circumferential Stiffness

Continuing from the previous simulation, an analysis is performed to estimate the circumferential stiffness of the structure. The procedure for determining the circumferential stiffness is given below

- The vertical displacement-based boundary condition (BC) is maintained and a coefficient of friction of 1.0 is prescribed between the structure and the road surface.

- A rotational degree of freedom about the tyre's axis is allowed and the structure is rotated by 10 degrees.
- The resistive torque offered by the structure is recorded. The test is conducted to mimic the effect of rolling.

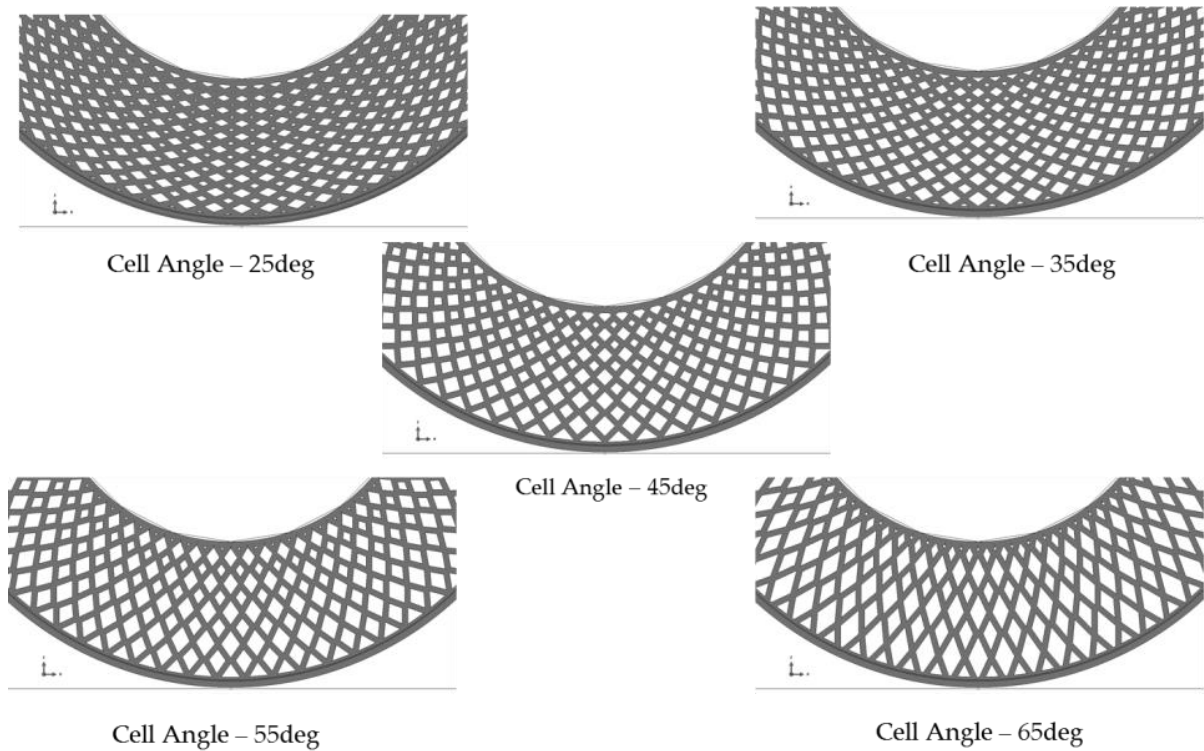


Figure 3.5: Variation in spoke configuration with Half Cell Angle (HCA)

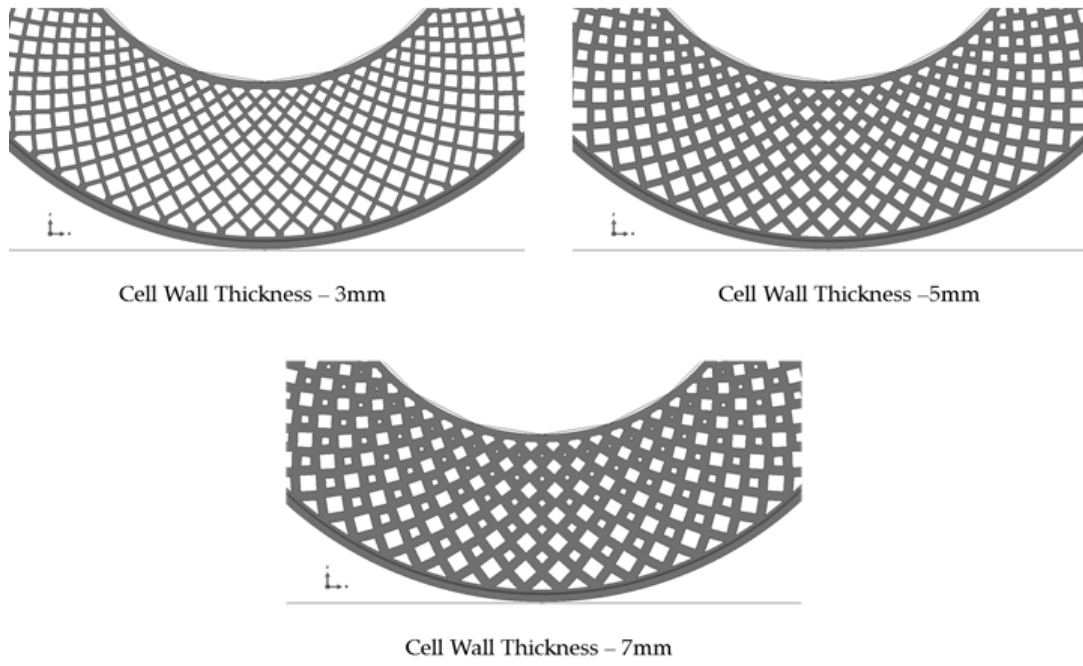


Figure 3.6: Variation in spoke configuration with Cell Wall Thickness (CWT)

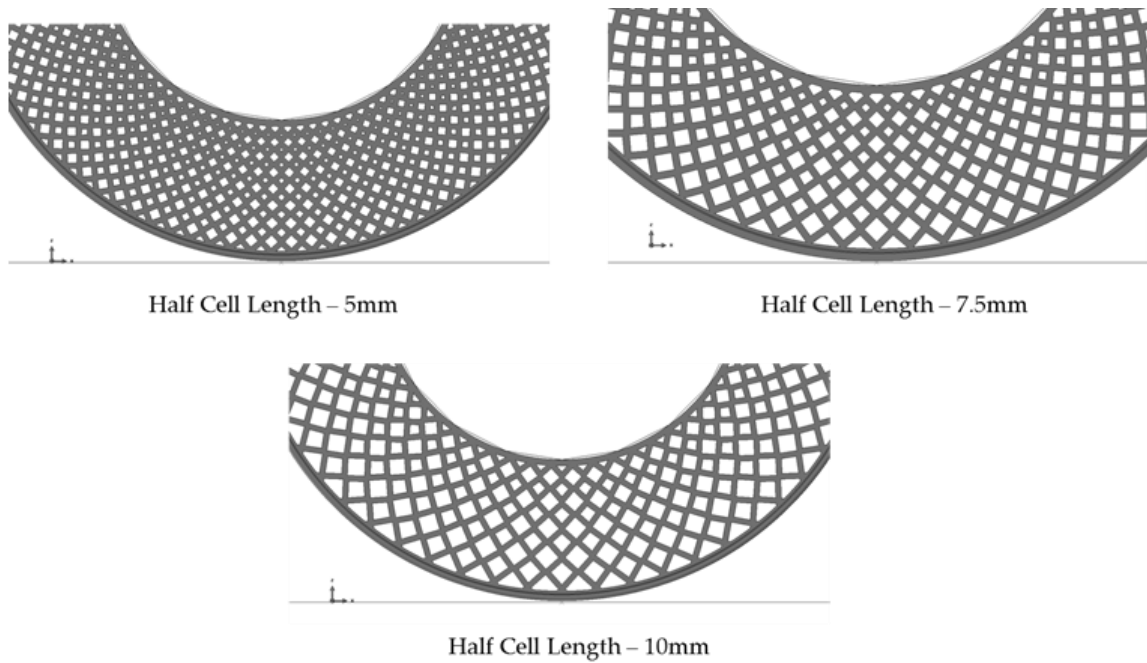


Figure 3.7: Variation in spoke configuration with Half Cell Length (HCL)

3.6 RESULTS AND DISCUSSION

The results from the parametric study are reported and its behaviour with respect to its geometric properties analysed. The preliminary design characteristics such as radial stiffness, contact pressure profile and stress distribution in the spoke for the three tyre models are highlighted. A procedure similar to that proposed by Rao *et al.* (2006) has been adopted for the NPT model to capture the process of tyre force generation and the F&M characteristics of the equivalent pneumatic tyre.

3.6.1 Radial Stiffness

The load-deflection curves for the range of HCAs, HCLs and CWTs are recorded and explained in the following section. The following observations can be made from the derived load-deflection curves

- Increase in the HCA decreases the relative density of the cell. The relative density is defined as the ratio of the density of the structure to the density of the structure's constituent material. The relative density of a rhombi tessellated structure is given by

$$r = \frac{\rho^*}{\rho_s} = 2 \frac{t}{l} \left(1 - \frac{1}{2} \frac{t}{l} \right)$$

where r is the relative density, ρ_s is the density of the material used, ρ^* is the density of the structure, t is the cell wall thickness and l is the length of the cell wall. Increase in the HCA increases the overall l of the structure. Relative density variation can also be characterised by the mass of the structure. Relative density is directly proportional to the mass of the structure. Increase in the HCA consequently decreases the mass of the structure, due to the drop in the structure's relative density and this is observed in Table 3.5.

- Table 3.5 also reveals that the stiffness of the structure is not necessarily proportional to the relative density of the structure. For higher values of θ_h , despite the lower values of relative density, the structure still manages to exhibit very high stiffness.

- There exists an angle θ_h for which the structure exhibits the lowest radial stiffness. This angle was found to be 45 degrees. Below this angle, the volume of material causes a rise in the stiffness. Above 45 degrees, increase in θ_h consequentially decreases θ_v . When F_{45} , (as observed in Figure 2.8), acts on a unit cell with very high θ_h , the cell walls begin to carry the loads by axial compression rather than bending, as conventionally observed, thereby exhibiting very high stiffness.

Similar tests are performed on these structures by varying the other two parameters; CWT and HCL. It can be intuitively understood that, as the cell wall thickness of the structure increases, consequently does the relative density and thus there is an increase in the radial stiffness as shown in Figure 3.9. Likewise from Figure 3.10, it observed that, as the HCL of the structure increases, the cell wall length increases, consequently increasing the void area in the cell, thereby lowering the relative density of the structure and thus compromising on the radial stiffness.

Table 3.5 - Radial stiffness with relative density

Cell Angle (deg)	Relative Density	Mass (kg)	Stiffness (kN/m)
25	0.93	17.90	221.42
35	0.96	16.60	186.78
45	0.99	14.50	171.20
55	0.97	13.80	203.35
65	0.66	13.25	221.64

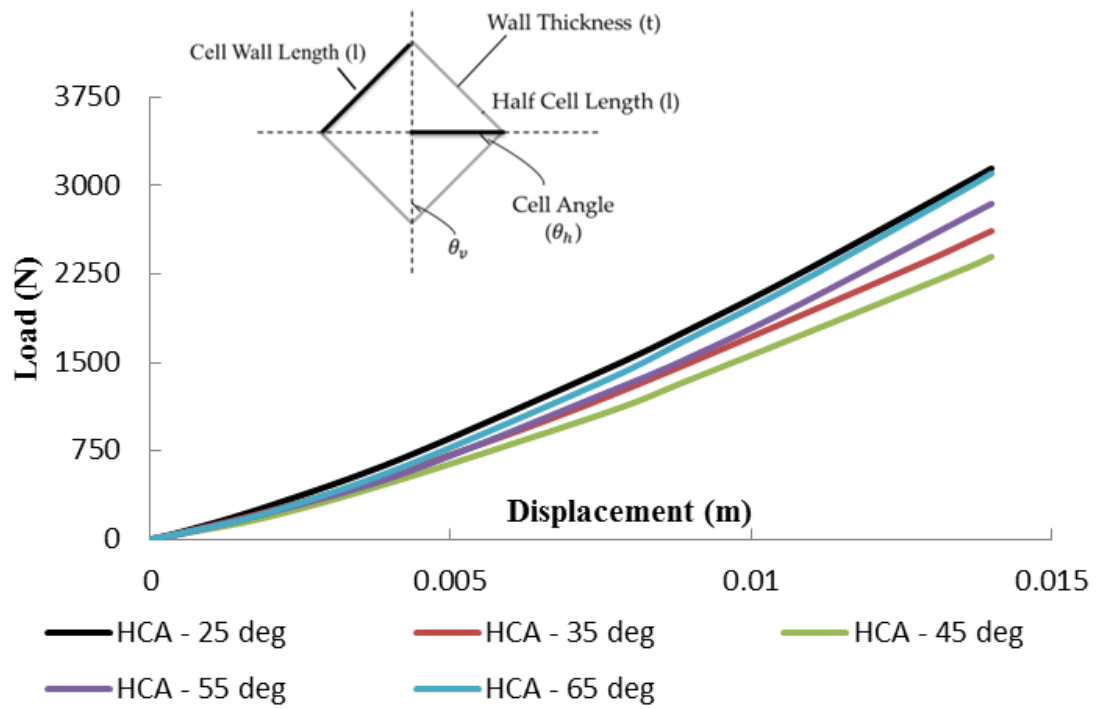


Figure 3.8: Half Cell Angle (HCA) and its effect on vertical stiffness

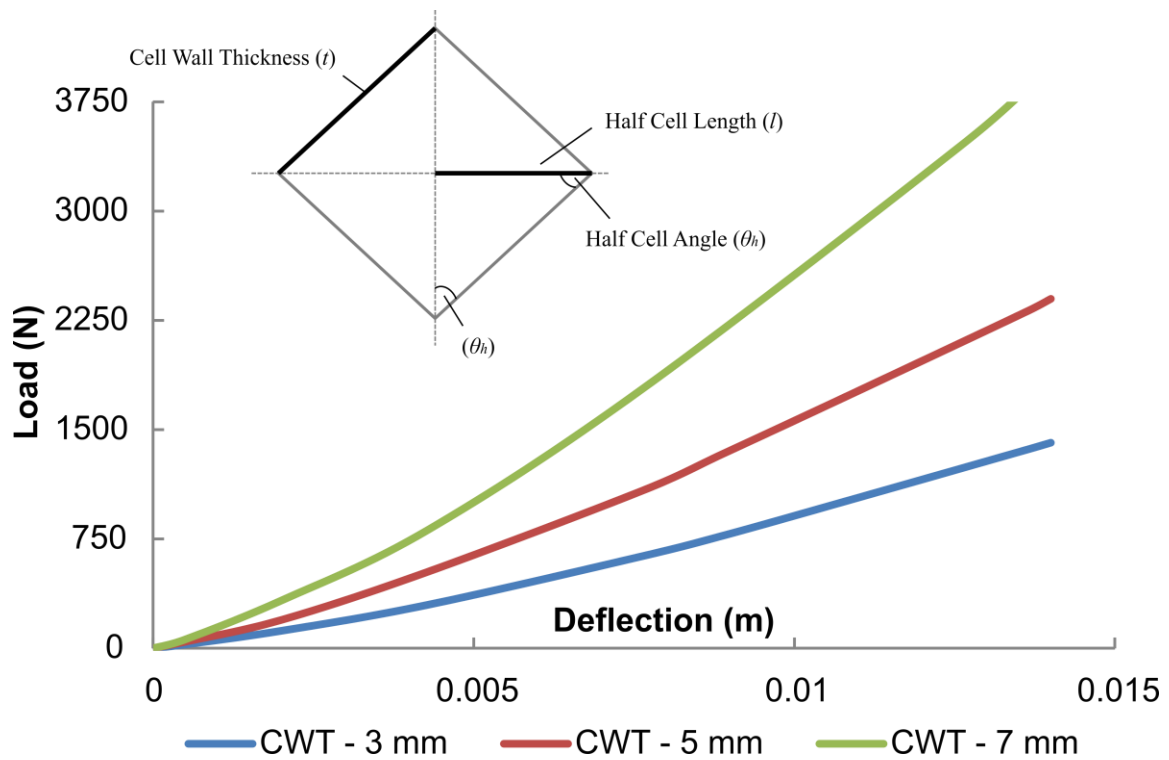


Figure 3.9: Cell Wall Thickness (CWT) and its effect on vertical stiffness

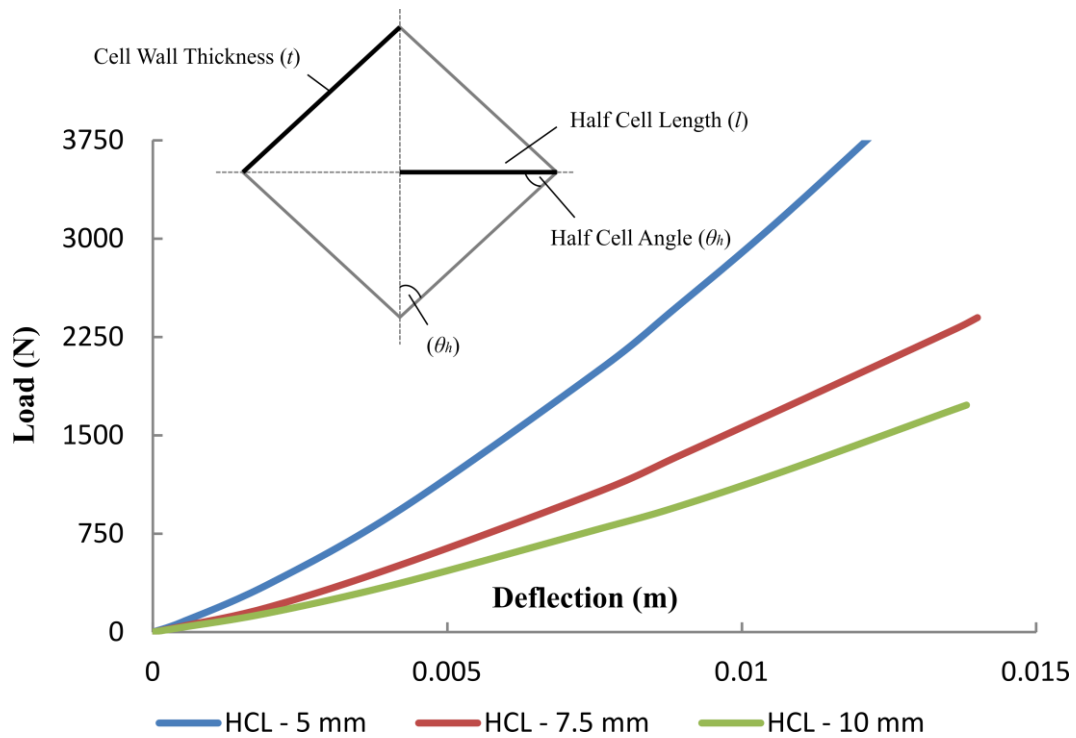


Figure 3.10: Half Cell Length (HCL) and its effect on vertical stiffness

3.6.2 Circumferential Stiffness

Wang *et al.* (2004) showed that the properties of planar honeycombs did not vary in the two principal directions due to the structure's geometric symmetry and this phenomenon is consistent in annular structures as well. The structure's circumferential stiffness with respect to the three unit cell parameters are shown in Figures 3.11, 3.12 and 3.13 respectively. The consequence of a structure having inadequate circumferential stiffness is shown in Figure 3.14. The final spoke configuration is based on the weight of the structure and the stiffness offered in the two principal directions for which the spoke does not contort when rolling.

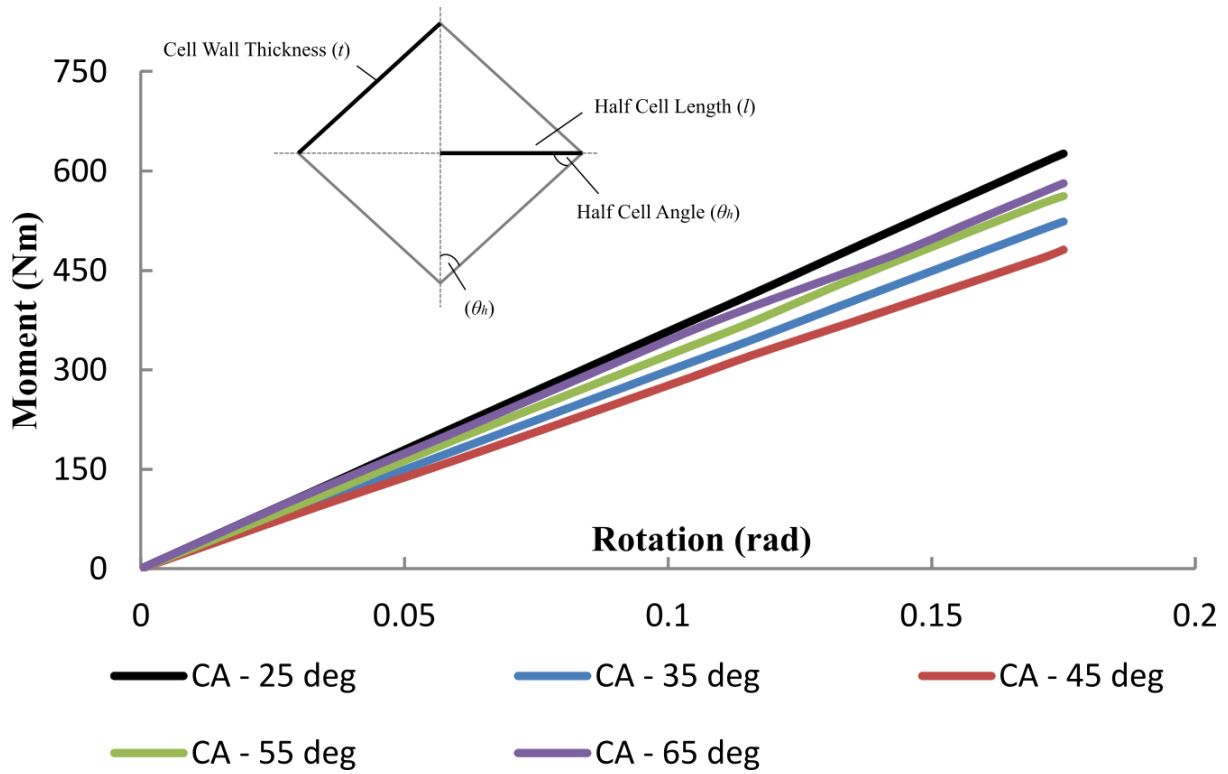


Figure 3.11: Cell Angle (CA) and its effect on the circumferential stiffness

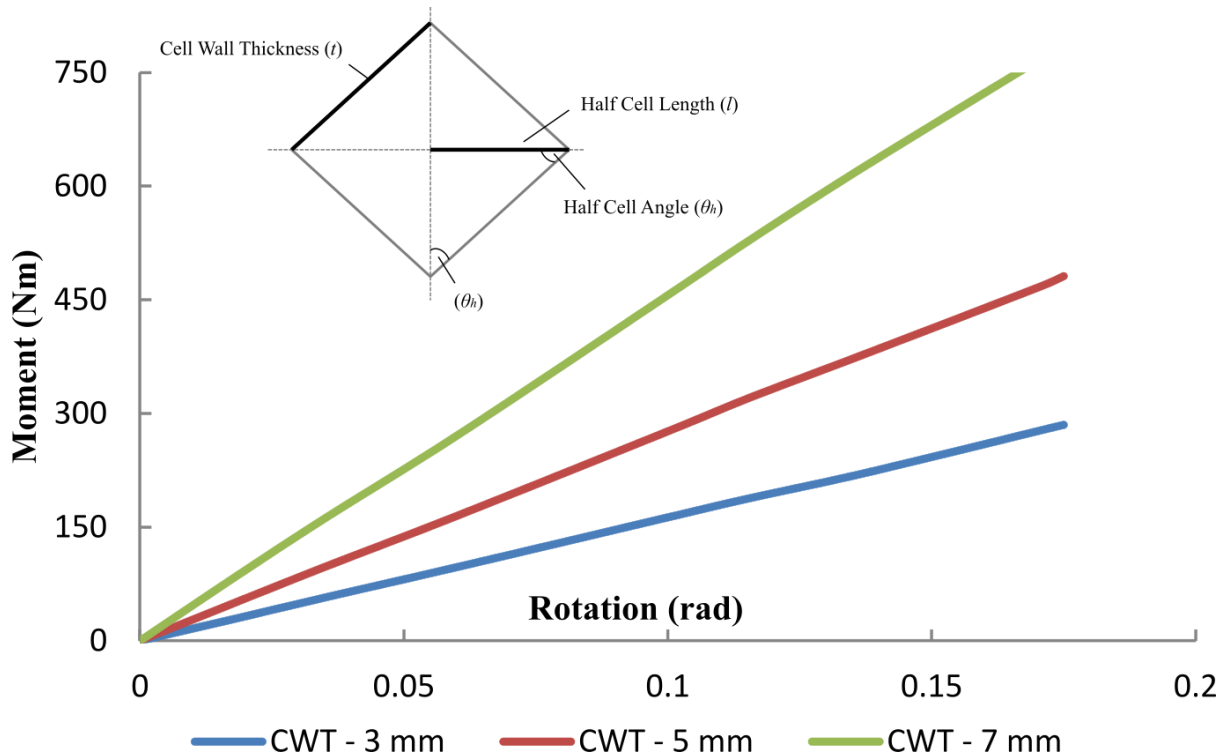


Figure 3.12: Cell Wall Thickness (CWT) and its effect on the circumferential stiffness

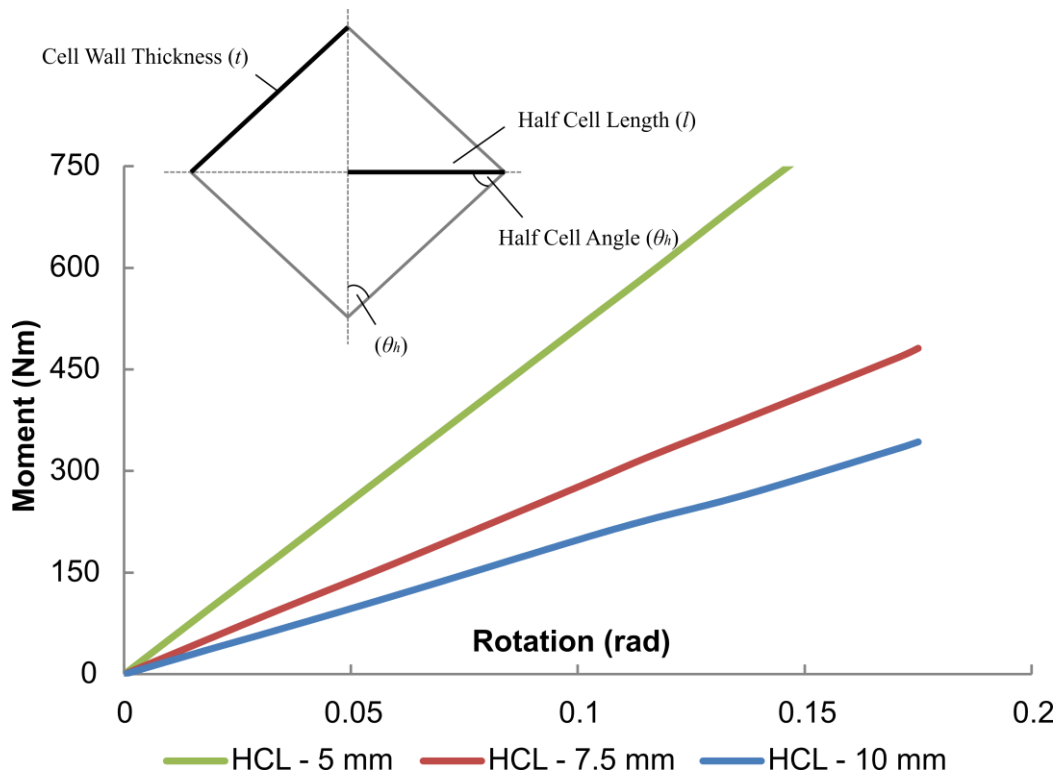


Figure 3.13 - Half Cell Length (HCL) and its effect on circumferential stiffness

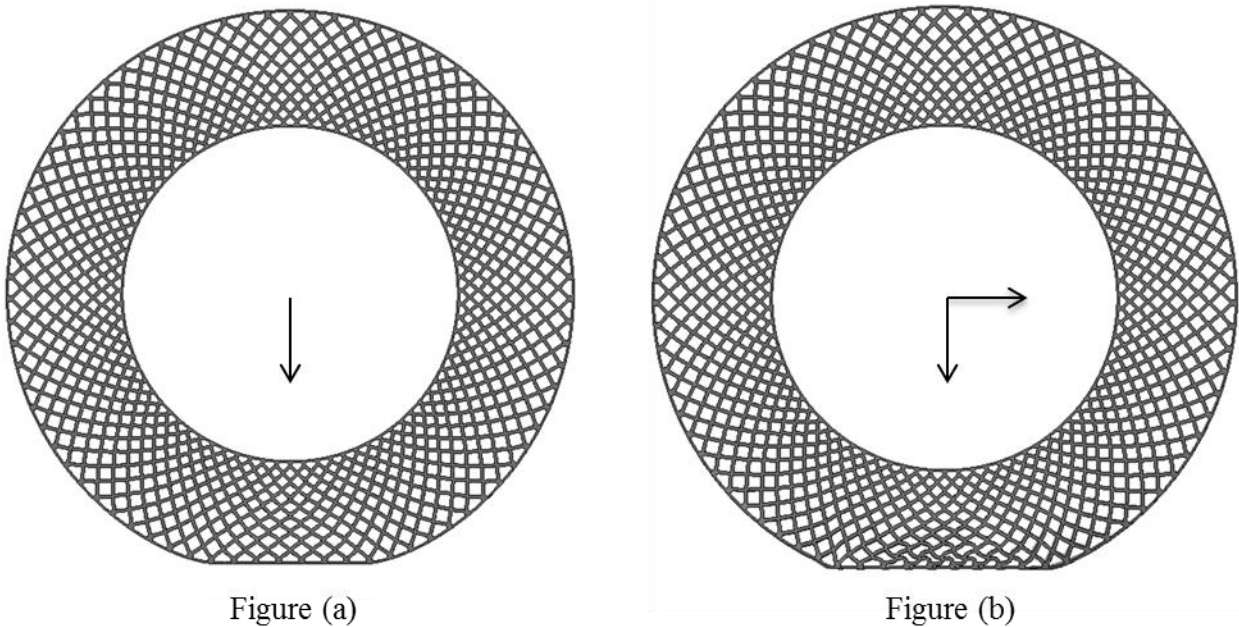


Figure 3.14: Figure (a) illustrates an NPT with adequate vertical stiffness. Figure (b) show the same spoke configuration with inadequate circumferential stiffness and the resultant contortion of the structure when subjected to rolling.

3.7 STATIC LOADING AND STEADY STATE ROLLING

The preliminary design characteristics such as radial stiffness, contact pressure profile and stress distribution in the spoke (in the case of NPT) for the two tyre models are highlighted in this section. All the analyses are performed for a rated load of 3000N. The loading simulation is conducted with a frictionless contact between the tyre and the road whereas a coefficient of friction of 0.7 is prescribed for the rolling simulation.

3.7.1 Loading

The load-deflection plot of a 165/70R14 passenger car tyre and the steel ringed NPT model are shown in Figure 3.13. For a load of 3000 N, a maximum deflection of 20.81 mm for the pneumatic tyre, 12.5 mm for the steel ringed NPT is observed. Since the NPT is a bottom loader, the region above the contact area is the load bearing region in the tyre. The stress distribution in the flexible spoke of the two NPTs is shown in Figure 3.14. Unlike the pneumatic tyre, all the loads are taken in compression rather than tension.

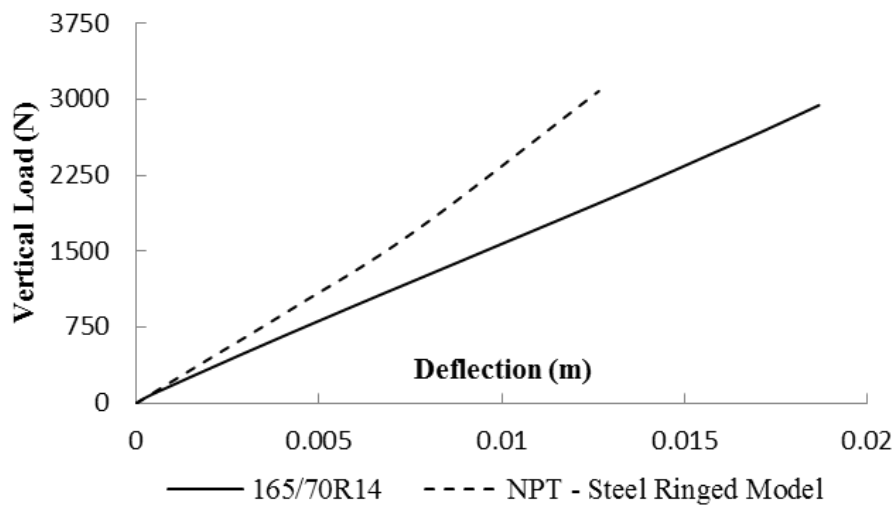


Figure 3.15: Vertical load – deflection curves for different tyre models

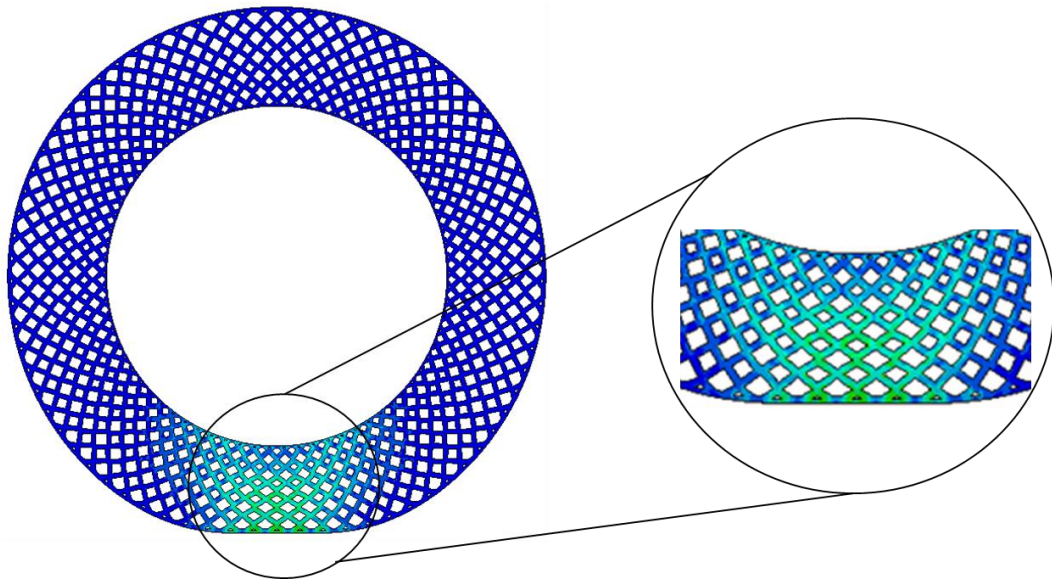


Figure 3.16: Illustration of the 'bottom-loading' phenomena in the Steel Ringed NPT

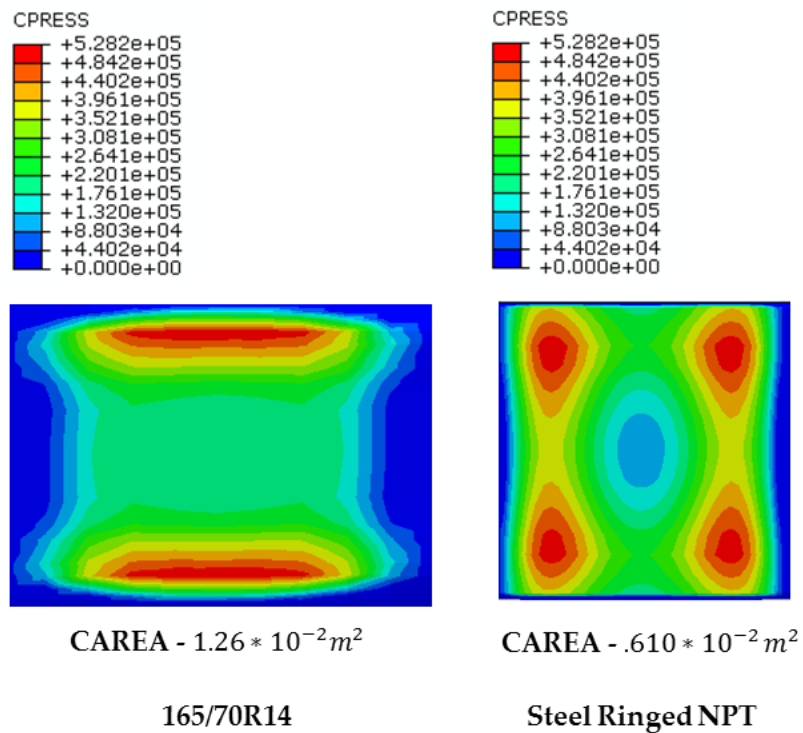


Figure 3.17: Contact pressure distribution and contact area variation for different tyre models
(Contact Pressure in **Pa**)

3.7.2 Contact Patch

Figure 3.15 shows the variation in the contact pressure distribution and the contact area for the NPT and its pneumatic counterpart. The high vertical stiffness exhibited by the steel ringed NPT manifests in the form of a smaller contact patch. A maximum contact area of $1.26 * 10^{-2} \text{ m}^2$ for the pneumatic tyre and $0.610 * 10^{-2} \text{ m}^2$ for the NPT is obtained. The other major difference lies in the contact pressure distribution of the two tyre models. In the pneumatic tyre, the region of maximum contact pressure is oriented along the direction of travel. The magnitude of contact pressure begins to decrease as we move towards the center of the contact patch. The concentration of high contact pressures at the shoulder of the tyre is due to the bending stiffness of the sidewall. In the steel ringed NPT, the region of maximum pressure is oriented in the lateral direction along the leading and the trailing edge of the contact patch. This is in accordance to the contact patch obtained by Kim *et al.* (2013). This phenomenon is also observed in all NPTs which consist of shear beams in their assembly. This is due to the high bending stiffness of the steel ring. The length of the contact patch and the region of the maximum contact pressures are due to the longitudinal buckling of the steel ring. Since shear beams consists of 2 inextensible rings, a similar phenomenon is observed.

3.7.3 Longitudinal Force

Figure 3.16 shows the variation of the longitudinal force with its slip ratio. The magnitude of the maximum traction force is in accordance with Coulomb's law of friction. A peak longitudinal force of 2099 N is produced. The steel ringed NPT model reaches the peak longitudinal force at 6% slip ratio whereas the pneumatic tyre peaks at 8% which is a desirable trait for an NPT to processes. The tyre is capable of producing the required traction force without torsional buckling of the spoke structure.

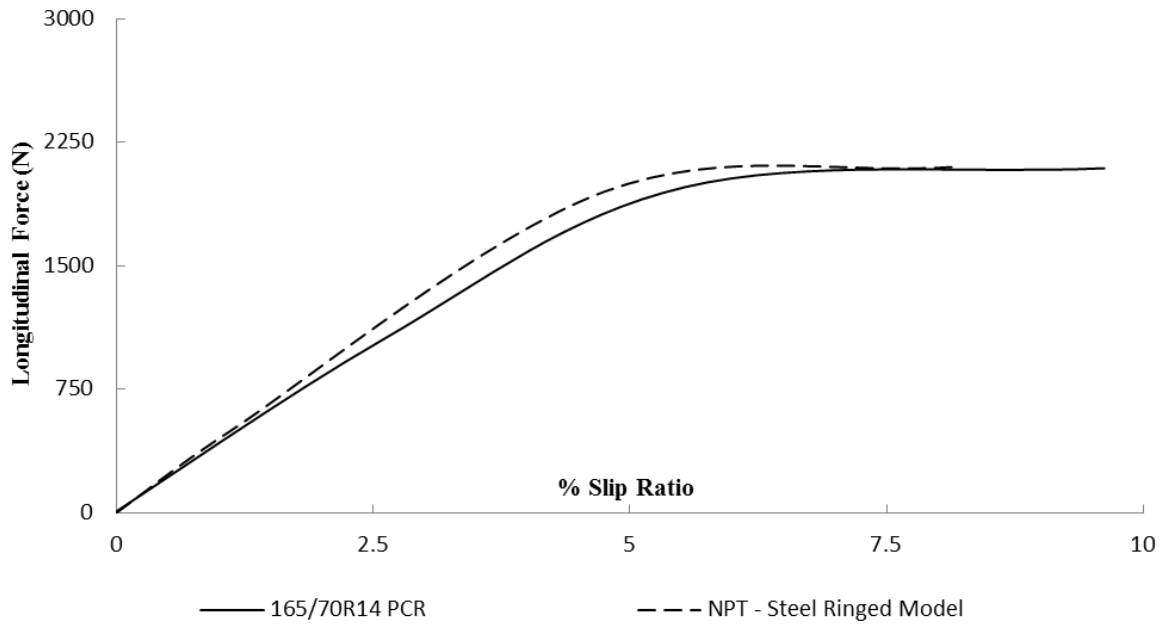


Figure 3.18: Longitudinal force variation for different tyre models

3.7.4 Lateral Force

Figure 3.17 shows the variation in the lateral force generated for the two tyre models. The lateral force peaks at a slip angle of 4.5 degrees for the pneumatic tyre and 2.8 degrees for the steel ringed NPT. A pneumatic tyre exhibits a cornering stiffness of 539 N/deg whereas the steel ringed NPT has a cornering stiffness of 753.96 N/deg. A tyre with high cornering stiffness is a desirable quality to possess as it enhances the handling characteristics of the vehicle. Conventionally, the stiffness of the tyre at 1 degree slip angle is assumed to be the cornering stiffness and tyres usually operate in the linear range of 1-2 degrees. The NPT is more than capable of producing the required lateral force.

3.7.5 Self-Aligning Torque (SAT)

Figure 3.18 shows a variation in the SAT between the two tyre models with increasing slip angle. A large disparity in the magnitude of SAT values is observed. The maximum SAT value of 20 Nm is achieved by the pneumatic tyre, but the steel ringed NPT only manages to achieve a peak torque of 4.9 Nm. The low magnitude of SATs can be attributed to the low contact area of the steel ringed NPT. Figure 3.15 shows that the contact area of the steel ringed model is only half the area of its pneumatic counterpart. Rao (2005) captured the effect of contact area and coefficient of friction on SAT for pneumatic tyres. The work

highlighted that the SAT magnitudes increase with increasing coefficient of friction whereas the SAT values decreased with increasing inflation pressure. Higher inflation pressure results in a lower contact area thereby lowering the SAT values. This is in agreement with the phenomenon observed in the case of the steel ringed NPT.

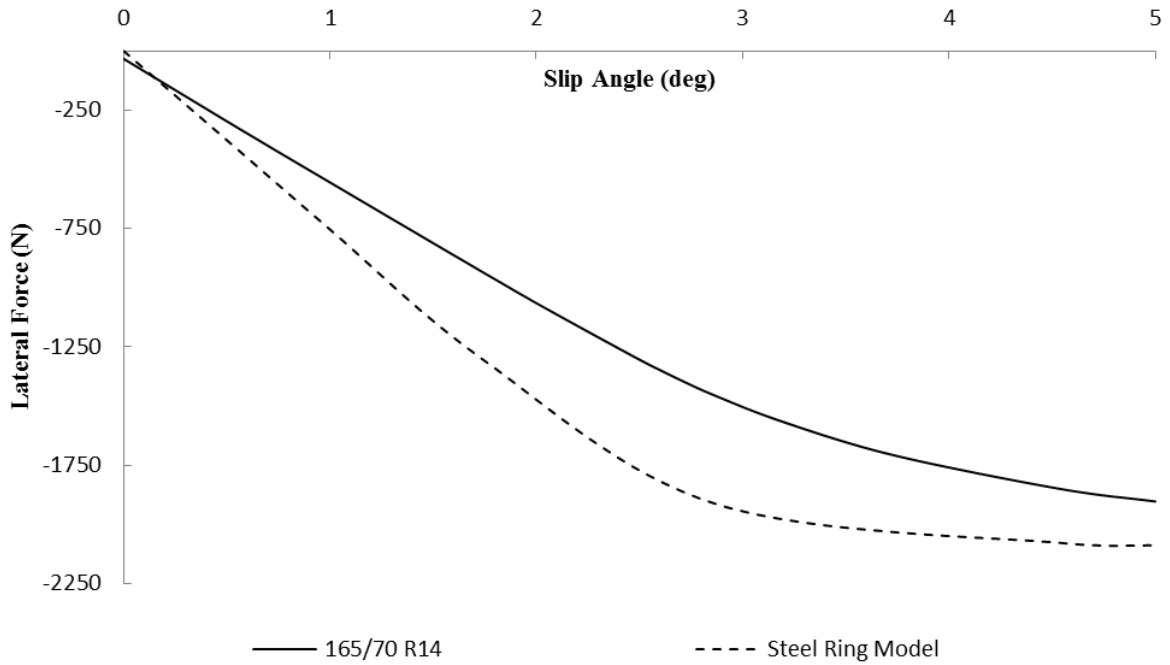


Figure 3.19: Lateral force variation for different tyre models

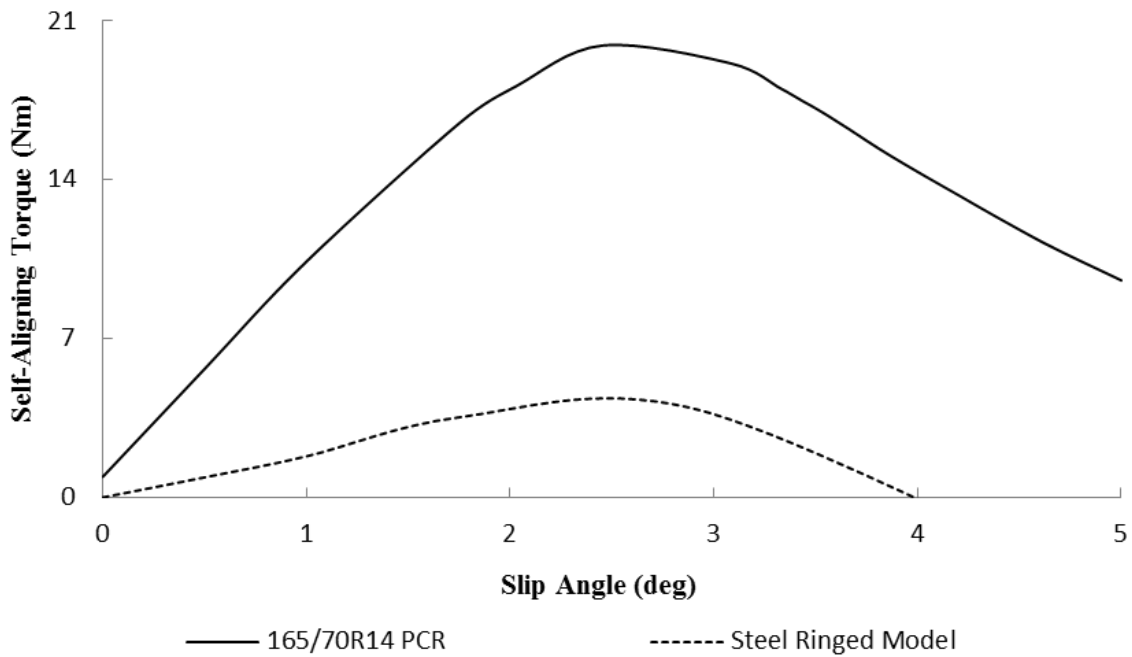


Figure 3.20: Self-Aligning Torque variation for different tyre models

3.8 SUMMARY

A study on the effect of geometric parameters in the overall in-plane mechanical behaviour of the structure has been highlighted. With the FE element model the pneumatic tyre and the steel ringed NPT developed, various simulations are conducted to extract both static and steady-state characteristics of the tyre. It was found that the designed tyre is capable of matching the NPT's longitudinal and lateral force requirements but is incapable of producing the required SAT.

CHAPTER 4

EFFECT OF DESIGN ATTRIBUTES ON THE FORCE AND MOMENT CHARACTERISTICS

4.1 INTRODUCTION

A major advantage of the pneumatic tyre is the number of design handles available in terms of extracting the desired performance. With the current Non-Pneumatic Tyre (NPT) assembly, it is difficult for a designer to deliver varying performance without making a major change in the spoke design. This chapter addresses one such method to incorporate varying performance characteristics with minimalistic change in the overall design of the tyre. The effect of material properties on the performance of the tyre has also been highlighted. Additionally, a new circumferential spoke design has been conceived in order to decouple the circumferential stiffness from the longitudinal and lateral stiffness.

4.2 EFFECT OF IN-PLANE GEOMETRY ON LATERAL STIFFNESS

The resistance exhibited by the tyre to deformations when subjected to loads acting in the axial direction, determines the lateral stiffness of the tyre. In the previous chapter, the effect of geometric parameters on the in-plane mechanics was performed using a FE study. Similarly, in order to characterize the lateral behaviour of the NPT, it is imperative to understand the effects of the geometric properties on the lateral stiffness of the tyre. A FE simulation was conducted to capture these effects. In the first step, a displacement based boundary condition (BC) is assigned to the road. The road is displaced vertically by 15 mm towards the tyre. A coefficient of friction of 1.0 is assigned in the subsequent step. It is followed by a lateral displacement step, where the road is displaced by 10 mm in the lateral direction. The reaction force generated due to the friction in the tyre-road interface is recorded. This simulation is performed for spokes of various configurations as highlighted in the previous chapter.

The variation of the lateral force with respect to the in-plane spoke configuration is captured in Figures 4.1 to 4.3. It is observed that, variation in the lateral force is similar to that observed in the in-plane reaction force development. It is observed from Figure 4.1 that the structure which offers the least stiffness is the one with an Half Cell Angle (HCA) of 45

degrees and the highest stiffness for a HCA of 25 degrees when the Cell Wall Thickness (CWT) and Half Cell Length (HCL) are kept constant. As the magnitude of CWT increases, so does the stiffness of the structure in the lateral direction and vice versa in the case of HCL. Since the lateral stiffness of the spoke is determined by the out-of-plane bending stiffness of the spoke, a phenomenon similar to the in-plane behaviour is observed. In the case of CWT and HCL, variation in the in-plane geometry causes a rise (or drop depending on the parameter taken into consideration) in the volume of material which directly affects the lateral stiffness of the tyre.

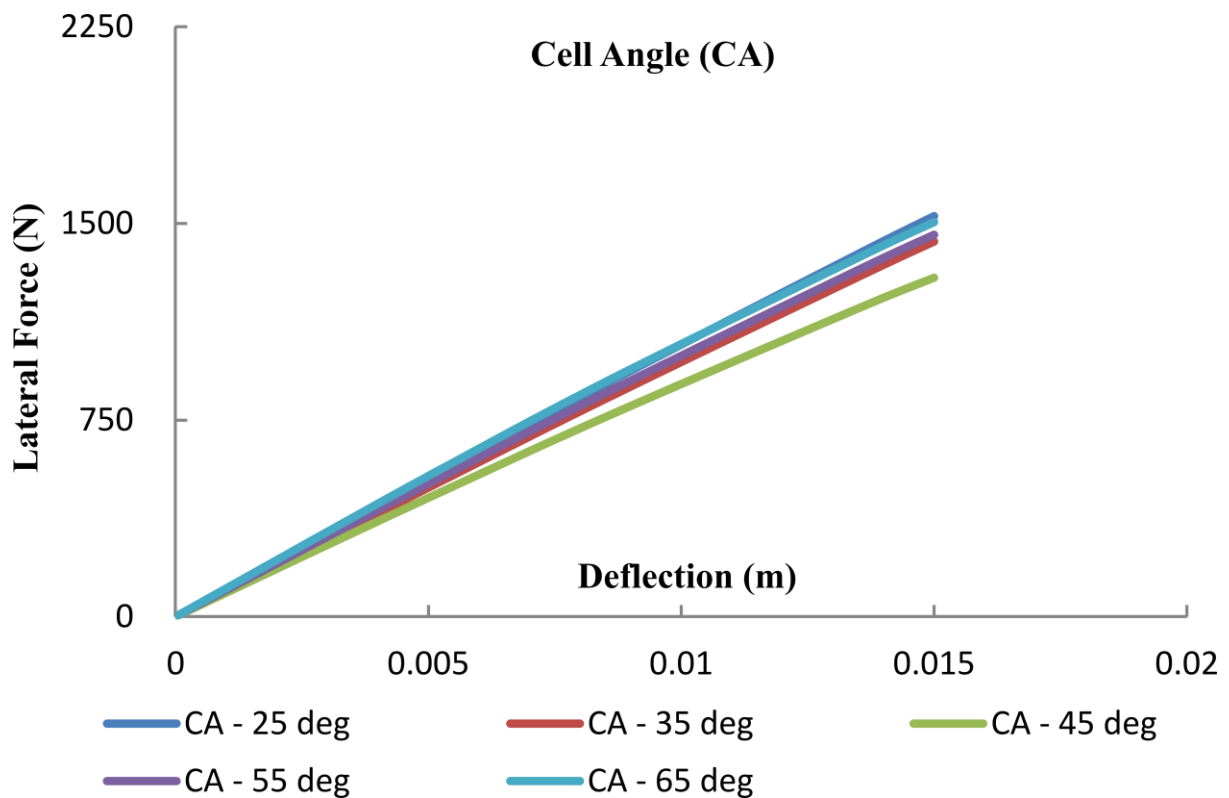


Figure 4.1: Variation of lateral force generation with Half Cell Angle (HCA)

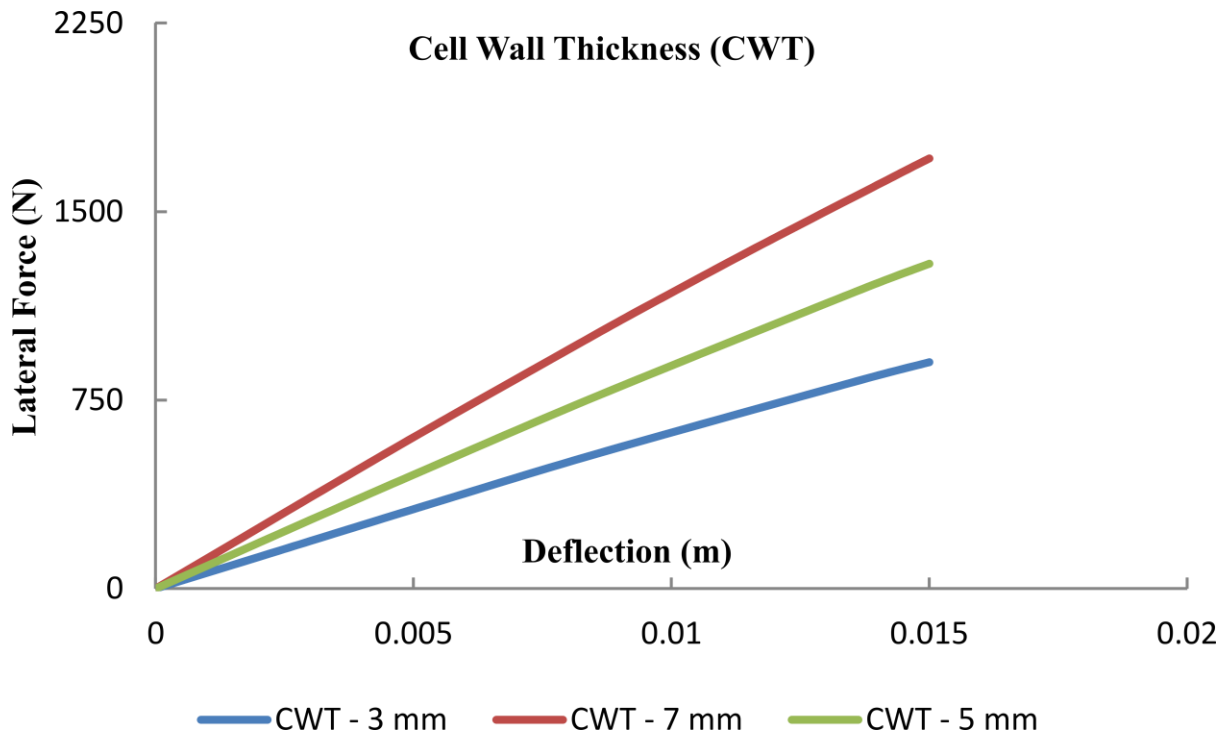


Figure 4.2: Variation of lateral force generation with Cell Wall Thickness

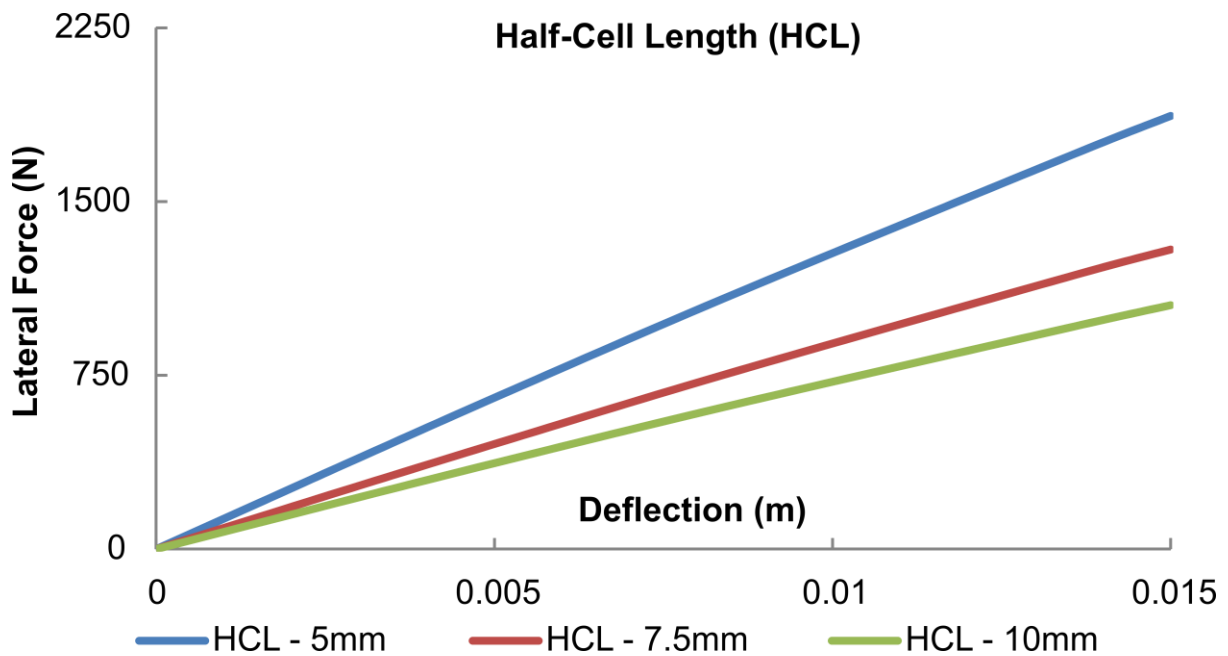


Figure 4.3: Variation of lateral force generation with Half Cell Length (HCL)

4.3 BELT MODEL AS REINFORCEMENTS

Apart from the inherent stiffness possessed by the structure due to the density of the material present in the lateral direction, the variation in lateral stiffness is also governed by the in-plane cell configuration. With inflation pressure capable of altering the stiffness properties of the pneumatic tyre and with the current steel ringed NPT, the number of modifiable design attributes available for a tyre manufacturer seems restrictive. As seen in the previous section, any change in the tyre's performance can only be achieved by changing the spoke design. Apart from the spoke, the outer steel ring is the only other component responsible for maintaining the structural integrity of the tyre. This can be proved by varying the material properties of the outer ring. A static loading analysis is conducted with the steel ringed NPT, where the steel ring's material properties are modified to the spoke's elastomeric properties. Figure 4.4 shows the load – deflection curves for this modified assembly. An immediate drop in the vertical stiffness of the tyre is observed. By changing the material of the steel ring, a drop in the vertical stiffness of 10% was observed, thus proving that the outer steel ring is an active participant in the load carrying process.

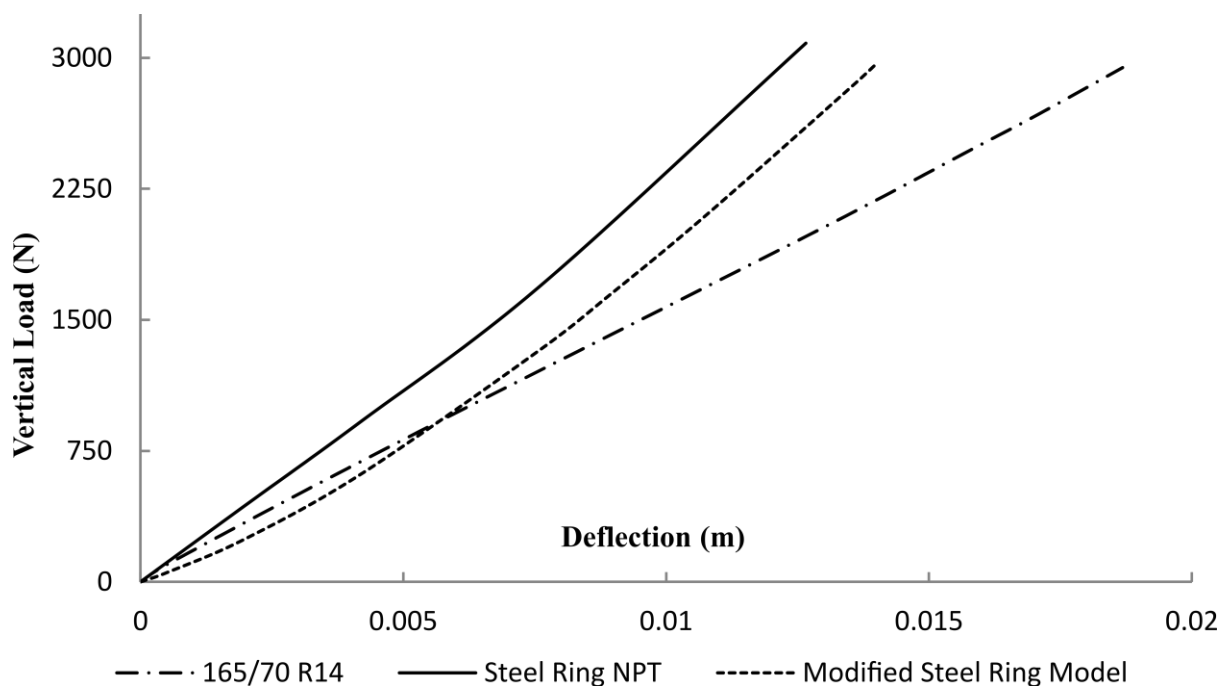


Figure 4.4: Variation of vertical load – deflection curves with varying outer ring material properties

It is imperative that the tyre exhibits a certain degree of flexibility, in terms of design and performance. In order to achieve these varying performance characteristics, a material was required, to replace the steel ring, which offered varying stiffness properties without affecting the radial stiffness of the tyre. Incorporating a new material altogether would involve going through a laborious process of testing the material for its applicability in tyres.

Composite materials are capable of exhibiting directionally dependent behaviour based on their constituent materials. A composite which is already in use, like reinforcing belts, was considered to replace the steel ring of the NPT. In the case of pneumatic tyres, belts are used to render stiffness to the carcass, as the structure is constantly in a state of tension. Belts are composites of elastomers with reinforcements embedded in them. The reinforcements are conventionally metallic in nature. These belts are anisotropic in nature and the anisotropic behaviour of cord-reinforced rubbers is dependent on the material of the host and reinforcements, area of reinforcement, number of reinforcements, reinforcement orientation etc. (Clark, 1981). The outer steel ring is replaced by reinforcing belts. In order to minimize variability, the belt package used in the NPT is similar to those used in the equivalent pneumatic tyre, without varying its material properties. By taking advantage of the composite's anisotropic behaviour through the variation of the reinforcement angles, belts have been used to mimic the shear strength of the steel ring. The construction of the belts are such that, a 0 degree belt angle indicates that all the reinforcements are aligned axially to the tyre whereas a tyre with 90 degree belt angle has reinforcements running circumferentially around the tyre.

4.4 FE MODEL OF BELT REINFORCED NPT

Figure 4.5 shows the unit sector and lateral section of the belt reinforced NPT. The same spoke configuration, as seen in the steel ringed NPT has been retained in order to maintain consistency between the models. The outer steel ring has been replaced by two reinforcing belts. The number of belts used and the belt properties assigned are similar to the belt properties of the equivalent pneumatic tyre. The host and embedded element properties are provided in Table 4.1 and Table 4.2. The material properties of all the other components have been retained as per the steel ringed model.

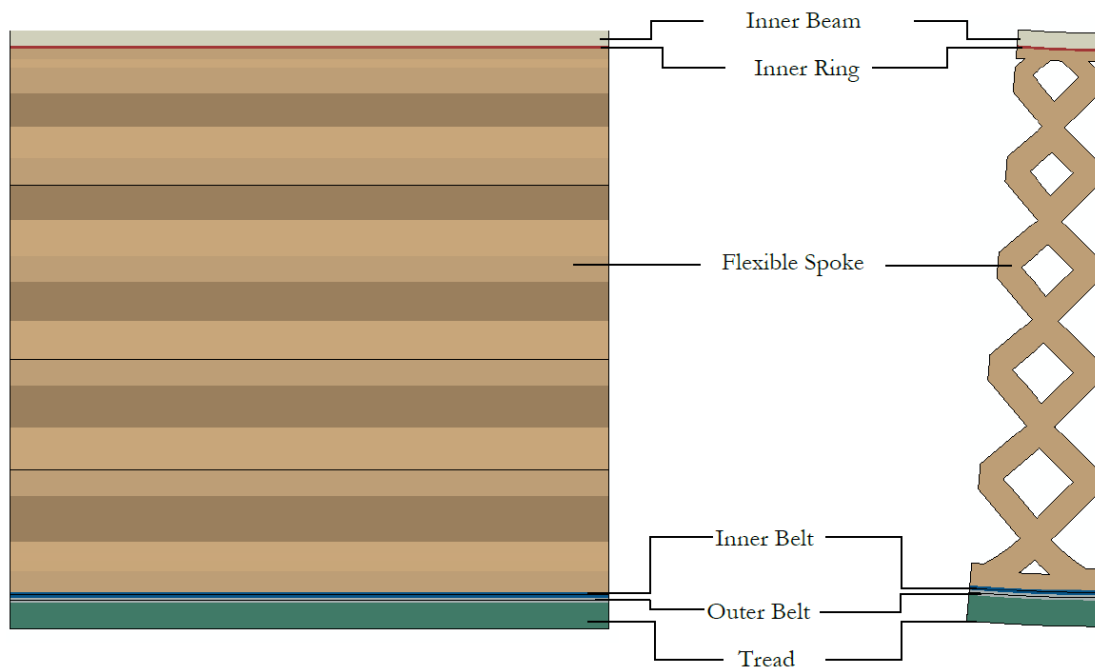


Figure 4.5: Lateral section and unit sector of Belt Reinforced NPT

Table 4.1: Embedded element – material properties

Tyre Component	Reinforcement cross-sectional area (m^2)	Reinforcement Spacing (m)	Orientation of Reinforcement (deg)
Belt 1	2.12 E-07	1.64 E-03	30,60,90
Belt 2	2.12 E-07	1.64 E-03	-30,-60,-90

Table 4.2: Host element – material properties

Tyre Component	Density kg / m^3	Young's Modulus (N / m^2)	Poisson's Ratio
Belt 1	7485	140.76 E+09	0.3
Belt 2	7485	140.76 E+09	0.3

4.5 RESULTS AND DISCUSSION

FE simulations are conducted in order to extract the static and steady-state behavior of the belt reinforced NPT. The results from these simulations are compared with both the steel ringed NPT as well as with the equivalent pneumatic tyre.

4.5.1 Vertical Stiffness

As observed from Figure 4.6 replacing the steel ring with an elastomer resulted in a drop in the vertical stiffness. Similarly, a drop in the vertical stiffness of approximately 10% is observed in the belt reinforced NPT. Since the pneumatic tyre's belts are designed to work in tension, they do not play a part in the load carrying process and hence it can be intuitively understood that variation of the belt angles do not affect the vertical stiffness in the belt reinforced NPT. This is captured in Figure 4.7. The effect of replacing the steel ring with a cord reinforced rubber is more pronounced in the contact pressure distribution of the tyres.

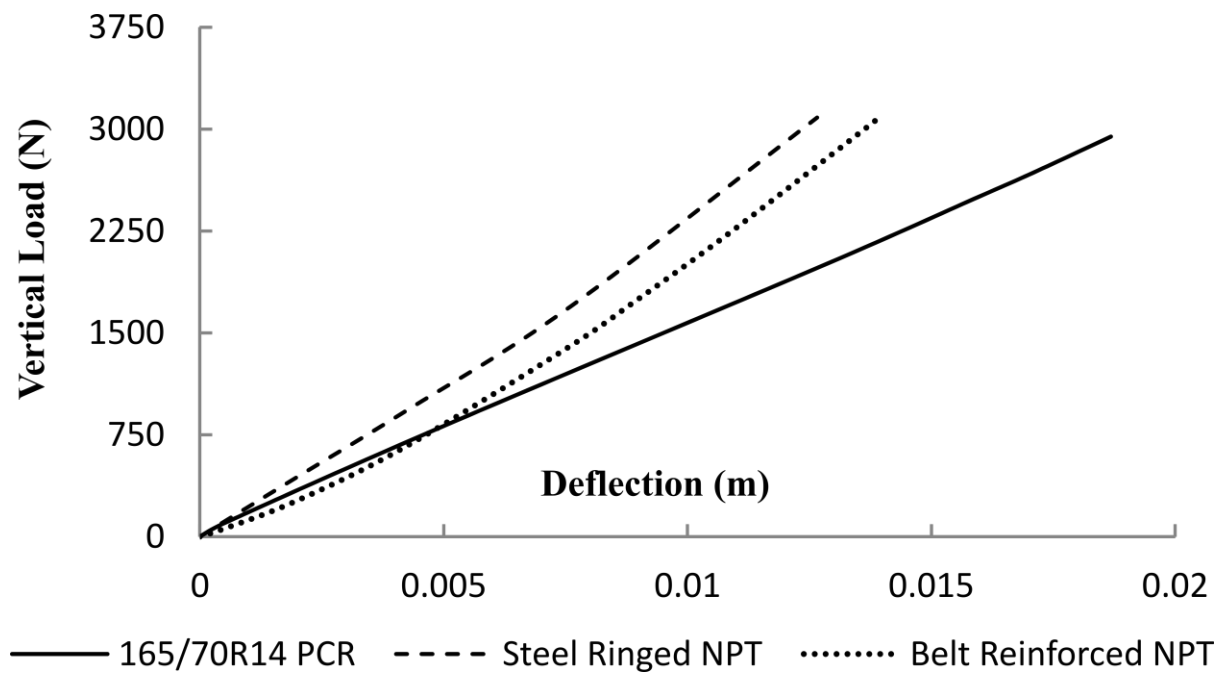


Figure 4.6: Vertical load – deflection curve for the different tyre models

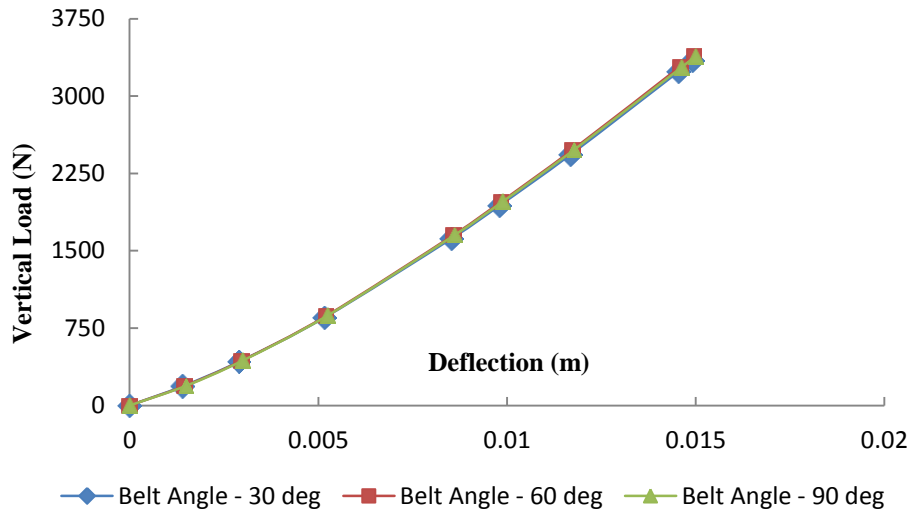


Figure 4.7: Vertical load – deflection curve for NPTs with varying reinforcement angles

4.5.2 Contact Patch

Figure 4.8 compares the contact pressure distribution and the contact area of the 3 tyre models. A marked difference is observed between the contact pressure distribution and the contact area of the steel ringed and the belt reinforced NPT. There is an absence of a high contact pressure band at the leading and trailing edge of the contact patch due to absence of the steel ring. A striated contact pressure distribution in the belt reinforced NPT reveals the participation of individual cell wall in the load bearing process. The contact pressures are lower and the drop in the vertical stiffness of the tyre is manifested as increase in the contact area. Due to the anisotropic nature of the belts, a difference is observed in the contact pressure distribution of the belt reinforced NPTs with varying reinforcement angles. Figure 4.9 shows the variation in the contact pressure distribution of the three belt reinforced tyre models. Table 4.3 shows the variation in the contact area of the different tyre models. It can be observed that the contact areas do not change with varying belt angles (as no change in the vertical stiffness is observed).

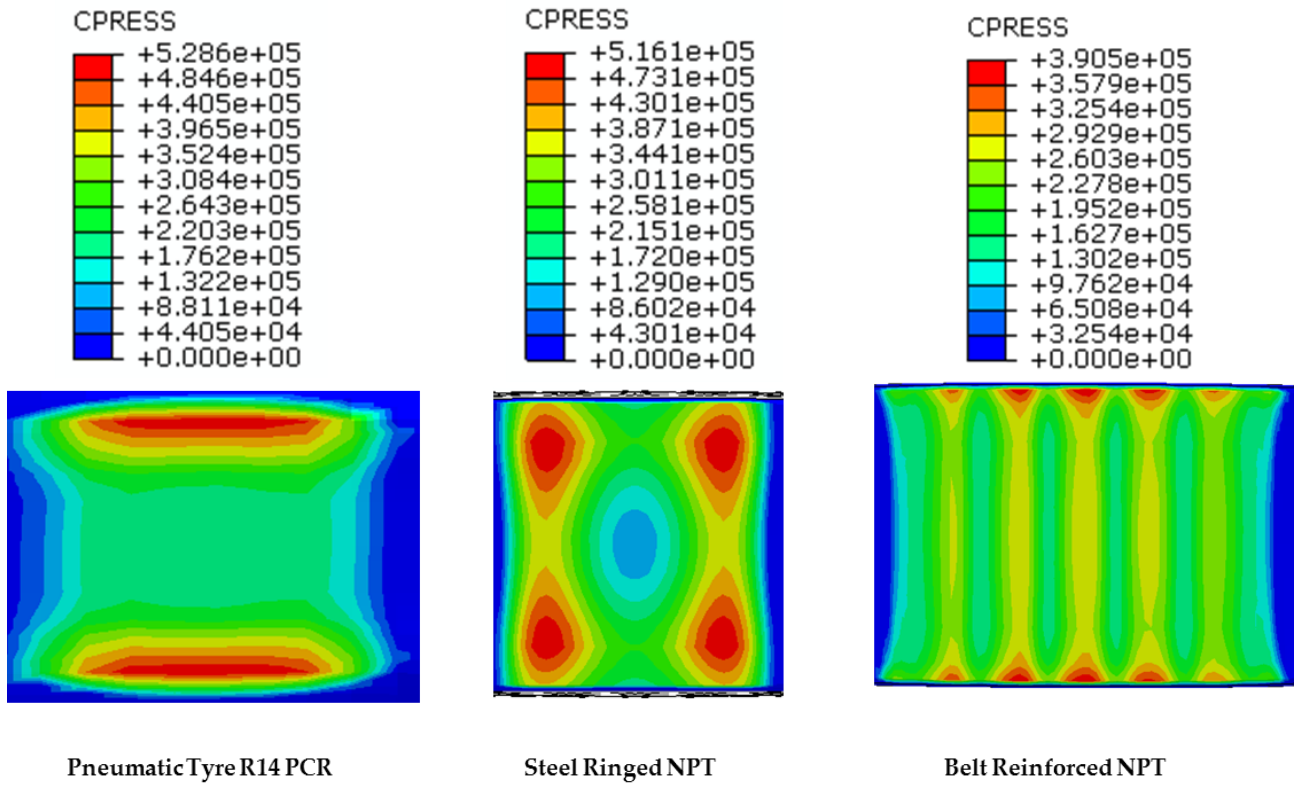


Figure 4.8: Contact pressure distribution for different tyre models (Contact Pressure in **Pa**)

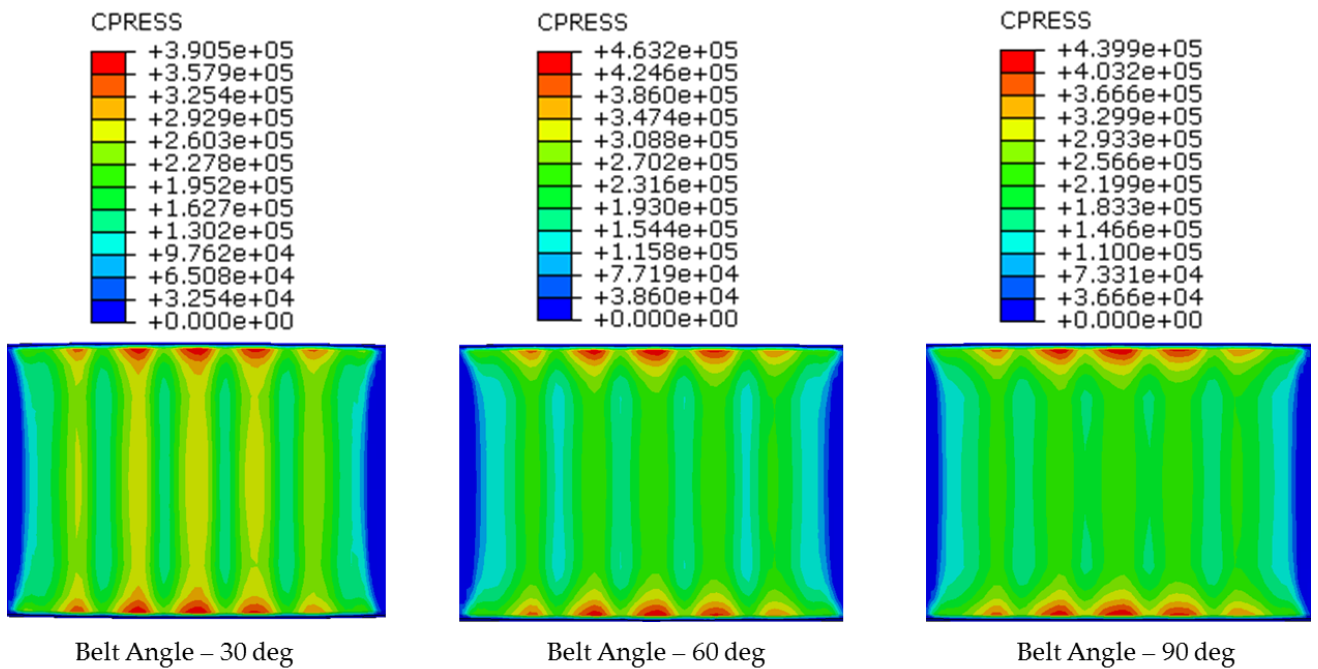


Figure 4.9: Contact pressure distribution for NPTs with different reinforcement angles (Contact Pressure in **Pa**)

Table 4.3: Contact area of different NPT models

Tyre Model	Contact Area (m^2)
165/70 R14	1.26E-02
Steel Ringed NPT	0.61E-02
Belt Reinforced NPT – 30 degrees	1.53E-02
Belt Reinforced NPT – 60 degrees	1.50E-02
Belt Reinforced NPT – 90 degrees	1.51E-02

4.5.3 Longitudinal Force

Figure 4.10 shows the variation in the longitudinal force developed in the three tyre models. The figure also illustrates the variation of the traction force produced with varying reinforcement angles. It is observed that, the NPT with the 30 degrees reinforcement orientation is capable of matching the equivalent pneumatic tyre's and the steel ring NPT's performance.

4.5.4 Lateral Force

Figure 4.11 shows the variation in lateral force for the three different tyre models. As observed in the previous chapter, the high out of plane bending stiffness of the steel ring caused the NPT to exhibit a high cornering stiffness. In the case of the belt reinforced NPT, the reinforcement angles predominantly affects the lateral stiffness of the tyre. The NPT with 30 degrees reinforcement angle was able to match the cornering stiffness of the equivalent pneumatic tyre. A maximum variation of 45% in the cornering stiffness is obtained by varying the reinforcement angles between 30, 60 and 90 degrees. The reinforcing belts are designed to work in tension, yet, variation in the belt angles significantly affects the cornering stiffness of the tyre. Thus prompting the designer to focus attention of the most optimum belt design which can be used in a bottom loading tyre.

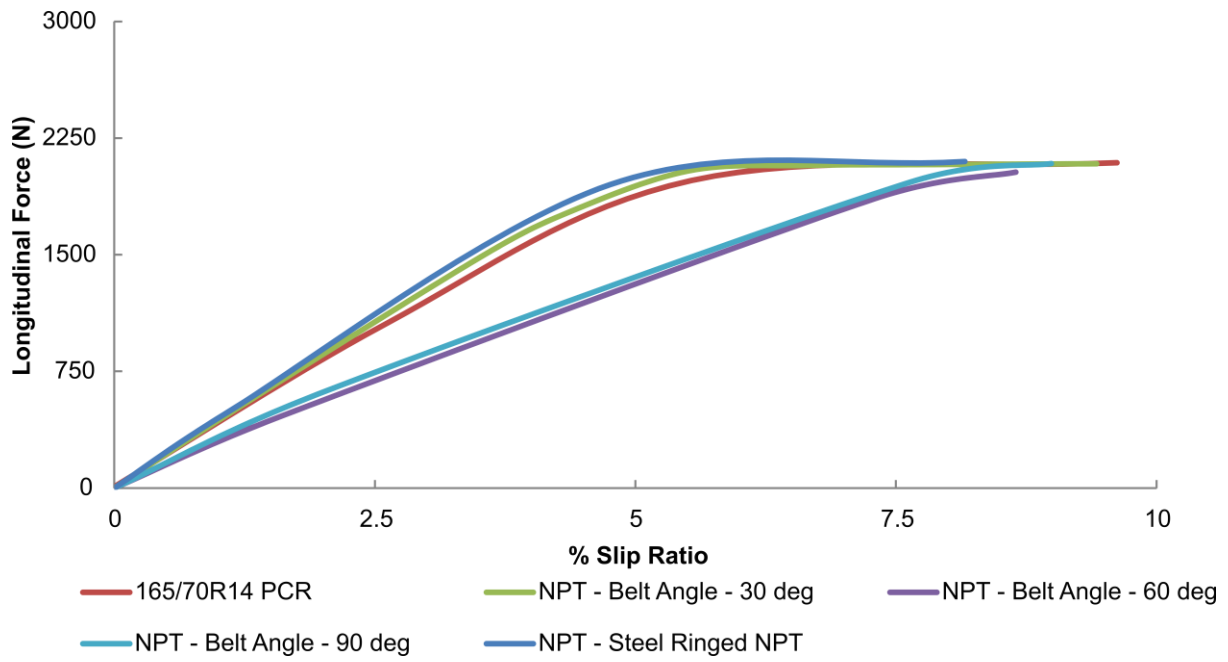


Figure 4.10: Variation of longitudinal force for different NPT models

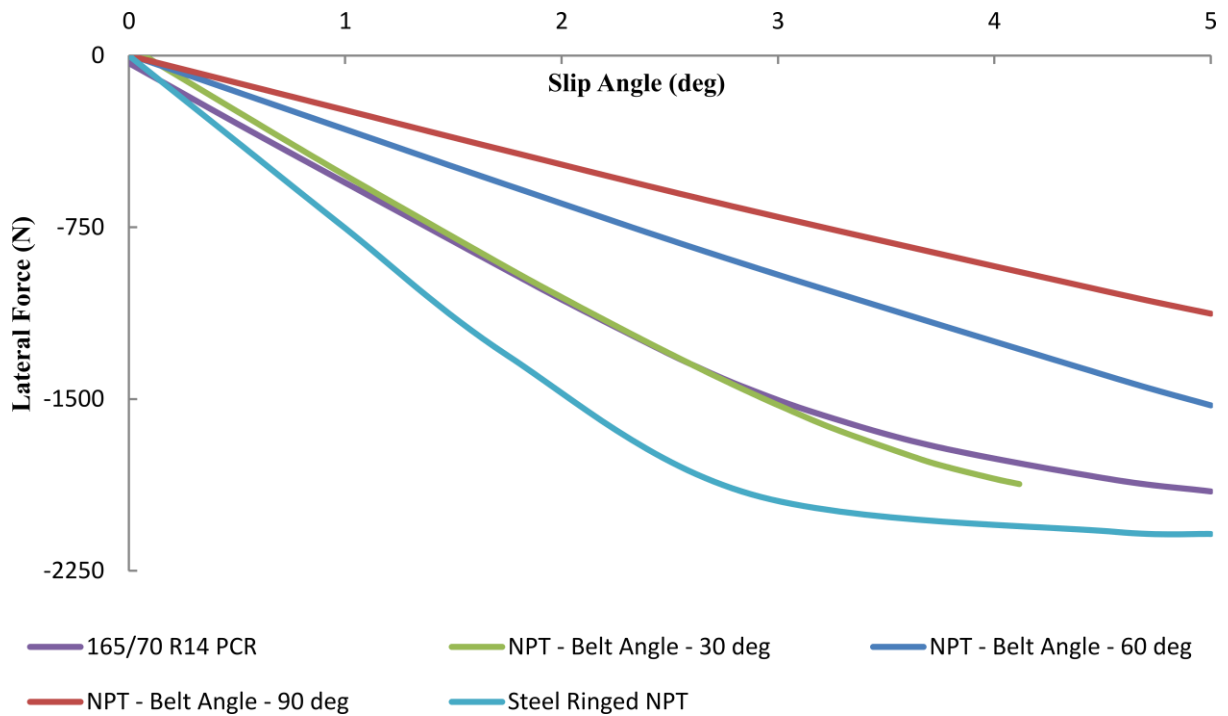


Figure 4.11: Variation of lateral force for different NPT models

4.5.5 Self-Aligning Torque (SAT)

It can be extrapolated from the previous analyses and Figure 4.11 that the participation of belts in the lateral force generation also affects the SAT magnitudes. Due to the lower contact area of the steel ringed NPT, the tyre is not able to produce the required SAT. The SAT value reaches zero for a slip angle of 4 degrees whereas other models peak around this slip angle range. Since SAT is a function of the contact area, the belt reinforced NPT is at an advantage due to its bigger footprint and thus produces the required torque. As the reinforcement angles vary, small variations in the SAT magnitudes in the linear range are observed. The differences in the SAT magnitudes get exaggerated at higher slip angle ranges.

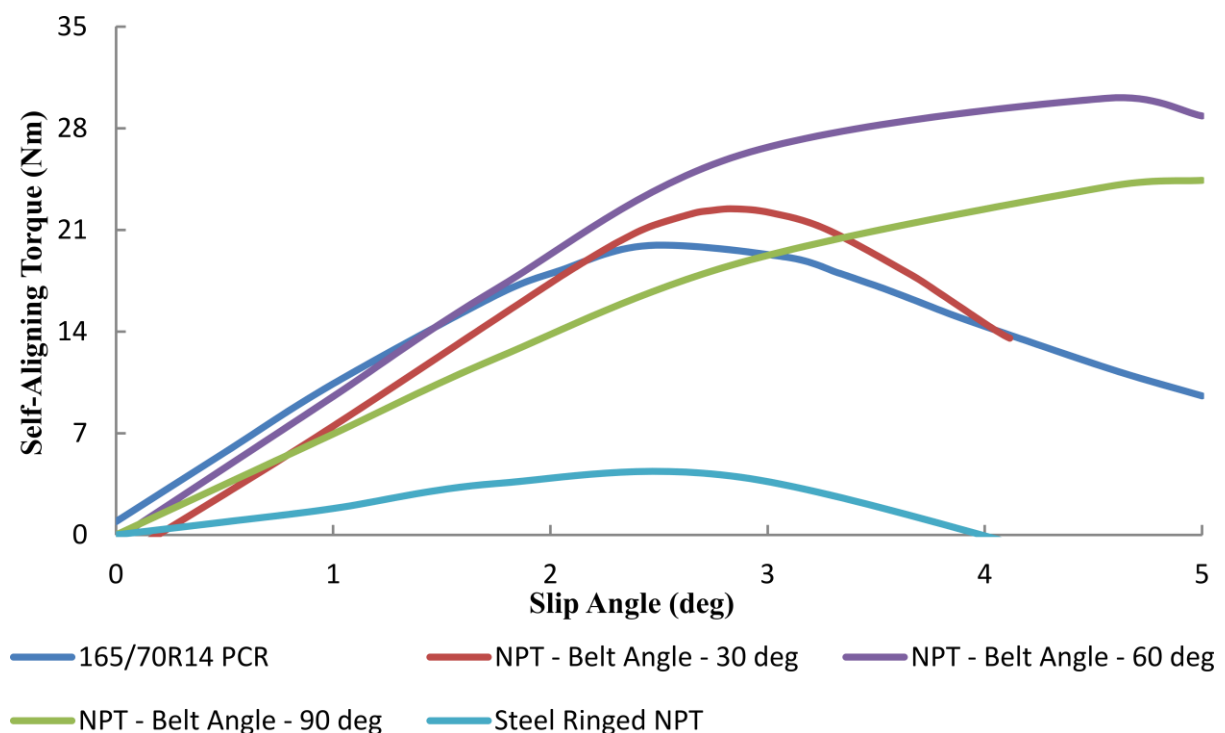


Figure 4.12: Variation of SAT for different NPT models

4.6 CHARACTERIZATION OF NPT's F&M BEHAVIOUR

It has been observed that the introduction of reinforcing belts in the NPT assembly has a significant role in affecting the F&M characteristics of the designed NPT. It was found that, the tyre with a 30 degree belt angle was able to match the performance characteristics of the equivalent pneumatic tyre. A large variation in the F&M characteristics (especially the lateral force generation) was observed by varying the reinforcement angles.

With the belt-reinforced model matching the performance characteristics of the pneumatic tyre, it is essential to characterize the NPT's F&M behaviour with varying design and operating criteria. In this section, the effect of variations in the spoke material stiffness, normal load and tread material stiffness is captured. Attention is predominantly focused on the lateral stiffness of the tyre since performance as well as the safety aspect is dependent on this parameter. All the simulations are performed under standard operating conditions wherein a steady-state rolling simulation of the tyre is conducted at 40 kmph with a rated load (except in the section where the effect of normal loads on the F&M characteristics is studied) of 3000 N and a coefficient of friction of 0.7. A 30 degree belt angle is chosen for all the simulations.

4.6.1 Spoke Material Variation

In order to study the effect of spoke's material properties on the F&M characteristics, FE simulations are conducted by varying the spoke material's properties from -20% to +20%. This is achieved by varying the material's hyperelastic coefficients C_{10} , C_{20} and C_{30} . Table 4.4 shows the variation in the vertical displacement of NPTs with varying material properties. Figure 4.13 shows the variation in the lateral force of the NPT models with their respective material properties. Among the belt reinforced models, a maximum variation of 14% is observed when the modulus of the material is varied from -20% to +20%.

Figure 4.14 shows the variation in the SAT values of the different NPT models. It can be observed that the material which offers lower stiffness exhibits the maximum SAT values whereas the material with the 20% increase in the overall material stiffness exhibits the lowest stiffness. This is in accordance with the behavior observed when comparing the steel ring NPT and the belt reinforced NPT. Higher vertical stiffness translates to lower contact area. Thus lowering the overall SAT magnitudes.

Table 4.4: Vertical deflection with varying spoke material stiffness

NPT Model - % variation in material modulus	Vertical Displacement (m)
-20%	0.01643
-10%	0.01496
Default spoke properties	0.01372
+10%	0.01272
+20%	0.01212

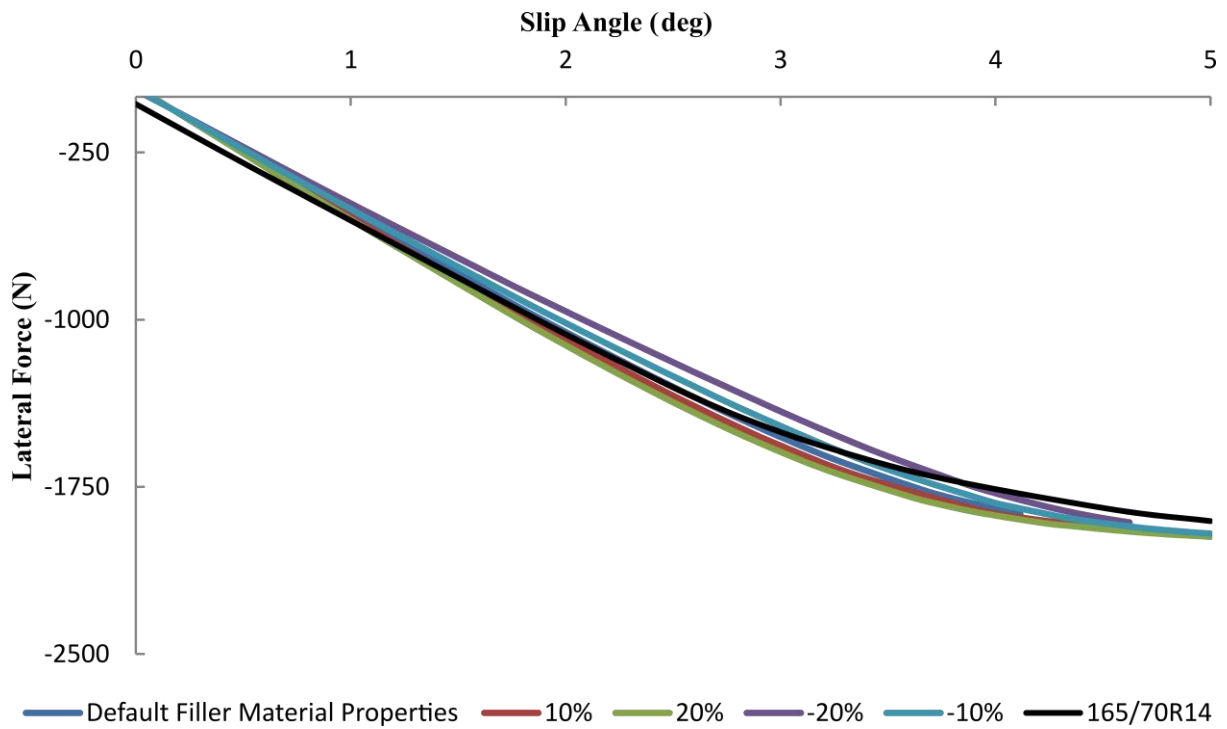


Figure 4.13: Variation of lateral force with varying spoke material stiffness

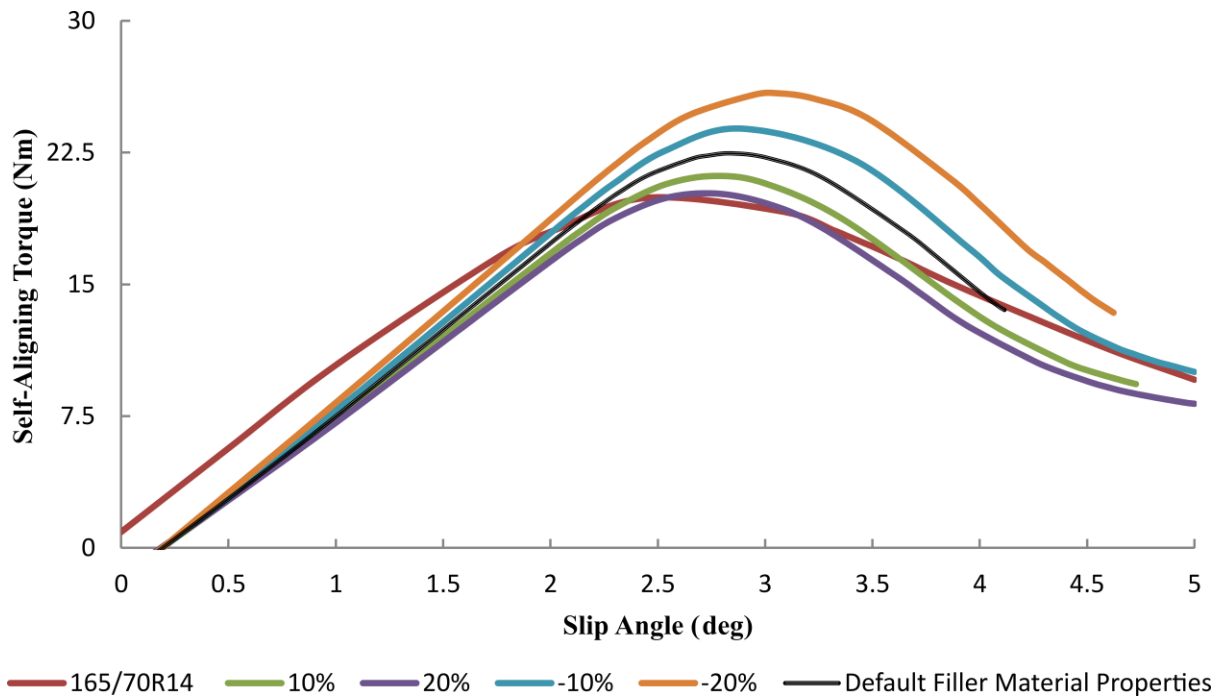


Figure 4.14: Variation of SAT magnitudes with varying spoke material properties

4.6.2 Normal Load Variation

The effect of normal load variation with the F&M characteristics of the NPT is highlighted in this section. The steady-state rolling simulations were conducted for three different loading conditions. Figure 4.15 shows the variation of the lateral force with the varying normal loads. The simulation is performed for the normal loads of 2500 N, 3000 N and 3500 N. It can be seen from Figure 4.15 that, in the linear (< 3 degrees) slip angle range, a maximum difference of approximately 10% is observed in the lateral stiffness between the maximum and minimum loads of 2500 N and 3500 N. The results observed are similar to the results obtained by Bakkar *et al.* (1987). The differences in the stiffness begin to show up for larger slip angles.

Figure 4.16 shows the variation of the SAT magnitudes with slip angles for different normal loads. As observed by Bakker *et al.* (1987), increase in the normal load increases the overall vertical stiffness and thus consequently, the contact area of the tyre resulting in higher SAT magnitudes. Despite the magnitude variations, the SAT values peak for the identical values of slip angle.

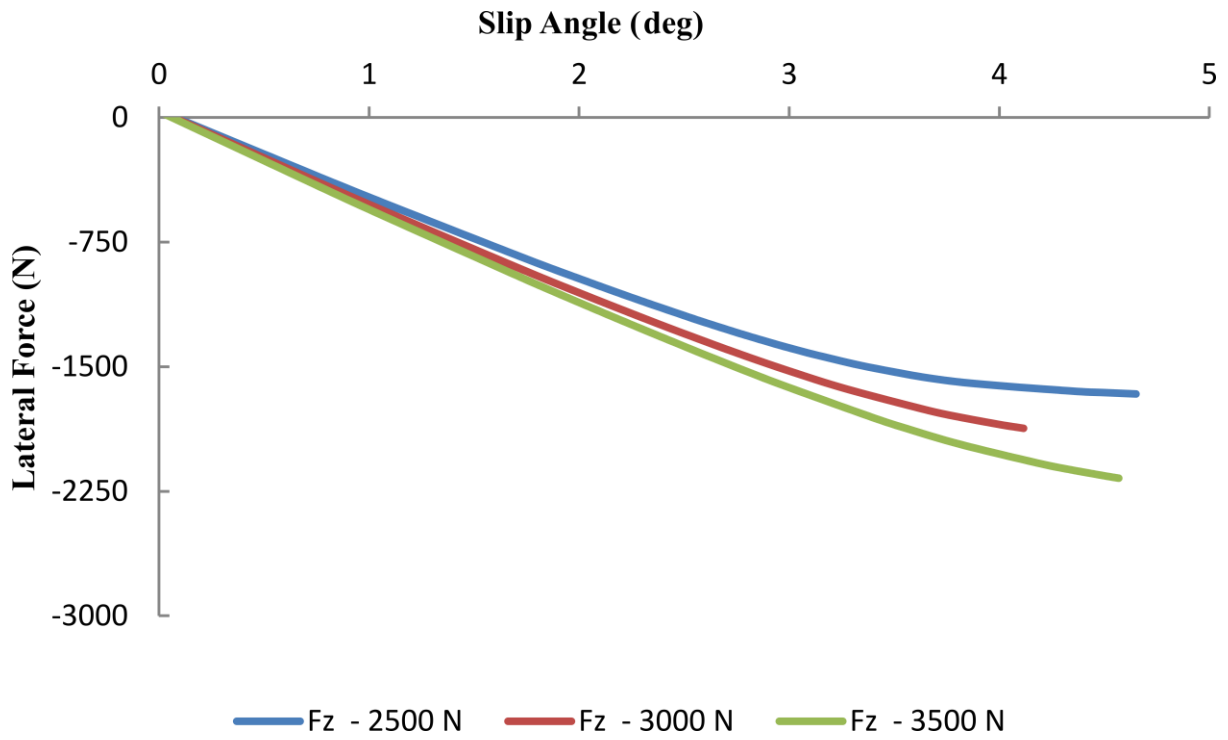


Figure 4.15: Variation of lateral force with varying normal load

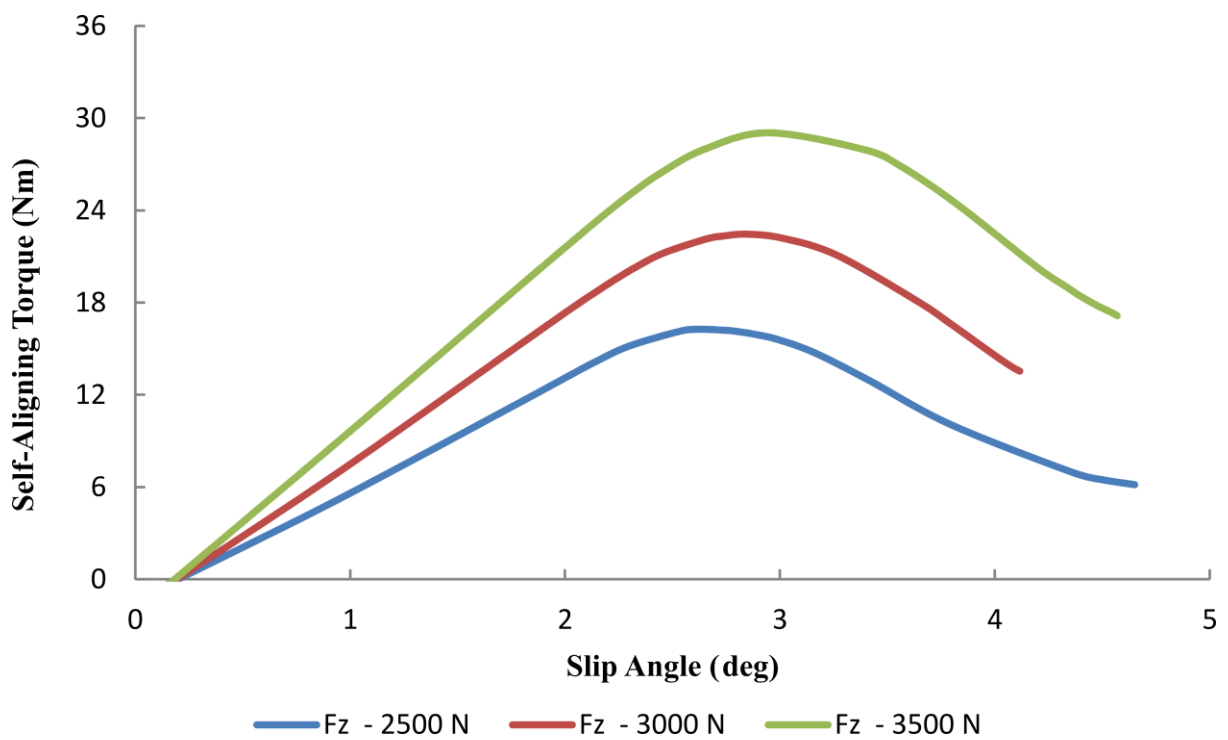


Figure 4.16: Variation of SAT magnitudes with varying normal loads

4.6.3 Tread Material Variation

Figure 4.17 shows the variation in the tread material's stiffness and its effect on the lateral force. It can be observed that, increase in the tread material does not increase the lateral stiffness of the tyre. A lateral stiffness variation of less than 5% is recorded. In the case of its pneumatic counterpart, as reported by Narasimha Rao (2005), increase in the tread stiffness caused a 10% rise in the lateral stiffness of the tyre.

Figure 4.18 shows the variation in the SAT magnitudes for NPTs with varying tread stiffness. As in the case of lateral force generation, varying the tread hyperelastic properties have no effect on the SAT magnitudes. Although this corresponds to the behaviour observed in the pneumatic tyre, there is an increase in the slip angle at which peak SAT magnitudes are achieved which is not observed in the case of the belt reinforced NPTs.

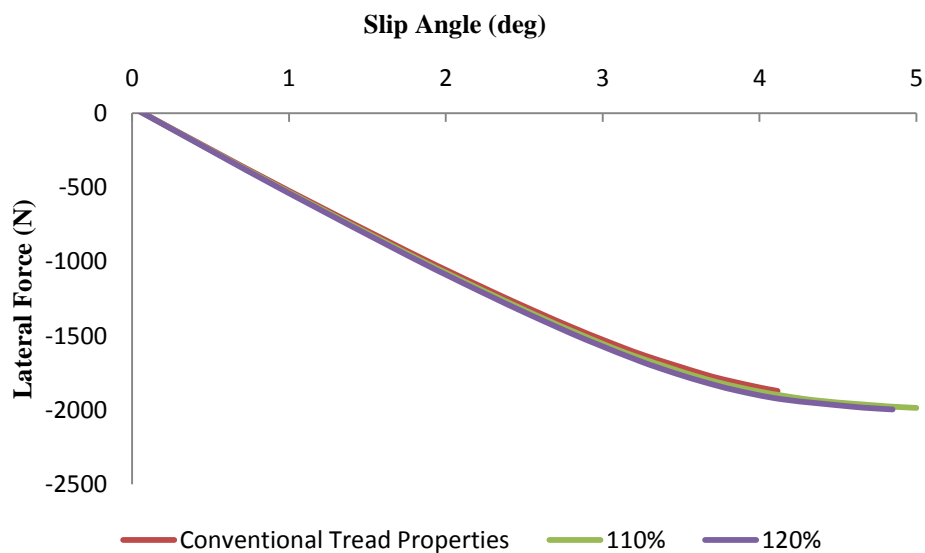


Figure 4.17: Variation of lateral force with varying tread hyperelastic properties

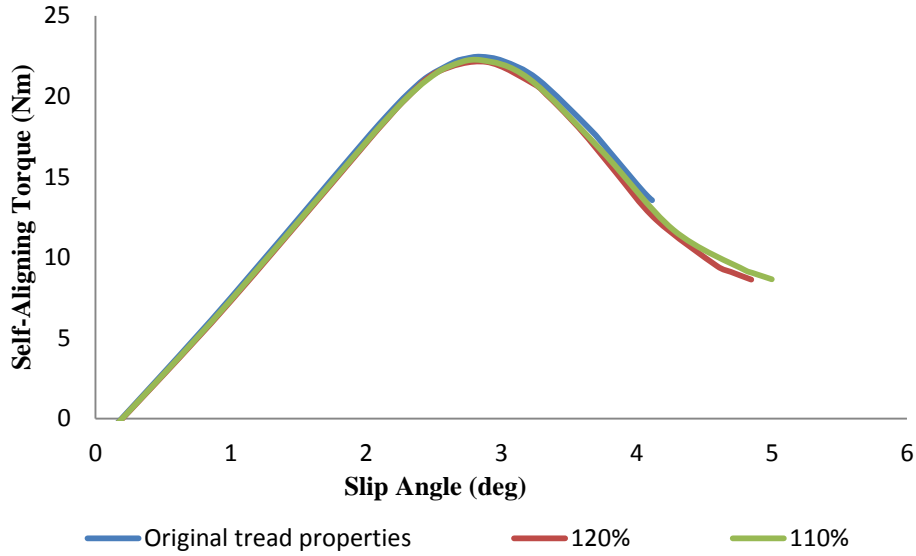


Figure 4.18: Variation of SAT magnitudes with varying tread hyperelastic properties

4.7 CIRCUMFERENTIAL SPOKE NPT

It was identified in the previous section that lowering the spoke material’s stiffness affected the circumferential stiffness of the spoke. It was also concluded from Figure 4.1 to Figure 4.3 that vertical, circumferential and lateral stiffness were coupled by design. Since NPTs do not require any inflation pressure, it is desirable to have a tyre where all the three stiffness are not coupled; thereby increasing the number of design attributes available and allowing the manufacturer to customize the tyre depending on the application. Since circumferential stiffness is the governing parameter in the design of NPTs, it was essential to decouple the circumferential stiffness from the vertical and lateral stiffness. This section explains a method of decoupling the circumferential stiffness from the vertical and lateral stiffness. This is achieved through the introduction of circumferential spokes.

Figure 4.19 shows the unit sector and the lateral section of the circumferential spoke NPT. In the case of circumferential spoke NPT, the entire tessellation is oriented in the circumferential direction rather than the axial direction as observed in the steel ringed as well as the belt reinforced NPT. All the design attributes of the unit cell is identical to the axial spoke model. The complete FE models of the two NPTs are shown in Figure 4.20. The assembly of components and all the material properties are identical to the axial spoke model. A continuous structure is obtained in the circumferential direction, when the unit sector is

rotated about its axis, which is responsible for rendering stiffness in the circumferential direction. In order to ensure that none of the tyres have unfair advantage in terms of volume of material used, the mass of the two tyres are kept as close to each other as possible. Due to the nature of construction, the axial spoke NPT weighs 5% more than the circumferential spoke NPT

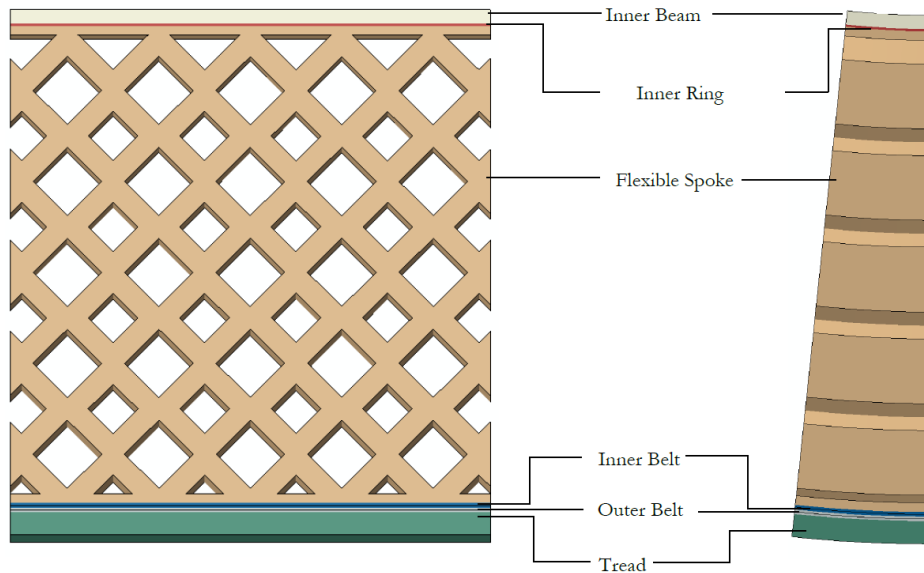


Figure 4.19: Unit Sector and lateral section of a circumferential spoke NPT

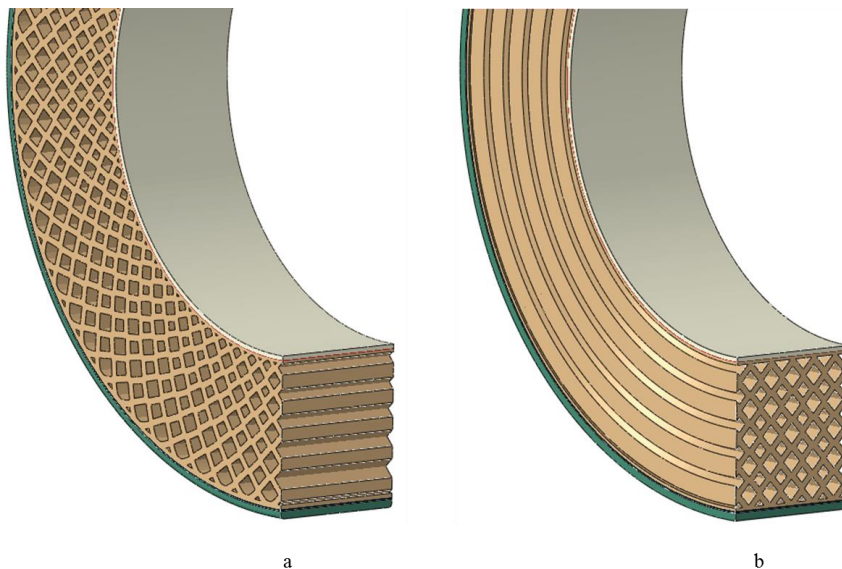


Figure 4.20: Sectional view of (a) axial spoke NPT and (b) circumferential spoke NPT

In order to evaluate the performance of the circumferential spoke model, a FE study similar to the one performed for the conventional NPT model is conducted. The analysis is performed for a rated load of 3000 N, coefficient of friction of 0.7 and a belt angle of 30

degrees. A static analysis to simulate the load carrying and phenomena and a steady-state rolling analysis for extracting the force and moment characteristics is undertaken.

4.7.1 Vertical Stiffness

Figure 4.21 shows the load-deflection plot for the four different tyre models. It can be observed, for a rated load of 3000 N, a maximum deflection of 16.6 mm is recorded for the circumferential spoke NPT. A drop in the vertical stiffness of almost 20% is observed. This increase in the compliance of the structure can be attributed to the Poisson's effect. In the axial spoked model, during loading, due to Poisson's effect, the structure tries to expand in both lateral and circumferential direction. The growth in the lateral direction is small due to the volume of material in the aforementioned direction whereas expansion in the circumferential direction is prevented due to the resistance offered by the adjacent cell wall members. In the case of the circumferential spoke NPT, the structure is free to expand on either side in the axial direction thus resulting in a structure with high compliance.

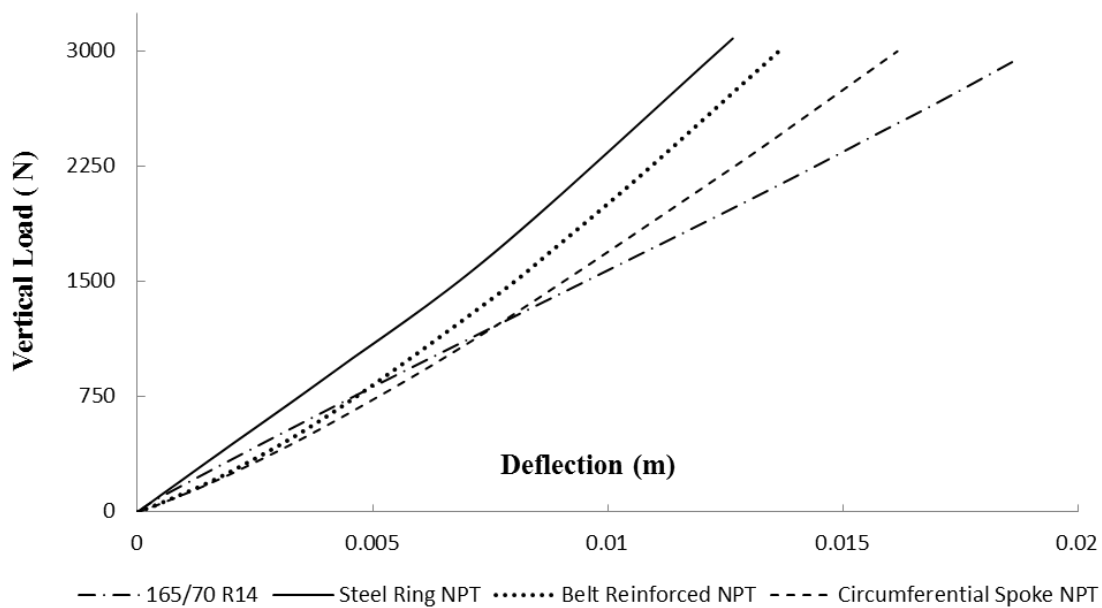


Figure 4.21: Load-deflection curves for different tyre models

4.7.2 Contact Pressure Distribution

Figure 4.22 shows the contact pressure distribution for the three tyre models. It can be observed that the circumferential spoke's contact pressure distribution is very similar to the pneumatic tyre's contact pressure profile. Apart from the identical profile, lower magnitudes of peak contact pressures are observed in the circumferential spoke model. Due to the increased compliance of the structure, a larger contact area is obtained. A contact area of $1.29E - 02 \text{ m}^2$ is recorded. As in the case of the axial spoke NPT a high contact pressure band is present, due to the structure's Poisson effect, which is oriented along the longitudinal direction. A longitudinal pressure band is obtained due to the participation of the tyre's circumferentially running cell walls. In order to focus on the region of maximum pressure, the scales of the contoured profile in Figure 4.22 have not been altered.

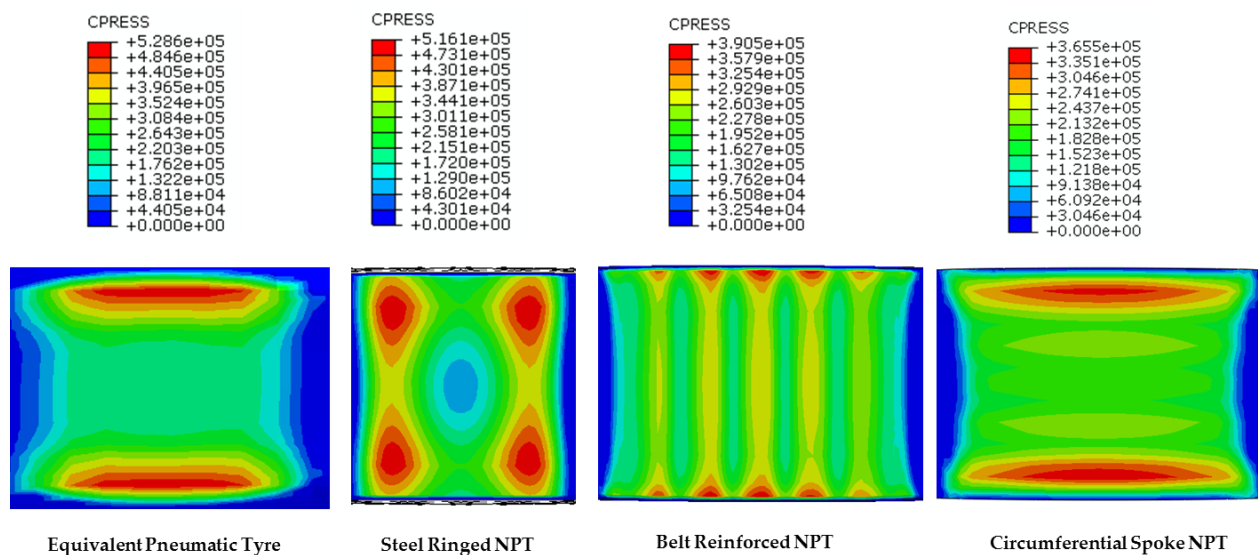


Figure 4.22: Contact pressure variation for different tyre models (Contact Pressure in Pa)

4.7.3 Longitudinal Force

Figure 4.23 shows the variation of the longitudinal force with respect to the slip ratio. The circumferential spoke NPT manages to reach its peak longitudinal force at 8% slip ratio whereas the other models manage to reach at 6% slip. Although the structure is continuous by design in the longitudinal direction, it exhibits lower stiffness when compared to other tyre models

4.7.4 Lateral Force

Figure 4.24 shows the variation of the lateral force with respect to other NPT models. The circumferential spoke model is able to match the pneumatic tyre's lateral stiffness but is lower than the steel ring NPT's stiffness. The tyre manages to match the peak lateral force as the steel ring NPT with increasing slip angle.

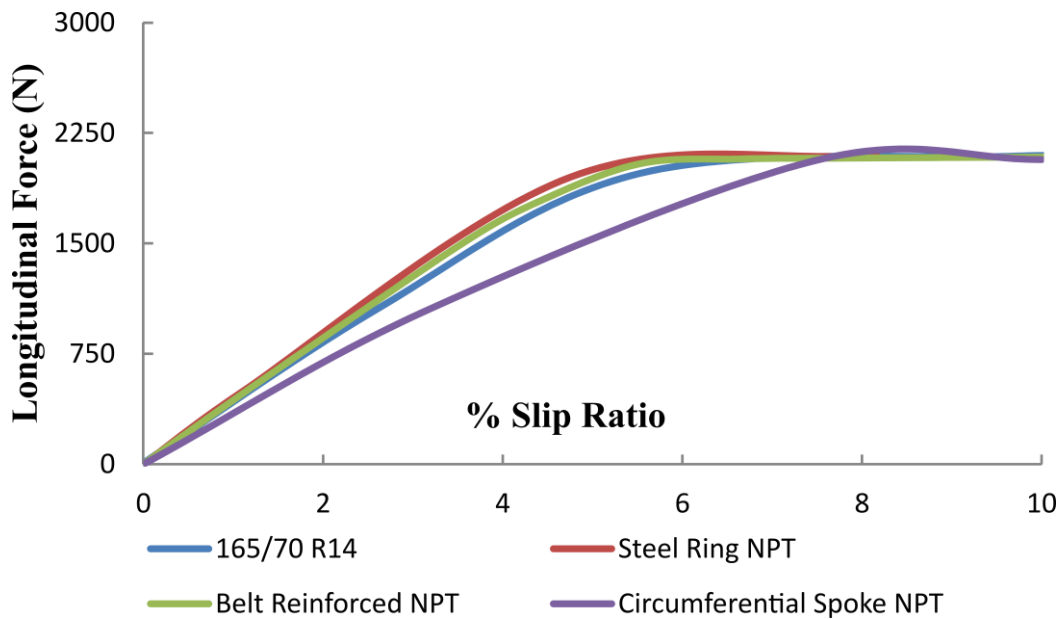


Figure 4.23: Variation of longitudinal force for different tyre models

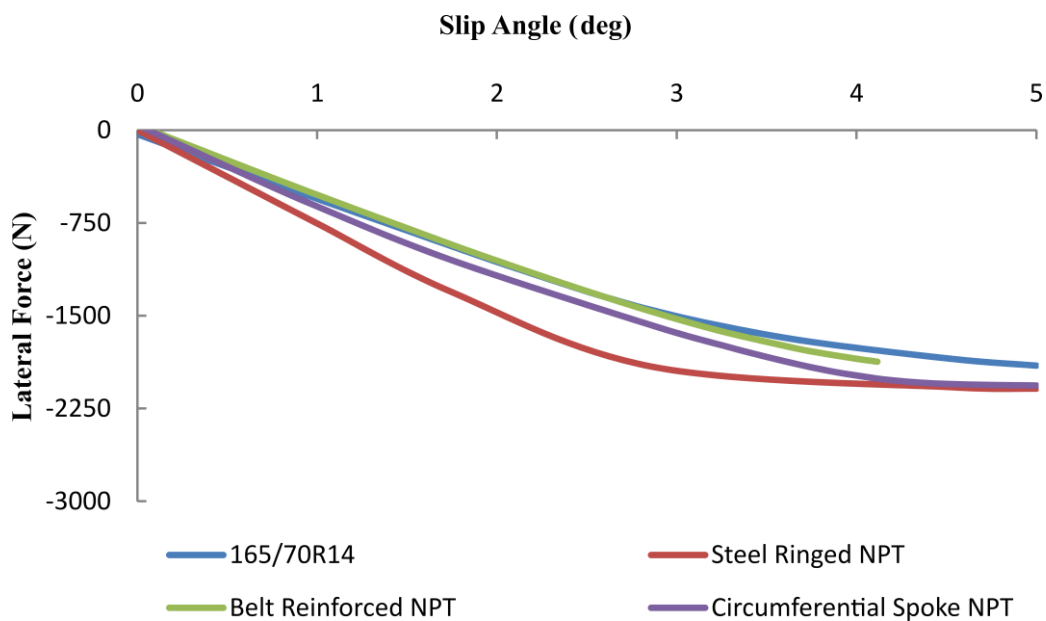


Figure 4.24: Variation of lateral force for different tyre models

4.7.5 Self-Aligning Torque (SAT)

It was observed from Figure 4.25 that the contact area of the circumferential spoke NPT was lower than the belt reinforced NPT. Owing to this, the SAT generated by the circumferential spoke NPT is lower than the belt reinforced NPT. The peak SAT magnitudes for the circumferential spoked NPT is closer to the pneumatic tyre's magnitude but the slip angle at which this is achieved is further away.

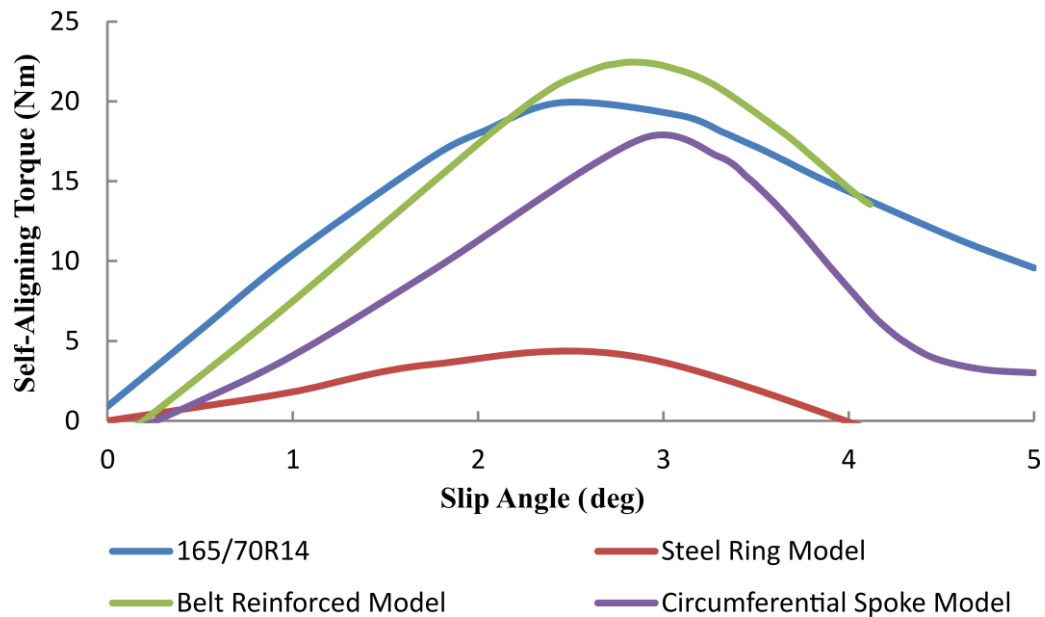


Figure 4.25: Variation of SAT for different tyre models

4.8 LIMITATION

Although the circumferential spoke NPT exhibits performance characteristics capable of matching the pneumatic tyre, there exists a complication with regards to manufacturing such a tyre. Conventionally, axially spoked NPT can be manufactured by moulding (Manesh *et al.*, 2012). In the case of circumferential spoked NPT, moulding is not a feasible manufacturing process as it is not possible to create a single mould for the entire tyre. A possible approach would be to mould two halves of the tyre and use suitable mechanical or chemical bonding process to hold the two halves together. The tyre model has been conceived with the notion of highlighting the freedom available in NPT design.

4.9 SUMMARY

The chapter throws light on the effect of reinforcements in a bottom loading NPT. It showed that cord reinforced rubbers had a major effect on the vertical and lateral stiffness of the tyre. The chapter also highlights the effect of different material properties on the F&M characteristics of the tyre. It was found that in the quest of lowering the stiffness by reducing the material properties, a significant drop in the circumferential stiffness of the tyre was also observed. The effect of load variations did not cause a significant change in the lateral stiffness in the linear range, thus ensuring the applicability of the tyre for different categories of vehicles. The concept of circumferential spokes has been introduced. It exhibited higher compliance without compromising on its performance. Both static and steady-state performance of circumferential spoke NPT closely conforms to the performance of the equivalent pneumatic tyre.

CHAPTER 5

CONCLUSION

5.1 CONTRIBUTIONS

A Non-Pneumatic Tyre (NPT) has been designed with the aim of replicating the conventional pneumatic tyres performance for passenger cars. As the first step towards manufacturing a product, a CAD model has been developed followed by a comparison of its performance with an equivalent 14" passenger car radial (PCR) tyre. A structure had to be conceived in order to replace the inflation pressure and the study of cellular structures is considered as the basis for the design of this structure. The following contributions have been made during the course of the research work

- An annular rhombi tessellated structure has been designed as the load carrying member, to replace inflation pressure using the philosophy of cellular structures. The governing parameters behind NPT design have been identified.
- A design methodology has been adopted wherein, the entire unit sector of the tyre can be created by using just the unit cell's geometric parameters. This is essential as it simplifies the entire design process. The designer can also choose to impose his/her own design strategy by increasing the number of governing geometric parameters.
- A change in the design assembly has been proposed wherein, conventional outer stainless ring has been replaced by the pneumatic tyre's reinforcing belts to replicate the performance of the equivalent pneumatic tyres and exhibiting varying performance in tyres of similar design.
- The concept of circumferential spoke has been introduced in this thesis. The new design eliminates the need for the structure to exhibit circumferential stiffness thereby allowing the NPT to be further compliant than its predecessor.

5.2 CONCLUSIONS

A 3D FE model of an aperiodic rhombi tessellated NPT has been developed and numerical experiments have been conducted to study the process of tyre force generation. The design warranted a spoke configuration which would neither buckle nor contort under the required operating conditions. A steel ringed NPT was initially designed and the model was capable of generating the required traction and cornering force as its pneumatic counterpart. In order to increase the number of design handles, the existing steel ring is replaced by conventional pneumatic tyre's belts. Since the pneumatic tyre belts are designed to work in tension, they are not involved in the load carrying process of the NPTs. Yet, variations in the belt angles affected the F&M characteristics, predominantly, the lateral stiffness of the tyre. The belt design inherently need not be similar to the pneumatic tyre's design and can be subjected to variations, but the introduction of cord reinforced elastomers has opened up a new facet in controlling the lateral stiffness of the tyre which was initially a function of the in-plane configuration and density of material in the transverse plane. The final part of the thesis introduces the concept of circumferential spokes. This design decoupled the circumferential stiffness from the lateral and vertical stiffness thereby further increasing the number of available handles when compared to conventional NPT models.

5.3 FUTURE WORK

One of the major advantages of the NPT is the flexibility in design. Unlike conventional pneumatic tyres the design does not demand a containment for holding the inflation pressure, thus eliminating a major design constraint. In order to a conduct a thorough validation of the presented designs, the following work can be performed in the future as an extension to this work.

- By including the viscoelastic effects, a study can be performed to calculate the rolling resistance of the tyre. A design strategy can be developed by identifying the correlation between spoke design and rolling resistance. This can also be extended to perform a temperature study in order to calculate the peak temperatures developed in the NPT during operation.
- Since the tyre behaves as a bottom loader, flat-spotting is a major issue. A study is essential in order to take into account such visco-plastic effects and consequently the durability of the tyre.

- The vertical stiffness of the pneumatic tyre is modelled as a single spring-damper system. This need not be the case for NPTs as the spoke can be conceived with varying geometric and material properties in the radial direction. A design can be developed to enhance its damping properties where the spokes attenuate a portion of the induced vibrations thereby working complementary to the suspension system.
- A comparative study of the ride/handling characteristics of a bottom and top loader could advocate the use of tyres of different load carrying mechanism for different surfaces or on different vehicles.
- An algorithm to recommend an optimized unit sector's dimensions depending on the equivalent tyre specifications like tyre size, rated load, operating conditions etc. with an available library of materials. This would help hasten the process of tyre design in order to test the tyre for its applicability.

REFERENCES

1. *Accidental deaths and suicides in India* (2013). National Crime Records Bureau,
2. **Alagappan, A. Vijay** (2014). *Magic formula tyre models using a realistic friction law*. Master's thesis, Indian Institute of Technology Madras.
3. **Arakawa, K., Masanori Iwase and Masahiro Segawa.** (2012). *Non-Pneumatic Tire*, U.S. Patent, US 8,113,253 B2
4. **Bakker, E., L. Nyborg, and H. B. Pacejka** (1987). Tyre Modelling for Use in Vehicle Dynamics Studies. *Society of Automotive Engineers*, 870421, 2.190 - 2.203.
5. **Berglind, L. A., Jaehyung Ju, and Joshua D. Summers** (2012) Aluminum Taper Bristle-Shaped Shear Band for a Nonpneumatic Tire, *Tire Science and Technology*, **40**(3), 152-170.
6. **Choi, E-H.** (2012). *Tire related factor in Pre-Crash Phase*, Technical Report, National Highway Traffic Safety Administration, Washington, DC.
7. **Clark, S. K** (1981) *Mechanics of pneumatic tires*. US Department of Transportation, National Highway Traffic Safety Administration.
8. **Fadel, G. M., Jaehyung Ju, Ashwin Michaelraj, Prabhu Shankar, Joshua D. Summers and John C. Ziegert.** (2011). *Honeycomb structures for high shear flexure*, US Patent, US 2011/0030866 A1
9. **Fiorletta, C. A.** (1994). *Tire pressure monitoring system*, U.S. Patent, US 5,289,160.
10. **Gardetto, W. W.** (1997). *Run-flat support for pneumatic tired wheel*, U.S. Patent, US 5,660,653.
11. **Gasmi, A., Paul F. Joseph, Timothy B. Rhyne and Steven M. Cron** (2012). Development of a two-dimensional model of a compliant non-pneumatic tire, *International Journal of Solids and Structures*, **49**(13), 1723-1740
12. **Gibert, J. M., Balajee Ananthasayanam, Paul F. Joseph, Timothy B. Rhyne and Steven M. Cron** (2013), Deformation Index–Based Modeling of Transient, Thermo-mechanical Rolling Resistance for a Nonpneumatic Tire, *Tire Science and Technology*, **41**(2), 82-108
13. **Gibson, L. J., and M. F. Ashby,** *Cellular solids: Structure and Properties*. Cambridge University Press, 1997

14. **Gillespie, T. D.**, *Fundamentals of vehicle dynamics*, Society of Automotive Engineers, 1992
15. Government of India. Available at <http://ncrb.gov.in/> [Accessed July 2014]
16. **Harris, A.** (2000), *The Mathematics of Tessellation*
URL: <http://ictedusrv.cumbria.ac.uk/math/pgdl/unit9/Tessellation.pdf>
17. **Hoppenheit, R., Siegfried Pooch, Bernd Backhaus, Lothar Salokat, Robert Pohlmann and Klaus Ehlers** (1996). *Solid rubber tire with wound overlay reinforcement structure*, U.S. Patent, US 5,579,818
18. **Humbrecht, E.** (1897). *Vehicle-wheel tire*, U.S. Patent, 576,072.
19. **Ju, J., D. M. Kim and K. Kim** (2012). Flexible cellular solid spokes of a non-pneumatic tire. *Composite Structures*, **94**(8), 2285-2295
20. **Kim, K., J. Ju, and D. M. Kim** (2013). Static contact behaviors of a non-pneumatic tire with hexagonal lattice spokes. *SAE International Journal of Passenger Cars – Mechanical Systems*, **6**(3), 1518-1527
21. **Manesh, A., M. Tercha., B. Anderson, B. J. Meliska, and F. Ceranski** (2012). *Tension-based non-pneumatic tire*, U.S. Patent, US 8,109,308
22. **Pajtas, S.R.** (1990). *Honeycomb Non-Pneumatic Tire with a Single Web on One Side*, U.S. Patent, US 4,945,962.
23. **Narasimha Rao, K. V.** (2005). *Design of Pneumatic Tyres with Finite Element Analysis*. Ph.D.thesis, Indian Institute of Technology Madras.
24. **Narasimha Rao, K. V., R. K. Kumar, R. Mukhopadhyay, and V. Misra** (2006). A study of the relationship between Magic Formula coefficients and tyre design attributes through finite element analysis. *Vehicle System Dynamics*, **44**(1), 33–63.
25. **Rhyne, T. B., and S. M. Cron** (2006). Development of a Non-Pneumatic Wheel *Tire Science and Technology*, **34**(3), 150-169
26. **Rhyne, T. B., Ronald H. Thompson, Steven M. Cron and Kenneth W. DeMino.** (2007) *Non-pneumatic tire*, U.S. Patent, US 7,201,194.
27. **Russell, B. A.** (2012). *Energy Efficient Wheel System*, U.S. Patent, US 8,127,809
28. **SIAM Report**,
URL - <http://www.siamindia.com/statistics.aspx?mpgid=8&pgidtrail=9>

29. **SIMULIA Inc.**, ABAQUS Version 6.14 documentation. Dassault Systemes, Simulia Corp., Providence, RI, USA, 2014.
30. **Stang, P. L.**, and **Joel V. V. O.** (1976). *Self-sealing vehicle tire and sealant composition*, U.S. Patent, US 3,953,893
31. **Wang, A. J.**, and **D. L. McDowell** (2004). In-plane stiffness and yield strength of periodic metal honeycombs, *Journal of Engineering Materials and Technology*, **126**(2), 137-156
32. **Weisstein, E. W.** (2001). Tessellation by Mathworld
URL: <http://mathworld.wolfram.com/Tessellation.html>
33. **Willard Jr, W. L.** (1996) *Run-flat tire with three crescent-shaped reinforcing members*, U.S. Patent, US 5,511,599.
34. **Wilson, J. L.** (2013) *Sealant material composition, self-sealing pneumatic tire, and preparation thereof*, U.S. Patent, US 8,360,122.

LIST OF PUBLICATIONS

Papers in Refereed Journals

1. Anand Suresh Kumar and R. Krishnakumar, “Force and Moment Characteristics of a Rhombi Tessellated Non-Pneumatic Tyre”, *Tire Science and Technology*. (Accepted for publication, email dt: 23/11/2015)

Conferences

1. Anand Suresh Kumar and R. Krishnakumar, *Force and Moment Characteristics of a Rhombi Tessellated Non-Pneumatic Tyre*, **34th Annual Meeting and Conference on Tire Science and Technology**, Akron, Ohio, USA, 9th – 10th September 2015.

CURRICULUM VITAE

NAME : Anand Suresh Kumar
DATE OF BIRTH : 3rd January 1990

EDUCATIONAL QUALIFICATIONS

Master of Science (by Research)

Institution : Indian Institute of Technology Madras
Specialization : Engineering Design

Bachelor of Engineering (2011)

Institution : VelTech Engineering College, Chennai
Specialization : Mechanical Engineering

GENERAL TEST COMMITTEE

CHAIR PERSON:

Prof. Nilesh J. Vasa

Dept. of Engineering Design

GUIDE:

Prof. R. Krishna Kumar

Dept. of Engineering Design

MEMBERS:

Dr. Shankar Krishnapillai

Dept. of Mechanical Engineering

Dr. G. Saravana Kumar

Department of Engineering Design